THE UNIVERSITY OF MANITOBA

# SEISMIC APPROACHES FOR MINERAL EXPLORATION IN THE SUDBURY BASIN OF ONTARIO, CANADA

By

Derbew Messfin

A Thesis

Submitted to the Faculty of Graduate Studies

In partial fulfillment of the requirements for the degree of

Master of Science

In

Geophysics

Department of Earth Sciences

Winnipeg, Manitoba

October, 1983

# SEISMIC APPROACHES FOR MINERAL EXPLORATION IN THE SUDBURY BASIN OF ONTARIO, CANADA

BY

DERBEW MESSFIN

A thesis submitted to the Faculty of Graduate Studies of the University of Manitoba in partial fulfillment of the requirements of the degree of

MASTER OF SCIENCE



# ABSTRACT

This study investigates the feasibility of using seismic techniques in the search for ore deposits, with particular emphasis given to locating ore-bodies at great depths. The basic procedure followed was essentially an understanding of the forward problem, whereby the effects of the subsurface structure in a typical mining district was thoroughly studied. Such a study presupposes that there is a substantial knowledge of the subsurface geology and the seismic velocity distribution of the area under consideration. Consequently, the initial stage of the study was devoted to determining the elastic parameters. This was accomplished by laboratory measurement of seismic velocities and densities of core samples obtained from the Sudbury Basin.

The measured data shows that unlike most young sedimentary rocks, the velocity of crystalline rocks strongly depends on the chemical composition and density of the rock type, even in the low pressure region. Mafic igneous rocks have substantially higher velocities than felsic rocks. The computed acoustic impedance reveals a very high value for massive sulphides, followed by oxide-rich quartz gabbro and mafic norite. The reflection coeficient of possible interfaces in the Basin shows exceptionally high values for all interfaces formed with massive sulphides, and moderately high values for micropegmatite/oxide-rich quartz gabbro and mafic norite/granite gneiss interfaces.

By virtue of its capability to handle lateral as well as vertical inhomogeneities, fast computing time and flexibility, the asymptotic

ray theory was found more suitable for studying the effect of geological structures typically found in the Sudbury Basin. Hence, all the analysis and the numerical simulation undertaken in this study are based on this theory.

Most of the seismic models are large scale models ranging in depth from 5 km to 10 km and they represent actual geological conditions in Sudbury. The seismic response of these models shows that the micropegmatite/oxide-rich quartz gabbro and the mafic norite/granite gneiss contacts are characterized by substantially strong reflections. This suggests that these interfaces can serve as marker horizons in future seismic surveys. Besides, the intimate association of sulphide mineralization with mafic norite sub-layer indicates that the seismic method could be a powerful exploration tool in Sudbury-like environments.

Small scale models up to 1.6 km deep were constructed to simulate typical mineralized structures in Sudbury. In all the models considered, the sulphide body is outlined by a distinctly high amplitude of reflection. Both the travel time and the dynamic characteristics of these models have features that are indicative of the presence of mineralized structures.

From the model studies it is learned that conventional seismic reflection methods can be effectively used in mapping major geological structures in Sudbury, but the identification of mineralized zones, on the other hand, requires the use of new high resolution seismic techniques.

## ACKNOWLEDGEMENT

The author expresses his deep gratitude to Dr. W. Moon for continued inspiration and guidance in the course of this study. Sincere gratitude is extended to Dr. D.H. Hall for his advice and encouragement in the early part of my graduate program. Thanks is due to Dr. G.S. Clark for the invaluable suggestions and comments made on the geology of the study area. Drs. B.Kraus, Ebehard Berrer, and N.L.Anderson of INCO Ltd.(Copper Clif, Ontario) kindly offered velocity data and geological information used in this thesis. Dr. B.I. Pandit of The Department of Geological Sciences, University of Saskatchewan kindly explained the laboratory procedure for the velocity measurement. This project is part of an ongoing research programme being undertaken by The Center For Precambrian Studies of the University of Manitoba.

Financial support by the Department of Technical Co-operation for Development of the United Nations in the form of fellowships is gratefully acknowledged.

# TABLE OF CONTENTS

## LIST OF FIGURES

# LIST OF TABLES

# Chapter 1

## INTRODUCTION

The great majority of mineral deposits are beneath the surface of the earth, and their detection depends upon the physical characteristics which differentiate them from the surrounding media. Seismic methods are based on the detection of the variations in the elastic properties of rocks for determining geological structures associated with hydrocarbon accumulation, such as faults, anticlines and synclines. Similarly, variations in electrical conductivity and in natural currents in the earth, the rates of decay of artificial potential differences introduced into the ground, local changes in gravity, magnetism, and radioactivity, all provide us with valuable information as to the nature of the subsurface structures. The knoweledge acquired from these properties will be used to determine the most favourable places for locating the mineral deposits we seek. The choice of a method to locate a particular mineralization depends on the nature of the mineralization and of the host rock. A method may give a direct or indirect indication of the presence of a mineral deposit. An example of the former is the magnetic method when used to find magnetic ores of iron or nickel. The same method can be indirectly used to find placer gold deposits associated with magnetite.

Seismology is at present the only branch of geophysics that offers a feasible method by which subsurface investigation can be carried out to the greatest depths, as well as with correspondingly high resolution

and accuracy. The high resolution and accuracy stems from the fact that seismic waves have the shortest wavelength of any wave that can be observed after modulation by passing through structures inside the earth. Seismic waves undergo the least distortion in amplitude, as compared with other observables, such as heat flow, electromagnetic phenomena, strain, and static displacement (Aki and Richards, 1980).

The prime objective in exploration seismology is the mapping of geological structures almost invariably in the uppermost part of the earth's crust. The general theoretical background of seismic prospecting has much in common with earthquake seismology, the principal difference being in the frequency of the seismic waves employed. In contrast to earthquake waves, the waves used in seismic prospecting are of very short wavelength with frequencies ranging from about 10 Hz to 100 Hz. The basic principles of the instruments used are generally the same, but their technical specifications and operational details are greatly different.

Exploration seismology is broadly classified into the refraction method and the reflection method. The reflection method has been used far more than any other geophysical method for the mapping of subsurface structures in relatively young sedimentary areas favourable for hydrocarbon accumulation. The conventional method is less promising for deep crustal studies, its optimum practical applicability being confined to studies at intermediate depths, from a few hundred meters to a few kilometers.

The refraction method, which applies Snell's law of optics to seismic waves, is less popular at present in the oil industry but is widely

used in crustal studies and has considerable application in engineering and groundwater problems. In a reconaissance survey, the refraction method has some important advantages over the reflection method. In contrast to reflection surveys, which in the absence of velocity data can give only the geometry of the subsurface formations, refraction surveys yield data on the seismic velocities and large scale geometry of the formations (Sharma, 1976). On the other hand, the refraction method has some serious disadvantages in comparison with the reflection method: a) the method is inherently blind to detect a low velocity layer sandwitched between two layers of higher velocity, b) if one of the layers is thin in comparison with the depth, the refracted wave from this layer may never reach the surface as a first arrival, and c) for the same depth of penetration, the refraction method requires more energy and substantially large source-detector distance than the reflection method.

The usual procedure in exploration seismology is to generate seismic waves by a near-surface explosion(or a mechanical vibration), record the resulting waves which reach the surface at various distances through different paths, and deduce the position of reflecting and refracting interface by the analysis of travel times of identifiable wave groups. Both refraction seismics and reflection seismics need a device for generating and detecting seismic pulses. By far the most common method of generating seismic waves is by exploding a dynamite charge in a hole. The amount of dynamite used depends on many factors, one of which is the depth to the geologic structure to be investigated.

Tremendous progress has been made in seismology in the last two dec-

ades primarily because of the advent of modern computers and improvements in data acquisition systems, which are now capable of digital and analog recording of ground motion over a wide range of frequencies. Such advances in technology have enabled seismologists to make measurements with far greater precision and sophistication than was previously possible. A correspondingly high degree of computational analysis have been applied to high-quality data and elaborate theoretical models have been devised to interpret them.

Traditional seismic interpretation techniques have put more emphasis on determining the velocity and layer structure based primarily on travel times. Recently, it has been realized that both the arrival time and shape of a seismic wavelet provide information regarding the fine structure and physical properties of the material through which the wave has propagated (Braile and Smith, 1975). Then it is the task of the exploration seismologist to determine the subsurface structure and the physical properties from the data obtained at the earth's surface. This is what is known as the solution of the inverse problem and requires an understanding of the forward problem, i.e., the effects of earth structures on seismic waves. The main objective of this thesis is to demonstrate the effects of various seismic velocity distributions on the resulting seismic record sections using synthetic seismograms, and to apply the results to base metal exploration at unusually greater depths. The overall procedure is essentially a forward problem and it is based on seismic velocity distributions derived from laboratory-measured seismic velocities and the geological sections from which the rock samples for velocity measurement were obtained. The samples were obtained from the well known mining district of Sudbury, Ontario.

Most of the existing techniques for generating synthetic seismograms are designed to handle seismic problems associated with horizontally layered structures with no lateral variation in physical properties. On the other hand, most ore-bodies are known to occur in moderately-to-steeply dipping and often irregular structures. Consequently, the "asymptotic ray method", which allows both lateral and vertical inhomogeneity, but not necessarily as exact as the wave methods used for laterally homogeneous layers, was found more appropriate to model geological structures typical of the Sudbury Basin.

In the first half of the thesis, the geological background and the laboratory seismic velocity measurements are presented (chapter 2 and chapter 3). Chapter 4 lays the theoretical basis of the seismic modelling to be described in the next chapter. Finally, the role of some of the existing data processing operations with respect to seismic data collected for mineral exploration is investigated in detail.

## 1.1 Seismic methods in mineral exploration

Seismic techniques have had limited application in mineral exploration compared to petroleum prospecting. This is mainly because of the complexity of geologic conditions with many rock types, faulting, fracturing etc., that are commonly associated with areas of ore deposition. Consequently, velocity contrasts are likely to be uncertain and variable with resultant complex seismic wave propagation paths, which makes data interpretation far from unique. Besides, other geophysical methods, such as electrical and EM methods are more ideally suited to direct detection, so that seismic methods could not offer any advantage

for shallow ore deposits.

Both conventional refraction procedures and shallow refraction techniques with hammer energy sources have been successfully used to determine the depth to bedrock, probable composition of the bedrock material, and thickness of overburden for diamond drill hole locations. Seismic methods have been used to locate placer deposits in overburden materials above bedrock by outlining preglacial depressions in the bedrock topography (Hobson, 1966; Hobson and Grant, 1964). Nonmetallic mineral deposits such as gypsum, limestone, and cement can also be delineated using the same procedures as in engineering applications.

The most noteable applications to detect metallic ore-bodies, primarily sulphides, were made by Elliot (1967), Wabaso and Mereu (1978), and Overton (1972, 1976). In the first two studies, the technique used was a combination of fan shooting and ray path tracing. Nevertheless, all studies directed toward delineating sulphide ore-bodies were experimental in nature and some of the results were not encouraging.

The present trend, along with the advancement of electronic technology, is that of using seismic reflection techniques to map major geological features favourable for metallic ore-deposits as well as detecting the ore-bodies themselves. Consequently, there is a growing interest in using conventional and new high resolution petroleum prospecting instrumentation in sedimentary basins within the shield areas and in regions where there is appreciable layering or diversity of the different rock types.

## 1.2 Seismic surveys in the Canadian Precambrian Shield.

Since the early sixties, there has been a growing interest in understanding the various geological processes in the deeper parts of the Earth's crust. This has resulted in an increased crustal seismic activity in many parts of the world, particularly in Europe (Meissner, 1967; 1973; Dohr and Meissner, 1975), the U.S.S.R. (Kominskaya and Riznichenko, 1964), and North America (Berry, M.J., 1973; Oliver and Kaufman, 1977; Smithson et al., 1977; Green et al., 1980).

In North America, there are a number of groups from the university and government that are presently engaged in large scale seismic crustal studies. Noteable examples of such groups are the COCORP (Consortium for Continental Reflection Profiling), (Cook et al., 1980) in the United States and COCRUST (Green et al., 1980; Delandro and Moon, 1982) in Canada.

The Bulk of the seismic surveys in the Canadian Precambrian Shield are crustal in nature, with refraction profiles as long as 400 km. These surveys have resulted in a better understanding of the two most often quoted parameters, crustal thickness and upper mantle velocity, in the Canadian Shield. It has been established that the crust is generally thinner in the Superior Structural Province than in the Churchill Province (Mereu and Hunter, 1969). It is also known that the upper crust in the northeastern part of the Canadian Shield is characterized by low velocity zones (Berry, 1973; Berry and Fuchs, 1973). Whereas in the southwestern part of the Shield, Manitoba and Northwestern Ontario, the crustal velocity structure is given by a three layer model with step-like velocity increases with depth (Hall and Hajnal, 1969; 1973).

In recent years, seismic surveys, both reflection and refraction, have been utilized to map granite-greenstone contacts, fault zones, and structural province or subprovince boundaries (Green et al., 1979; Green, 1981; Young, 1979). In some parts of the Shield, the contact between volcanic rocks and sedimentary rocks has been mapped by seismic reflection techniques (Hajnal and Stauffer , 1975). These and several other seismic studies in the Shield give substantial evidence for the increasing role of the method in the area. Hence, it appears that deep seismic mapping continues to be an important factor in developing answers to major geological questions.

The Sudbury Basin is one of the largest mining district in the Canadian Shield. Considerable use of conventional mining geophysical methods has helped in locating metallic ore-bodies in the area. However, their applicability has been limited to shallow ore-bodies, not exceeding 500 m in depth. In this study an attempt will be made to investigate the feasibility of using the seismic method, which has a much greater depth of penetration, in Sudbury-like environments. Laboratory-measured seismic velocities of core samples obtained from the area were utilized to compute seismic models of geological structures typically found in the Sudbury Basin. On the basis of the computed seismic responses, it was possible to make a detailed study of the seismic discontinuity in the District.

# Chapter 2

# G E O L O G Y

## 2.1 General geology of the Canadian Shield

The Canadian Shield is a vast region of Precambrian rocks that occupy nearly half the area of Canada, with a total bed-rock area of nearly 4.5 million square km. Except on the northeastern side facing the Greenland Shield, the Canadian Shield is surrounded by Phanerozoic sedimentary rocks forming a platform cover of relatively undisturbed rocks protected by the virtually stable Precambrian basement (Stockwell et al., 1970). The Shield is believed to have remained esentially stable since the end of Precambrian time, however, it has been disturbed by Phanerozoic faults especially along the southern boundary and along the borders of the Bothia Uplift in the north. The more stable western boundary of the Canadian Shield is free from any disturbance caused by Phanerozoic faults.

On the basis of the overall differences in internal structural trends, style of folding and geologic ages, the Shield is divided into structural provinces and subprovinces (Figure 2.1). The structural divisions, although based primarily on geological evidence, have been greately strengthened by isotope age studies of orogenies. The boundaries between provinces are drawn where one trend is truncated by another, either along major unconformities or, in their absence, along orogenic fronts.

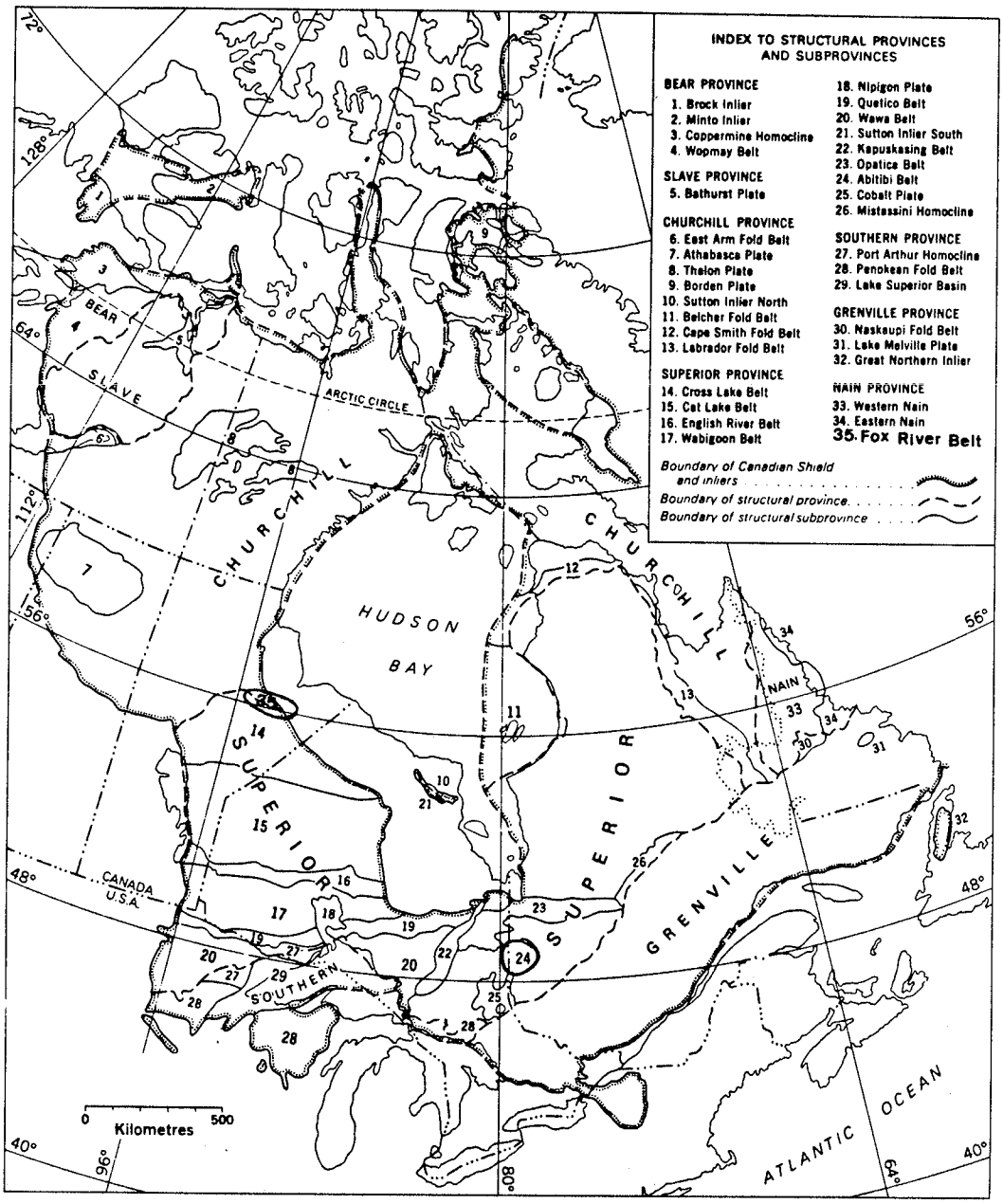


Figure 2.1. Structural provinces and subprovinces of the Canadian Shield (modified after Stockwell et al., 1970). Stockwell et al., 1970).

Four major orogenic periods have been recognized, named, and defined in the Canadian Shield. The Kenoran Orogeny (with mean K/Ar mica age of 2480 Ma) is defined as the last important period of widespread folding, metamorphism, and intrusion in the Superior Province, and is also well established in the Slave and Nain Provinces. Similarly defined are the Hudsonian Orogeny (mean k/Ar age of 1735 Ma) of the Churchill Province as the type region (has also been established in the Bear Province and Southern Province), the Elsonian Orogeny (mean K/Ar mica age of 1370 Ma) with Western Nain Province, as the type region; and the Grenvillian Orogeny, (mean K/Ar age of 955 Ma) of the Grenville Province being the type region (Stockwell et al., 1970).

The Canadian Shield is broadly classified into two first-order time units, the Archean and the Proterozoic. The Archean includes rocks involved in the Kenoran Orogeny and all other older rocks. The Proterozoic, on the other hand, spans the time from the close of the Kenoran Orogeny to the beginning of the Cambrian Period.

The Superior Province is the largest Archean province in North America (Condie, 1981), with dominant whole-rock Rb-Sr and U-Pb zircon ages ranging from about 2500 to 3000 Ma. Nearly all known mineral occurrences in Archean rocks are located in volcanic-sedimentary belts, or greenstone belts, and most occurrences, whether they consist of massive sulphides, gold bearing quartz veins, nickeliferous mafic intrusions or iron deposits, are closely associated with the volcanic rocks themselves (Lang et al., 1970).

The primary interest in shield geology is the occurrence of a wide range of economic mineral deposits including precious metals, base met-

als, ferrous and ferro-alloy metals, uranium and some non-metals. Noteable mining districts of the Shield include : banded iron formations of Quebec and Labrador, Nickel copper deposits of Sudbury, Ontario, and the Thompson-Moak Lake areas of Manitoba and the silver-cobalt deposits of Cobalt, Ontario.

## 2.2 Regional geological setting of the Sudbury Basin

Sudbury is uniquely located near the junction of the Superior, Southern, and Grenville structural provinces of the Canadian Shield (Figure 2.2). The Grenville Front, the northeast-trending contact zone between the Grenville Province and the Southern and Superior Provinces, is located about 10 km southeast of the Sudbury Basin. The Sudbury Structure also lies along the line of junction of two major fault systems, the east to northeast-trending Murray system of the north shore of Lake Huron, and the north-northwest-striking Onaping system of the Superior Province and the Cobalt plain (Card and Hutchinson, 1972). The major and minor axes of the Sudbury structure are aligned parallel to the Murray and Onaping fault systems respectively (Figure 2.2).

Both the location and shape of the Sudbury structure are clearly related to regional tectonic features, including the junction of three stuctural provinces and two main fault systems. The whole structure is believed to lie within a possible major Precambrian rift system. Regional stratigraphic evidence indicates that some of these tectonic features predate intrusion of the Sudbury Nickel Irruptive due to their apparent influence on Aphebian sedimentation (Card and Hutchinson, 1972).

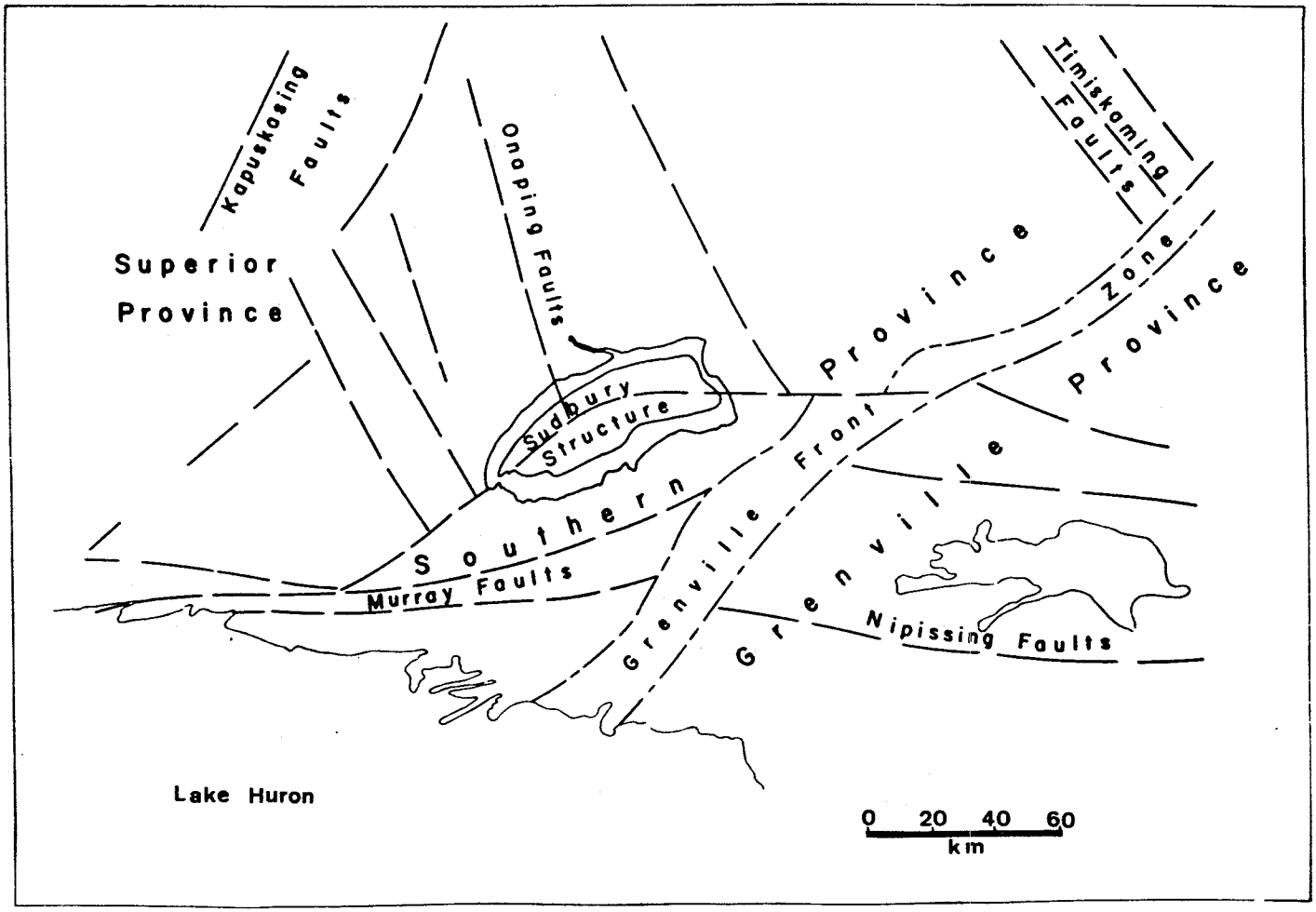


Figure 2.2. Location of the Sudbury Structure with respect to structural province boundaries and major fault systems (after Card and Hutchinson, 1972).

## 2.3 General geology of the Sudbury Basin

The Sudbury Basin is outlined by the Nickel Irruptive, an intrusion which encloses an elliptical basin (Figure 2.3) of approximately 60 km in an east-northeast direction and 27 km across. The irruptive consists of a lower gabbroic portion known as the "norite" and an upper granitoid portion known as the "micropegmatite". The lower contact of the irruptive on the south dips northward at angles of about 45° to 70° but, in some locations, it is vertical, or even south-dipping (Card and Hutchinson, 1972). The northern contact dips southward at angles of approximately 30° to 50° . At depth, the Nickel Irruptive is commonly believed to be basin or funnel-shaped, with rocks of the South Range thrust faulted 5 km upwards relative to the North Range.

In the north, the Nickel Irruptive intrudes Archean granitic and migmatitic rocks of the Superior Province. South, east and west of the Irruptive there are rocks of the Southern Province consisting of Proterozoic metavolcanic and metasedimentary rocks of the Huronian Supergroup, felsic intrusions of several ages including the Murray, Creighton, and Grenville Front granites, as well as mafic intrusions of various ages. Inside the Irruptive, there are rocks of the Whitewater Group, which include a lower tuff-breccia sequence (Onaping formation), carbonaceous slate unit (Onwatin formation) and an upper turbidite-greywacke sequence (Chelmsford formation). The group has a combined thickness of about 2,400 m. The Onaping formation is intruded by the micropegmatite and consists essentially of metasedimentary and granitoid rock and mineral fragments and devitrified and crystallized glasses.

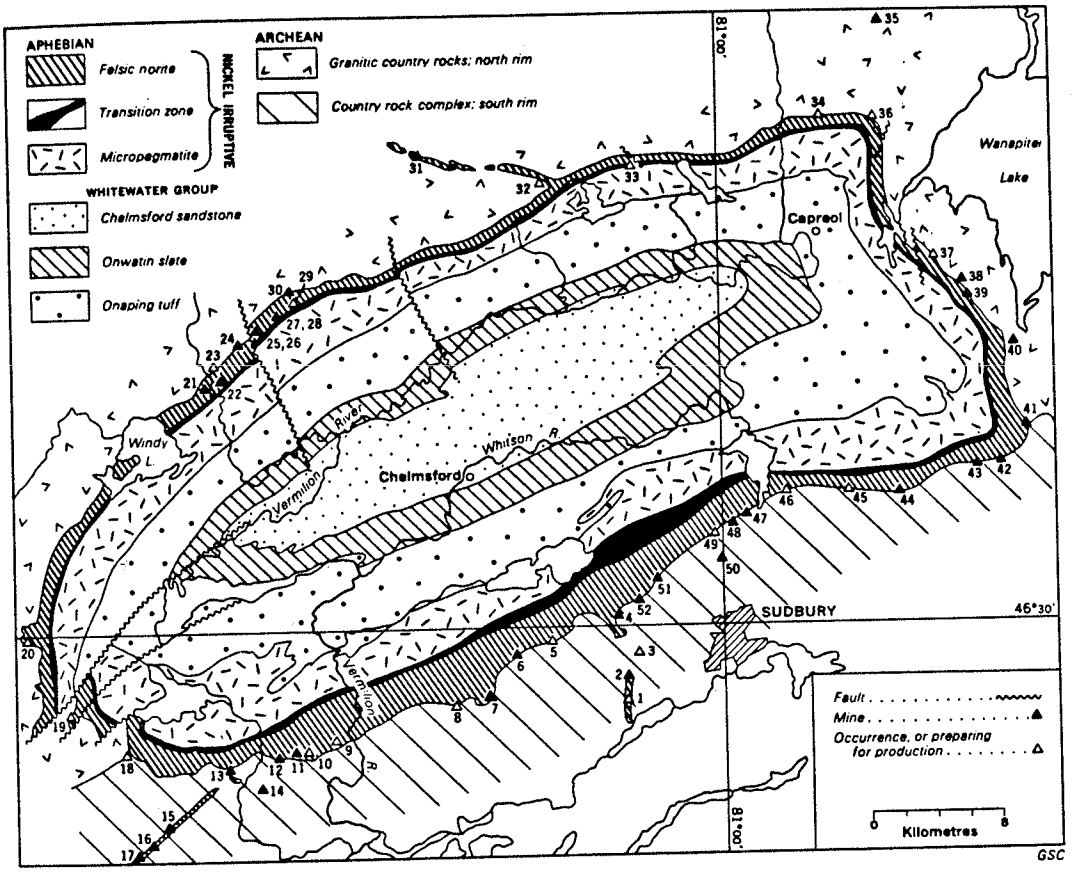


INDEX TO PROPERTIES

(Numbers in brackets according to Map 1252A)

1. Copper Cliff South
2. (89b) Copper Cliff No. 1
3. (89c) Copper Cliff North
4. (89a) Clarabelle
5. Tam O'Shanter
6. (90b) North Star
7. (90a) Creighton
8. Gertrude
9. McVittie Graham
10. Lockerby
11. (78b) Ellen
12. (78a) Crean Hill
13. (78c) Victoria
14. Vermilion
15. Kidd
16. (79c) Worthington
17. (79b) Totten
18. Chicago
19. Sultana
20. Trillabelle
21. (80a) Hardy
22. (80b) Onaping-Boundary
23. Levack West
24. (82b) Levack
25. (82a) Fecunis Lake
26. (82d) North
27. (82e) Strathcona
28. Coleman
29. Longvack South
30. (82c) Longvack
31. (83) Nickel Offset
32. W.D. 150, 155
33. North Range Shaft
34. New Dominion
35. (85) Milnet
36. Whistle
37. Capre Lake
38. Victor
39. (86) Nickel Rim
40. (87e) Maclennan
41. (87f) Norduna
42. East
43. (87a) Falconbridge
44. (87c) Garson
45. (87d) Kirkwood
46. Sheppard
47. (88a) Blezard
48. (88c) Mount Nickel
49. Little Stobie
50. (88b) Frood-Stobie
51. (89g) McKim
52. (89h) Murray

Figure 2.3. General geology and nickel deposits of the Sudbury District, Ontario (after Lang et al., 1969).

Many fragments show evidence of melting, and many display features considered distinctive of shock metamorphic origin. These features and the discovery of shatter cones gave support to the theory that the Sudbury structure could be explained by an explosive meteorite impact (Dietz, 1964; French, 1972). According to this hypothesis, the Onaping formation is interpreted as a fallback breccia deposited immediately after impact in the original crater.

Rubidium-strontium ages, estimated using mineral-whole rock pairs from the Sudbury Basin indicate that the Sudbury event, marked by the development of shock metamorphism and intrusion of the Nickel Irruptive, is 1900 Ma old (Gibbins and McNutt, 1975). More recently two independent high precision U-Pb zircon ages measured using norite samples from the North and South Ranges give ages of 1849.6 and 1849 Ma respectively(Krogh et al., 1982). Huronian formations, that lie unconformably on the Archean basement complex, are believed to have been deposited between 2,300 and 2,500 Ma (Fairbairn and Hurley, 1969). Archean granitic and migmatitic rocks of the Superior Province, mainly on the northern rim of the basin, are at least 2,500 Ma old (Van Schmus, 1965).

Another source of valuable information regarding the age relationship of the Irruptive rocks is paleomagnetism. A series of paleomagnetic studies on the Irruptive (Hood, 1961; Sopher, 1963; Larochelle, 1969) characterizes the norite as having an unusual magnetic stability with negligible isothermal contribution. The micropegmatite on the other hand has a substantially lower magnetic homogeneity, suggesting that an appreciable fraction of its remanent magnetization may be due

to minerals formed long after the original cooling phase of the Irruptive. The analysis also shows that the mean directions of magnetization of the norite and of the micropegmatite are not significantly different in the undisturbed sectors of the Irruptive (Larochelle, 1969). This led to the conclusion that the two rock units are probably contemporaneous. Also, the observed significant divergence in the direction of magnetization in the North and South Ranges has been attributed to post-irruptive folding towards the interior of the basin (Sopher, 1963).

## 2.4 On the origin of the Sudbury Basin

There are two main hypotheses on the origin of the Sudbury Structure. The older one has undergone various changes in detail but it rests upon broad conventional consideration of regional structure (location at the intersection of several major lineament(s), petrology (association of Fe-Ni-Cu sulphides with layered basic intrusions; proximity to other ring complexes) and geochronology ( Dence, 1978).

According to this theory, the Sudbury Structure represents volcanic-tectonic explosion processes. A broad dome, involving Huronian and older rocks, was uplifted by the presence of igneous magma. Successive periods of uplift followed by tensional release gave rise to the Sudbury breccia dikes and finally led to caldera collapse at the apex of the dome. Magma escaping around the rim of the caldera and flowing into the collapsed center produced the Onaping formation. The Nickel Irruptive was emplaced between the caldera walls and the downsagged Onaping volcanics (Speers, 1957). The Onwatin and Chelmsford forma-

tions may have been formed in a lake within the caldera.

More recently, Dietz (1964; 1972) suggested that the circularity and brecciation characteristics of the Sudbury Structure could best be explained by an explosive meteorite impact. This is based on the interpretation of shatter cones discovered in the area. Inspired by this theory, French (1967) found microscopic features characteristic of shock metamorphism in inclusions in the Onaping formation. Since then, more evidence has been accumulated which finally resulted in the classification of the Basin as one of the confirmed impact structures in Canada (Robertson and Grieve, 1975). In the more accepted version of the impact theory, the explosion acts as a trigger for endogenic magmatism with associated sulphide mineralization ( Dence, 1978). Shock waves radiating from the point of impact produced brecciation, melting, microscopic shock features and shatter cones, and excavated a circular crater. Part of the material blasted from the crater fell back as a poorly sorted breccia - the Onaping formation. Because of its great magnitude, the Sudbury event triggered magmatism by offloading the lower crust and mantle and by adding shock heat (Dietz, 1964), which initiated the evolution of the Nickel Irruptive. A saucer-shaped pool of magma, including the ores, was emplaced between the brecciated crater wall and overlying crater-filling breccias in the central zone of the structure. A body of water subsquently occupied the basin, in which the Whitewater sediments were deposited. Subsequent rebound, isostasy, tectonism and erosion played a great role in giving the present shape of the structure.

## 2.5 The ore-bodies

The ores in Sudbury are part of a sulphide and inclusion-bearing facies of the Irruptive that occurs as a discontinuous sub-layer around its outer margin and in places as dikes that invade the surrounding country rock (Souch et al., 1969). The ore-bodies fall into three logical groups; those associated with offset dykes, those on the South Range and those on the North Range.

The offset environment, as in Frood-Stobie, consists of a sulphide-spotted, wedge-shaped body of inclusion-bearing sulphide. Three principal ore types are recognized : disseminated sulphide, inclusion massive sulphide, and contorted schist inclusion sulphide. The offset ore-bodies at Copper Cliff project outward from the norite contact and range in shape from thin sheets to steeply-plunging or vertical pipes.

On the South Range, the ore-bodies are typified by sulphide and inclusion-bearing mafic sub-layer rock that occupy a depression in footwall rocks at the base of the Irruptive. At Creighton and Murray, the quartz-rich norite is in abrupt but irregular contact with the underlying ore zone or sub-layer (Figure 2.4a). The proportions of both inclusions and sulphides in the sub-layer usually increase towards the footwall, although, the inclusions are commonly absent and a zone of massive sulphide is present immediately adjacent to the footwall contact.

On the North Range, the ore-bodies are also typically associated with mafic sub-layer rocks occupying depressions at the base of the Irruptive. However, along the contact between Levack and Langvack

a)

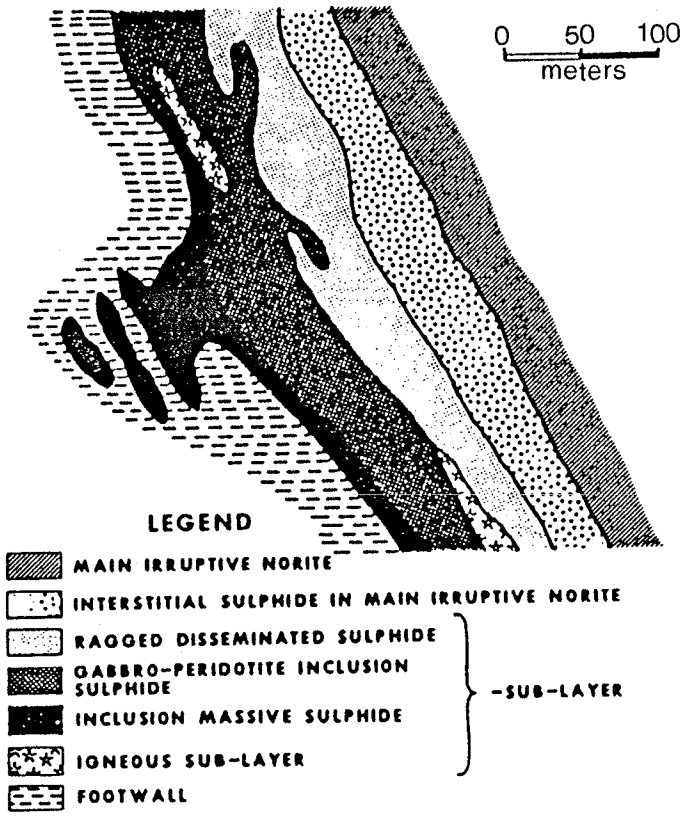


b)

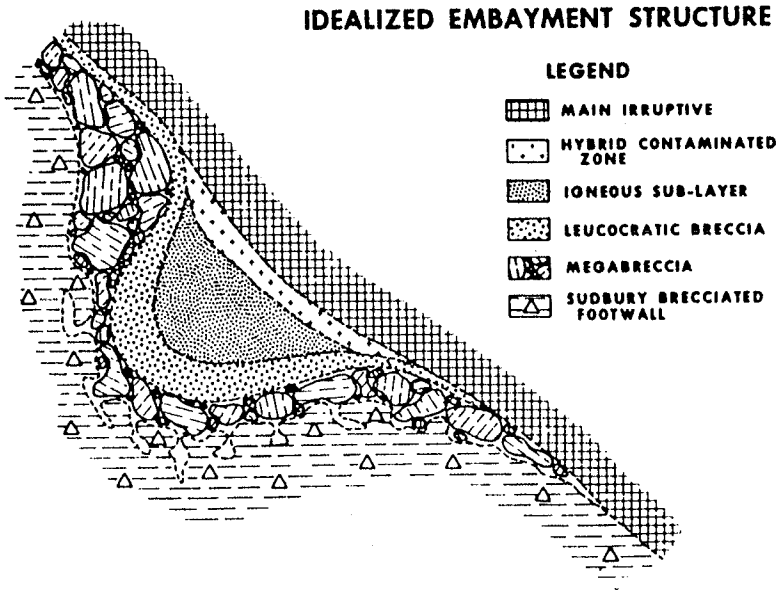


Figure 2.4. (a) Geological cross-section through the Creighton embayment (after Souch et al., 1969).
(b) Idealized embayment structure of the North Range enviroment (after Dence, 1978).

mines, the embayments project into zones of granite breccia, (Figure 2.5b), where the bulk of the sulphides occur in blebs that locally coalesce into pods or stringers and the bulk of the sulphides occur in the breccia. At Strathcona, a large nickel-copper-iron sulphide deposit on the northwest rim of the Basin, both field evidence and sulphide-silicate relationships indicate that the ore-body was emplaced by a combination of both gravitational differentiation of sulphides contained in the dark norite and injection of a sulphide magma into favourable structural sites (Cowan, 1968).

Laboratory seismic velocity measurements of drill core samples, that are representative of the major rock units in the North Range environment of the Sudbury Basin, were used to determine the seismic velocity distribution of the area (chapter 3). Based on the most accepted geological models, the velocity data will be utilized to construct a seismic model of the Basin in the subsequent chapters.

# Chapter 3

## LABORATORY SEISMIC WAVE VELOCITY MEASUREMENT

The behavior of seismic waves traveling in rocks has been the subject of extensive theoretical and experimental investigations since the beginning of the present century. Measuring the velocity of seismic waves in samples subjected to simulated overburden and pore pressures as well as temperature, has been aimed at understanding the major factors regarding the seismic velocity of rocks. Such studies have revealed that the seismic velocities in rocks are functions of porosity, chemical and mineral composition, overburden and fluid pore pressures, temperature, nature and amount of pore fluids, and pressure and thermal history. Of these, porosity, chemical and mineral composition, and pressures are generally considered to be the primary variables in affecting velocities.

Due to the intimate relationship between sedimentary rocks and hydrocarbon deposits, much attention has been given to the measurement of seismic velocities in sedimentary rocks (Hughes and Cross, 1951; Hughes and Kelly, 1952; Wyllie et al., 1958; King, 1966; Morgan, 1969). Recently, however, special emphasis has been given to the velocity of seismic waves in crystalline rocks. The most outstanding contribution made was Birch's compressional wave velocity measurements made up to 1000 MPa of pressure (Birch, 1960; 1961). This, combined with more recent work by Nur and Simons (1969), Spencer et al., (1976), Meissner and Fakhimi (1976), Christensen (1979), and Matsushima, (1981) provides some basic data for seismic modelling and quantitative interpretation of field seismic data.

The velocity measurement presented in this thesis differs from the measurements reported so far in three ways : 1) The rock samples used are all crystalline rocks, 2) The samples were all derived from rock units that are intimately associated with well known sulphide ore-bodies of the Canadian Shield, and 3) Unlike previous crystalline rock velocity measurements, aimed at investigating the crust and upper mantle, this study is primarily designed to examine the possibilities of observing reflections from discontinuities at depths of interest for drilling and production stages of a mine.

Laboratory study of elastic wave propagation for determining the elastic moduli of materials fall into two categories, depending upon whether wave pulses or continuous sinusoidal waves are used to obtain the necessary information (Kaarsberg, 1975). In the continuous method, one measures the velocity of some point on a sinusoidal wave using the relation $V=lf$ ( where V=velocity, l=wavelength, f=frequency ). In the pulse method, on the other hand, one measures the travel time of a pulse as it passes through a known distance of the medium, from which the velocity can be determined. This is the most popular and reliable laboratory method (Birch, 1960), and this is the method employed in the present study.

## 3.1 Apparatus and procedure

The essential elements of the apparatus used to measure P-wave (compressional wave) and S-wave (shear wave) velocities are depicted in Figure 3.1. In the center of the diagram, there is a laboratory press device (Carver Press) with a sample assembled in it. This particular

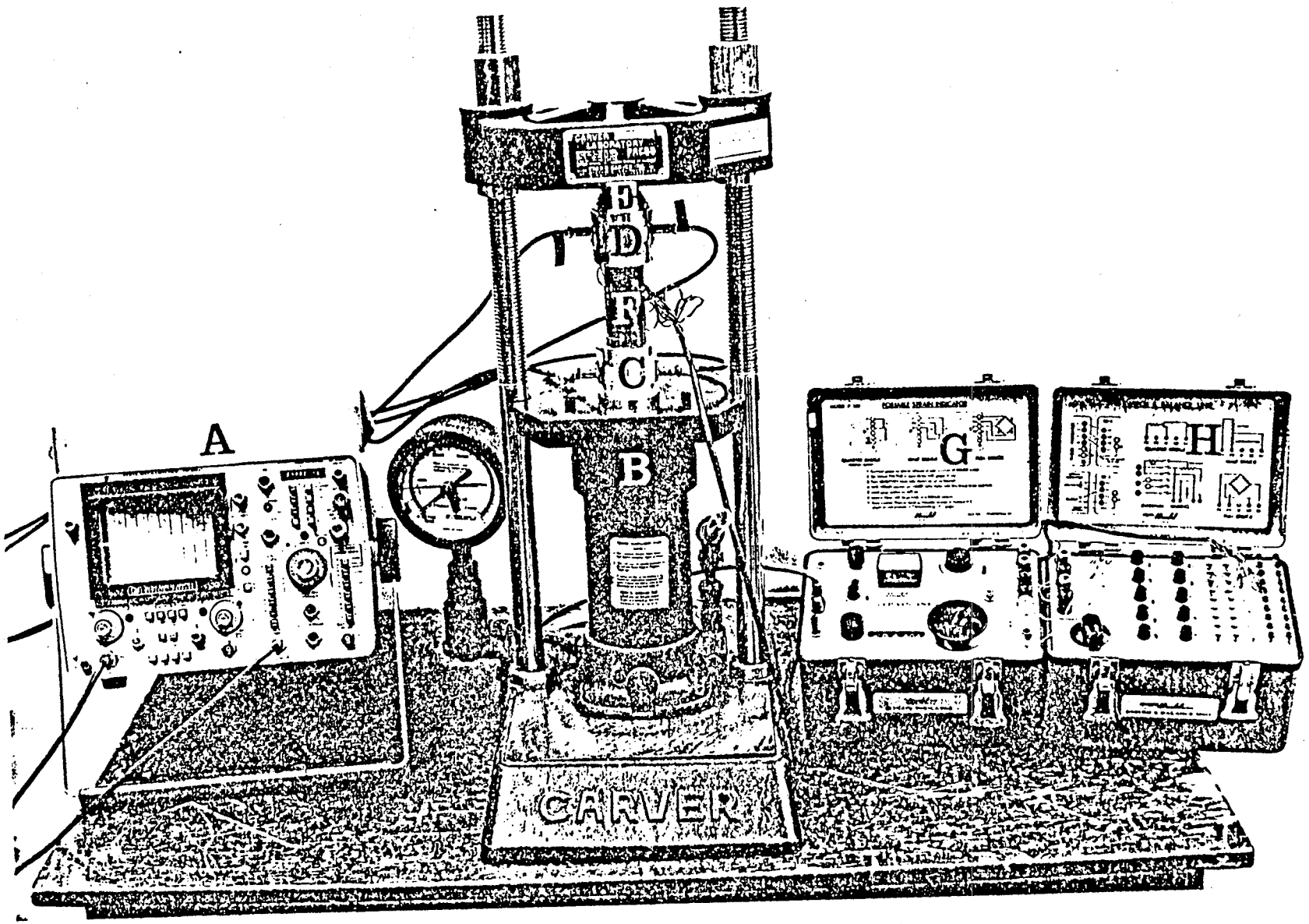


Figure 3.1. Assembly of the apparatus during experiment (after B.I. Pandit, 1982, personnal communication). Explanation of letters given given in the next page.

Assembly of the apparatus during experiment.

A = Oscilloscope with a P-wave signal displayed on its screen.

B = Laboratory press device with a sample assembled in it.

C = Transmitting transducer.

D = Receiving transducer.

E = Spherical seat.

F = The sample.

G = Strain indicator.

H = Switch and balance unit.

press device is mainly utilized when the velocity measurements are to be made as a function of axial stress. Located to the right of the press device are the strain indicator unit(G) and the switch and balance unit(H). Located to the left of the press device is an oscilloscope, on which the received signal (P-wave or S-wave) will be displayed. Both the transmitting and the receiving transducers are mounted in aluminum holders. To measure the seismic velocities as a function of axial stress, the holder-specimen assembly is placed between the platens of a Carver press. Then, P-wave and S-wave velocities are determined from measurements of time taken by an elastic pulse of either type to traverse the rock specimen. A pulsed oscillator with a frequency of 820 kHz is used to apply a repetitive (decaying sinusoidal) voltage pulse to the transmitter. The transmitter produces a pulse of mechanical energy that travels through the specimen. The receiving transducer detects the mechanical energy and converts it to an electrical signal which is displayed on the oscilloscope screen after suitable amplification.

The time taken by an elastic pulse to traverse the rock specimen and the transducer holders is read off the oscilloscope. The time taken by the pulse to traverse the rock specimen itself is calculated by subtracting the time taken by the pulse to travel the transducer holders in face-to-face contact.

It is important to note that an appropriate switching arrangement ensures that the two wave (P-wave and S-wave) velocity measurement can be carried out sequentially without any other change in the experimental set-up. Also, to provide a better contact and coupling at each end

of the transducer holders, a lead foil disc 0.04 mm thick is placed between the ends of the specimen and the transducer holders. On top of the upper transducer holder, a spherical seat was placed to correct any slight deviation from the parallelism at the top and bottom of the holder(s)-specimen assembly.

3.2 Sample description and preparation :

The rock samples for this thesis were obtained from the North Range environment of the Sudbury mining district of Ontario. A total of thirty one samples, representing eleven rock units of the Sudbury Basin, were selected from drill cores ranging in footage from 15 m to 2,100 m. Eight of these samples correspond to the major concordant rock units, namely, Onaping, micropegmatite, oxide-rich quartz gabbro, felsic norite, mafic norite sub-layer norite, granite breccia, and mafic and granite gneisses. The remaining three samples are for olivine diabase, steeply dipping dykes that often cut all the above units, with thickness varying from a few centimeters to 90 m, Sudbury breccia (a member of the footwall rocks), and massive sulphides.

The rock specimens were prepared in the form of cylinders of length 3.5 cm to 6.2 cm and diameter 2.5 cm to 5.4 cm. The flat faces are ground parallel such that the maximum difference in length across any diameter is less than 0.01 mm.

In order to take measurements on a dry specimen after the above preparation, the specimen is heated to about 105° C under vacuum (approximately 270 Pa) for approximately 24 hours (B.I.Pandit, personnal

communication). All the velocity measurements used in this thesis were done on dry specimens. If the measurements are to be carried out on water-saturated specimens, however, then after drying as above, the specimen is immersed in water and subjected to a vacuum. In this case, the specimen is covered with a rubber sleeve to prevent loss of moisture while the measurements are being made.

## 3.3 Results and discussion :

The dry P-wave and S-wave wave velocities shown in Table 1 were measured following the procedure described above. An average of three to four measurements were made for each of the major rock units and one measurement for each of massive sulphide, Sudbury breccia, and olivine diabase. Both dry and wet densities, porosity, and the length and diameter of each specimen were determined.

The measurements were taken by varying the axial stress from about 2 MPa to nearly 50 MPa, which corresponds to about 2 km of depth. Due to the inherent low porosity associated with all the rock units, no additional effort was made to investigate the seismic velocities under saturated conditions. It is also assumed that the change in density which results from the applied pressure is relatively small, hence only one density measurement was made.

Figures 3.2 through 3.4 show the dry P-wave velocities as a function of axial stress for the major rock units of the Sudbury Basin. The rocks in Figure 3.2 are the top three rock units below the Onwatin slate, followed by the middle three (Figure 3.3) and the lower most

Table 1. Laboratory measured physical properties of Sudbury rocks
(P-wave velocity, S-wave velocity, density, and porosity )

| BORE HOLE No | FOOTAGE (m) | ROCK TYPE | MODE | STRESS (MPa) 3.5 | 5.0 | 9.3 | 18.0 | 30.7 | 44.2 | LENGTH (mm) | DIAMETER (mm) | DENSITY ($kg/m^3$) (DRY) | DENSITY ($kg/m^3$) (WET) | POROSITY (PERCENT) |
|---|---|---|---|---|---|---|---|---|---|---|---|---|---|---|
| 52847 | 16 | ONAPING | Vp | 6.133 | 6.268 | 6.314 | 6.361 | 6.361 | 6.361 | 42.75 | 36.17 | 2745.9 | 2747.1 | 0.08 |
| | | | Vs | 3.669 | 3.669 | 3.638 | 3.638 | 3.654 | 3.669 | | | | | |
| 52847 | 277 | " | Vp | 6.181 | 6.219 | 6.219 | 6.257 | 6.257 | 6.296 | 50.50 | 36.20 | 2723.4 | 2724.0 | 0.06 |
| | | | Vs | 3.620 | 3.633 | 3.633 | 3.646 | 3.659 | 3.686 | | | | | |
| 52848 | 168 | MICROPEGMATITE | Vp | 6.041 | 6.083 | 6.212 | 6.168 | 6.301 | 6.346 | 43.92 | 36.20 | 2704.1 | 2707.4 | 0.33 |
| | | | Vs | 3.444 | 3.513 | 3.513 | 3.542 | 3.570 | 3.600 | | | | | |
| 52848 | 261 | " | Vp | 5.870 | 5.944 | 5.870 | 6.058 | 6.058 | 6.136 | 47.37 | 36.17 | 2681.4 | 2684.1 | 0.31 |
| | | | Vs | 3.384 | 3.420 | 3.420 | 3.433 | 3.445 | 3.458 | | | | | |
| 52848 | 506 | " | Vp | 5.837 | 5.992 | 6.073 | 6.073 | 6.156 | 6.241 | 45.06 | 36.07 | 2664.9 | 2670.4 | 0.54 |
| | | | Vs | 3.440 | 3.453 | 3.466 | 3.507 | 3.548 | 3.576 | | | | | |
| 52848 | 640 | " | Vp | 5.821 | 5.995 | 6.040 | 6.132 | 6.179 | 6.226 | 40.28 | 36.17 | 2695.7 | 2700.3 | 0.46 |
| | | | Vs | 3.414 | 3.414 | 3.428 | 3.458 | 3.488 | 3.503 | | | | | |
| 52848 | 775 | " | Vp | 5.971 | 5.971 | 6.156 | 6.252 | 6.252 | 6.302 | 39.83 | 36.17 | 2710.3 | 2713.0 | 0.27 |
| | | | Vs | 3.390 | 3.463 | 3.509 | 3.556 | 3.588 | 3.588 | | | | | |
| 58649 | 145 | " | Vp | 5.892 | 5.971 | 6.052 | 6.178 | 6.221 | 6.264 | 44.60 | 36.32 | 2709.0 | 2711.6 | 0.26 |
| | | | Vs | 3.498 | 3.498 | 3.485 | 3.512 | 3.540 | 3.568 | | | | | |

Table 1 ( Continued ).

| | | | | | | | | | | | | | |
|---|---|---|---|---|---|---|---|---|---|---|---|---|---|
| 60018 | 85 | OXIDE-RICH QUARTZ GABBRO | Vp | 6.340 | 6.444 | 6.552 | 6.664 | 6.721 | 6.721 | 39.12 | 36.17 | 2914.1 | 2915.1 | 0.10 |
| | | | Vs | 3.816 | 3.816 | 3.835 | 3.854 | 3.892 | 3.912 | | | | | |
| 60018 | 371 | " | Vp | 6.355 | 6.485 | 6.530 | 6.485 | 6.621 | 6.668 | 47.47 | 36.25 | 2918.3 | 2920.0 | 0.16 |
| | | | Vs | 3.638 | 3.638 | 3.652 | 3.753 | 3.798 | 3.813 | | | | | |
| 60072 | 679 | " | Vp | 6.310 | 6.325 | 6.350 | 6.410 | 6.525 | 6.510 | 34.82 | 46.84 | 2834.8 | 2836.7 | 0.18 |
| | | | Vs | 3.646 | 3.666 | 3.685 | 3.724 | 3.765 | 3.806 | | | | | |
| 52847 | 1164 | FELSIC NORITE | Vp | 5.555 | 5.626 | 5.662 | 5.699 | 5.811 | 6.010 | 43.99 | 36.07 | 2752.3 | 2757.4 | 0.51 |
| | | | Vs | 3.333 | 3.345 | 3.358 | 3.384 | 3.519 | 3.562 | | | | | |
| 60048 | 975 | " | Vp | 5.954 | 6.074 | 6.074 | 6.115 | 6.207 | 6.259 | 45.31 | 36.30 | 2834.1 | 2837.0 | 0.30 |
| | | | Vs | 3.397 | 3.407 | 3.425 | 3.464 | 3.491 | 3.499 | | | | | |
| 60072 | 1170 | " | Vp | 6.075 | 6.150 | 6.275 | 6.310 | 6.352 | 6.412 | 45.72 | 26.92 | 2789.5 | 2792.2 | 0.27 |
| | | | Vs | 3.313 | 3.349 | 3.374 | 3.399 | 3.425 | 3.451 | | | | | |
| 60005 | 1588 | MAFIC NORITE-SUB-LAYER NORITE | Vp | 6.070 | 6.080 | 6.152 | 6.300 | 6.350 | 6.480 | 38.23 | 54.33 | 2847.7 | 2852.4 | 0.47 |
| | | | Vs | 3.428 | 3.444 | 3.459 | 3.491 | 3.523 | 3.540 | | | | | |
| 40048 | 1576 | " | Vp | 5.912 | 5.898 | 5.988 | 6.117 | 6.102 | 6.168 | 51.26 | 36.25 | 2938.8 | 2940.3 | 0.15 |
| | | | Vs | 3.305 | 3.315 | 3.337 | 3.350 | 3.383 | 3.404 | | | | | |
| 60072 | 1383 | " | Vp | 6.250 | 6.275 | 6.277 | 6.350 | 6.401 | 6.450 | 50.11 | 47.22 | 2941.3 | 2943.2 | 0.18 |
| | | | Vs | 3.330 | 3.375 | 3.409 | 3.432 | 3.444 | 3.444 | | | | | |
| 60048 | 2097 | GRANITE BRECCIA | Vp | 5.647 | 5.684 | 5.722 | 5.960 | 6.001 | 6.043 | 43.03 | 36.37 | 2780.9 | 2785.2 | 0.42 |
| | | | Vs | 3.187 | 3.199 | 3.235 | 3.285 | 3.310 | 3.335 | | | | | |
| 52847 | 1520 | " | Vp | 5.879 | 5.951 | 6.062 | 6.100 | 6.100 | 6.133 | 48.62 | 36.20 | 2708.0 | 2712.8 | 0.48 |
| | | | Vs | 3.330 | 3.341 | 3.376 | 3.412 | 3.448 | 3.473 | | | | | |

Table 1 ( Continued ).

| | | | | | | | | | | | | | |
|---|---|---|---|---|---|---|---|---|---|---|---|---|---|
| 52847 | 1620 | " | Vp | 6.031 | 6.070 | 6.191 | 6.233 | 6.275 | 6.317 | 46.56 | 36.12 | 2741.7 | 2744.2 | 0.25 |
| | | | Vs | 3.514 | 3.514 | 3.527 | 3.554 | 3.568 | 3.581 | | | | | |
| 60019 | 1537 | " | Vp | 5.760 | 5.850 | 5.925 | 6.020 | 6.065 | 6.140 | 35.36 | 24.97 | 2919.9 | 2923.4 | 0.35 |
| | | | Vs | 3.253 | 3.289 | 3.305 | 3.352 | 3.368 | 3.384 | | | | | |
| 60001-L | 1206 | MASSIVE SULPHIDE | Vp | 4.914 | 4.979 | 5.046 | 5.069 | 5.185 | 5.209 | 56.36 | 36.20 | 4153.4 | 4160.8 | 0.74 |
| | | | Vs | 2.763 | 2.776 | 2.790 | 2.818 | 2.825 | 2.854 | | | | | |
| 52835 | 1362 | MAFIC GNEISS | Vp | 6.064 | 6.103 | 6.183 | 6.223 | 6.264 | 6.348 | 47.42 | 35.84 | 2869.6 | 2870.4 | 0.08 |
| | | | Vs | 3.412 | 3.412 | 3.399 | 3.424 | 3.461 | 3.474 | | | | | |
| 52847 | 1681 | " | Vp | 5.950 | 6.031 | 6.157 | 6.287 | 6.423 | 6.423 | 44.45 | 36.17 | 2774.6 | 2778.3 | 0.37 |
| | | | Vs | 3.342 | 3.367 | 3.380 | 3.393 | 3.432 | 3.459 | | | | | |
| 60048 | 2246 | " | Vp | 5.742 | 5.742 | 5.865 | 6.037 | 6.127 | 6.127 | 41.17 | 36.17 | 2749.3 | 2750.7 | 0.14 |
| | | | Vs | 3.445 | 3.460 | 3.489 | 3.519 | 3.549 | 3.565 | | | | | |
| 60072 | 1658 | " | Vp | 6.690 | 6.725 | 6.740 | 6.780 | 6.820 | 6.850 | 55.73 | 46.96 | 2888.0 | 2889.5 | 0.16 |
| | | | Vs | 3.678 | 3.691 | 3.715 | 3.728 | 3.740 | 3.753 | | | | | |
| 60005 | 2050 | GRANITE GNEISS | Vp | 5.568 | 5.568 | 5.673 | 5.783 | 5.858 | 5.936 | 44.93 | 36.14 | 2692.0 | 2698.1 | 0.61 |
| | | | Vs | 2.946 | 2.976 | 3.026 | 3.078 | 3.131 | 3.175 | | | | | |
| 60072 | 1730 | " | Vp | 5.835 | 5.875 | 5.981 | 6.066 | 6.125 | 6.141 | 62.38 | 47.42 | 2676.3 | 2678.3 | 0.20 |
| | | | Vs | 3.400 | 3.428 | 3.447 | 3.475 | 3.495 | 3.524 | | | | | |
| 60005 | 2135 | SUDBURY BRECCIA | Vp | 5.845 | 5.924 | 5.965 | 6.047 | 6.090 | 6.176 | 43.66 | 36.07 | 2831.8 | 2832.9 | 0.11 |
| | | | Vs | 3.479 | 3.493 | 3.521 | 3.521 | 3.550 | 3.564 | | | | | |
| 60072 | 1351 | OLIVINE DIABASE | Vp | 6.335 | 6.375 | 6.463 | 6.610 | 6.675 | 6.700 | 50.77 | 47.19 | 2989.2 | 2992.0 | 0.28 |
| | | | Vs | 3.466 | 3.466 | 3.490 | 3.502 | 3.526 | 3.551 | | | | | |

three units (Figure 3.4). The oxide-rich quartz gabbro has been repeated for illustration purposes.

The observed average porosity varies from 0.07% for the Onaping formation to 0.40% for granite gneiss. These values are all within the range of porosities expected from typical holocrystalline rocks (Birch, 1961). The mafic norite sub-layer has the highest average density of 2909.3 kg/m$^3$, and the rock with the highest porosity, granite gneiss, has the lowest density of 2684.1 kg/m$^3$ .

It can be seen that the observed P-wave velocities for the different rock types generally show a similar response to the applied pressure. There is a rapid increase in velocity up to about 10 MPa of pressure and then it levels off to an asymptotic behavior as the pressure is gradually raised to 44.2 MPa. In granites as well as in all crystalline rocks, the shape of pores plays a very important role. For a given concentration of pores, it appears that flatter (thinner) pores have a relatively greater effect on velocities than spherical pores (Toksoz et al., 1976). It is also well understood (Nur and Simons, 1969; Toksoz et al., 1976), that most low aspect ratio pores in granites close at about 50 MPa of applied pressure. Thus the rapid increase in velocity in the low pressure region is the result of the closing of very fine cracks in the rock samples. Beyond 20 MPa, the effect of pressure on velocity becomes less pronounced.

For the pressure values considered in this experiment, the effect of crack porosity cannot be completely eliminated. It appears to exist, even though it becomes very insignificant, up to about 200 MPa of pressure. Beyond this point, all cracks are closed and the observed veloc-

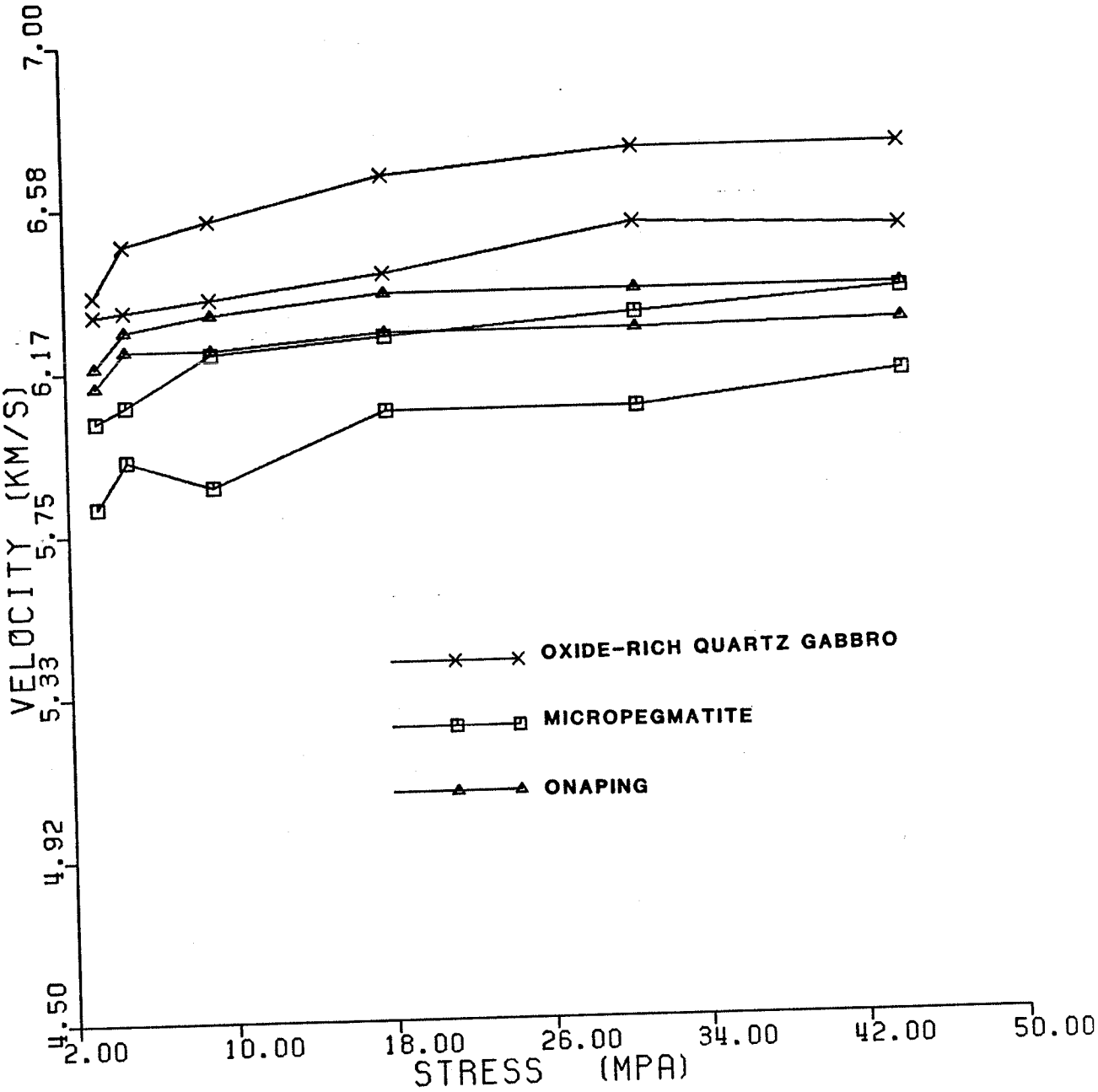


Figure 3.2. Dry P-wave velocity measurements as a function of uniaxial stress (for a given stress value, the maximum and minimum measured velocity are plotted. Hence all other measurements will lie between these two points, and the whole measurement for a particular rock unit will form an envelope outlined by the maximum and minimum values).

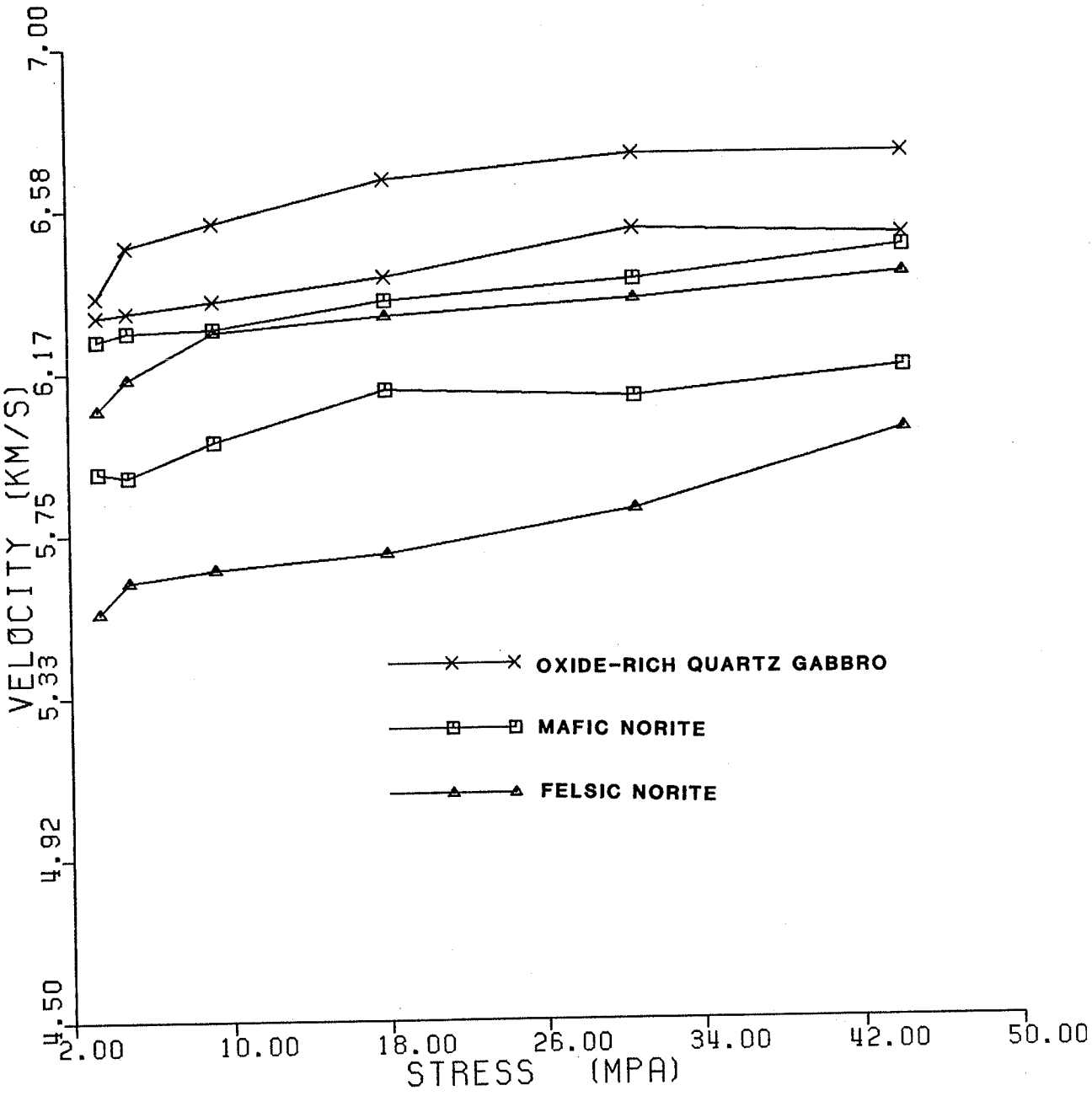


Figure 3.3. Dry P-wave velocity measurements as a function of uniaxial stress. The oxide-rich quartz gabbro has been repeated for explanation purposes (plotting scheme as in Figure 3.2).

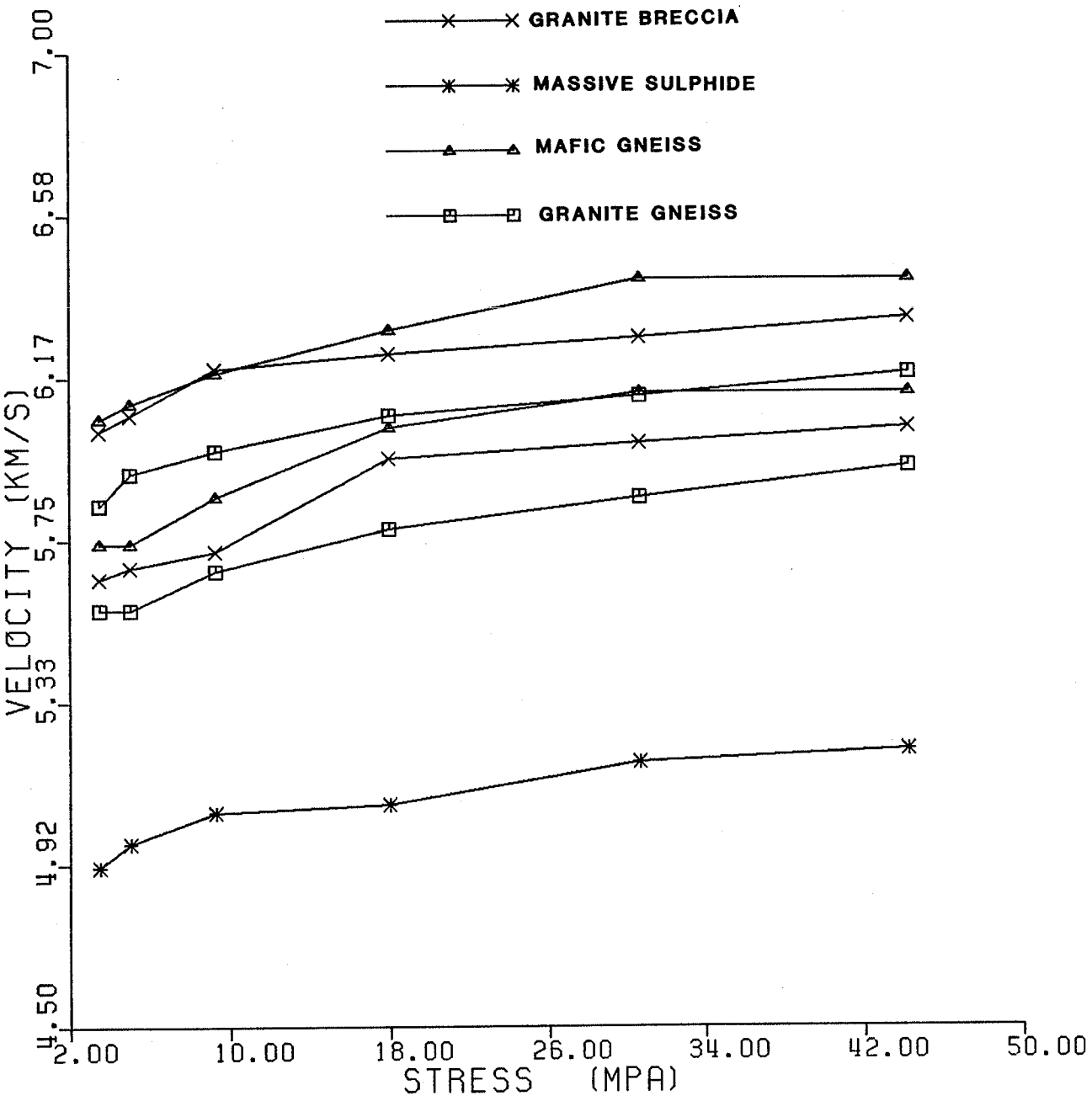


Figure 3.4. Dry P-wave velocity as a function of uniaxial stress (plotting scheme as in Figure 3.2).

ity will be the intrinsic velocity of the rock, which is a function of chemical composition and density (Simons, 1964; Young, 1979).

To establish whether there is any form of dependence between P-wave velocities and chemical composition, the measured velocities of the major rock units were broadly divided into two groups. The first group, composed of oxide-rich quartz gabbro, mafic norite, and mafic gneiss, contains the well defined mafic rocks in the Basin (Figure 3.5). The second group on the other hand contains the felsic rocks, i.e., micropegmatite, granite breccia, granite gneiss and felsic norite, (Figure 3.6). In the first group, the oxide rich quartz gabbro has a distinctly high velocity signature. The lowest value in this rock is higher than the highest value in the remaining two mafic rocks. There is a high degree of overlap in the velocities of the mafic norite and mafic gneiss. There is also a considerable degree of overlap in the measured velocities of the second group of rocks. It is significant to note that, the velocities associated with the felsic norite are closer to the velocities of the felsic rocks than to the mafic rocks. Hence, it is categorized in the felsic group of rocks. It is evident that the first (mafic) group as a whole has a significantly higher velocity than the second (felsic) group.

Despite the fact that the samples for each rock type were obtained from different bore holes and at different depths, measured velocities for each rock type are quite consistent. The standard deviation in the velocities measured at 44.2 MPa ranges from 0.046 km/s (0.70% of the mean) for Onaping to 0.203 km/s (3.3% of the mean) for felsic norite. On an average, there will be a 2.0% deviation from the mean value of

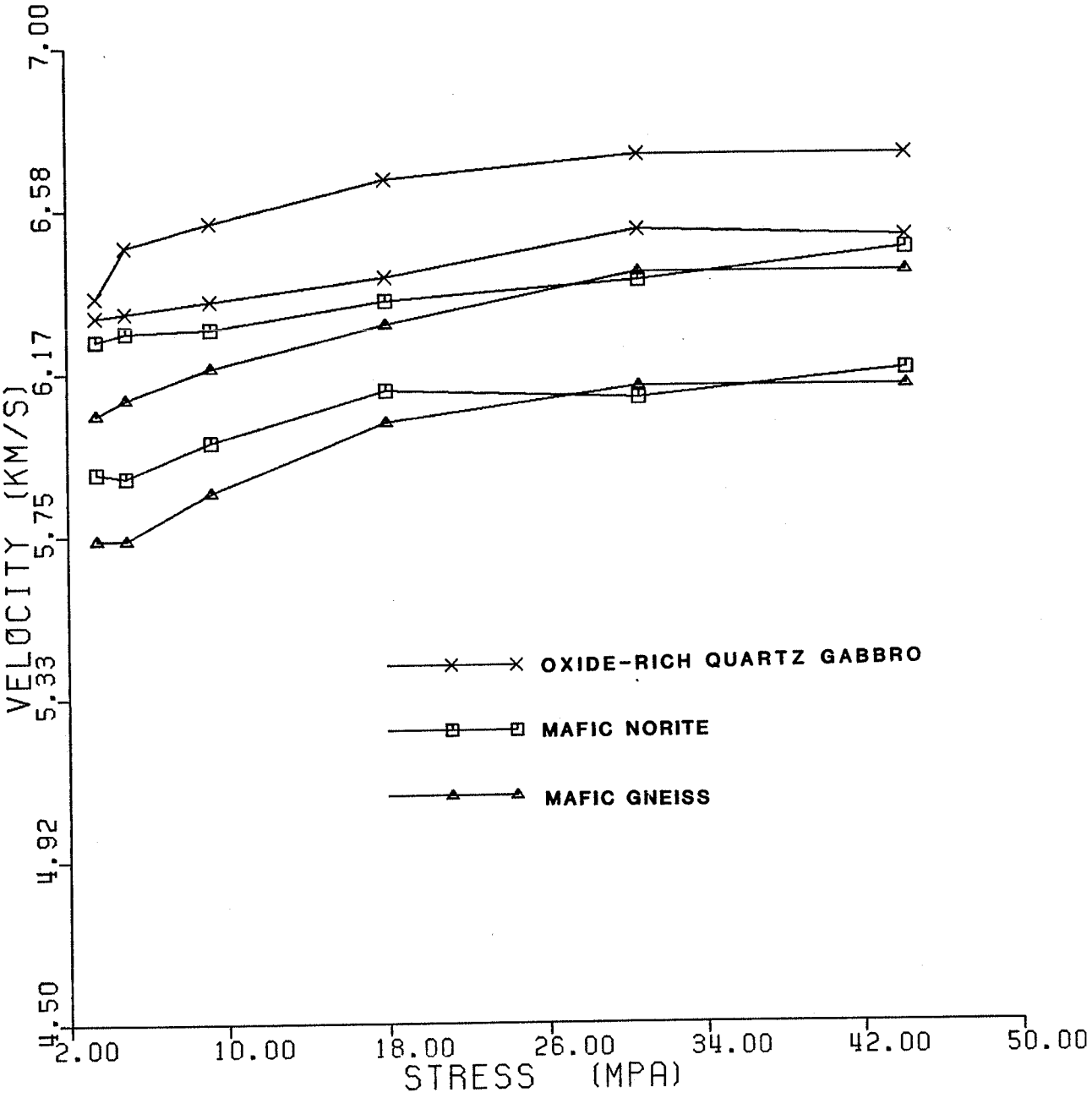


Figure 3.5. Dry P-wave velocity of mafic rocks (plotting scheme as in Figure 3.2).

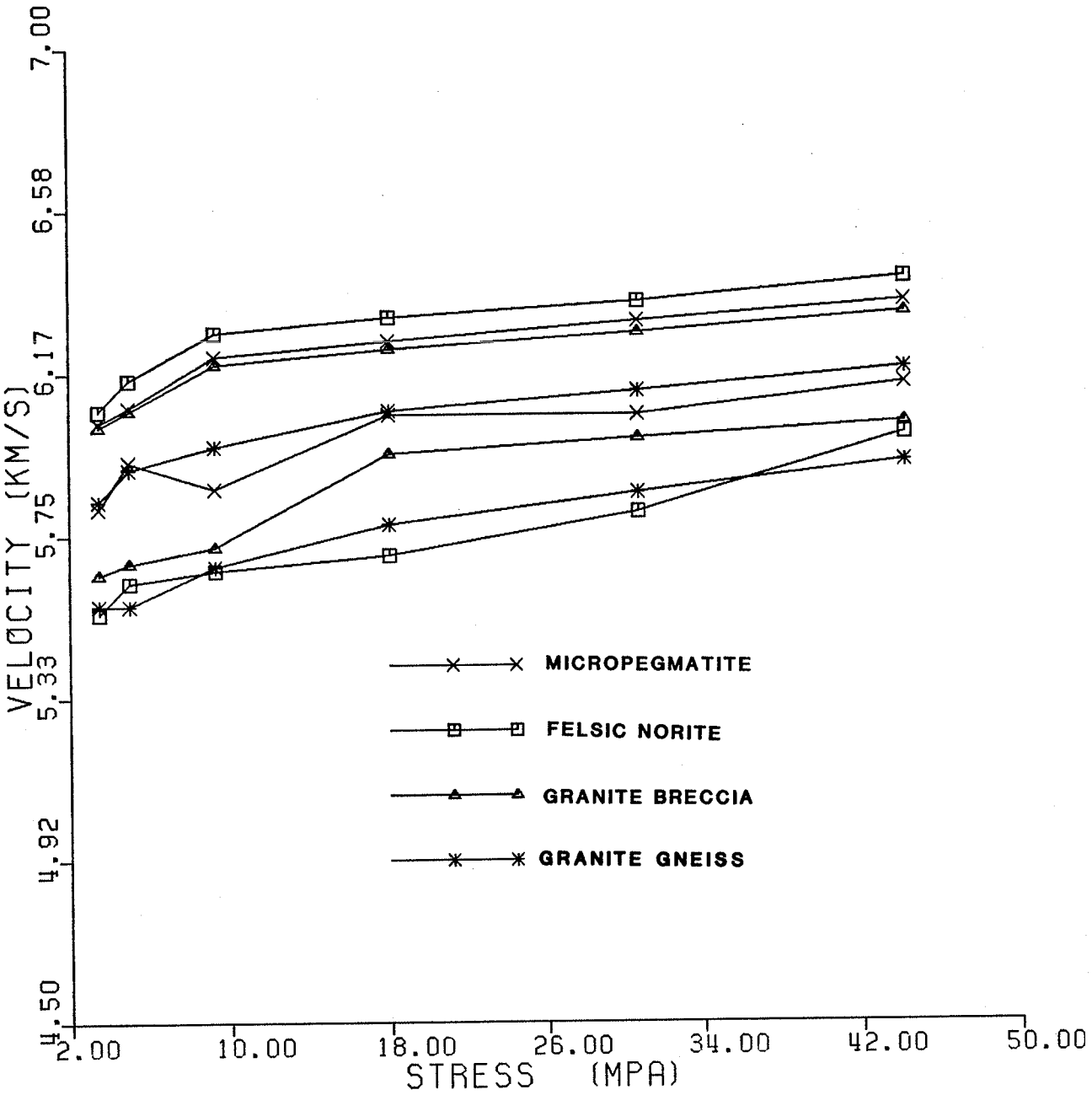


Figure 3.6. Dry P-wave velocity of felsic rocks (plotting scheme as in Figure 3.2).

the measured velocity of the particular rock; which is reasonably acceptable considering the 1.0% error introduced by the measuring equipment alone.

It is a common practice in laboratory measurements of seismic velocity to estimate how much one can predict P-wave velocity from the density of the material. Accordingly, a straight line of the form $V=a+b\rho$ (where V=velocity, $\rho$=density, and a and b are constants) has been fitted by the method of least squares to all observations at 44.2 MPa (except the data point for massive sulphides). The equation of the best fit line was determined to be $V = 2.5666 + 0.0013421\rho$, as shown in Figure 3.7. For the 29 data points, a standard deviation of 0.220 km/s with a correlation coefficient(r) of 0.58 was obtained. This gives $r^2$ (coefficient of determination) = 0.3377, indicating that 33.77 percent of the variation of velocity may be accounted for by correlation with density. This, obviously, is not a good correlation and shows that density alone has a minor role in determining P-wave velocity at a pressure of 44.2 MPa. The situation is quite different at high pressures (greater depths, eg. 1000 MPa), where a correlation of up to 0.94 can be obtained (Birch, 1961). The best correlation at high pressures is due to the absence of the effect of porosity (specially for crystalline rocks). On the other hand the poor correlation in the present experiment shows the importance of the effect of porosity at pressures of the order of 44 MPa.

Another contributing factor for the poor correlation could be the change of dimensions under pressure. Velocity will be affected by a change in the length of the sample, and density by a change in the

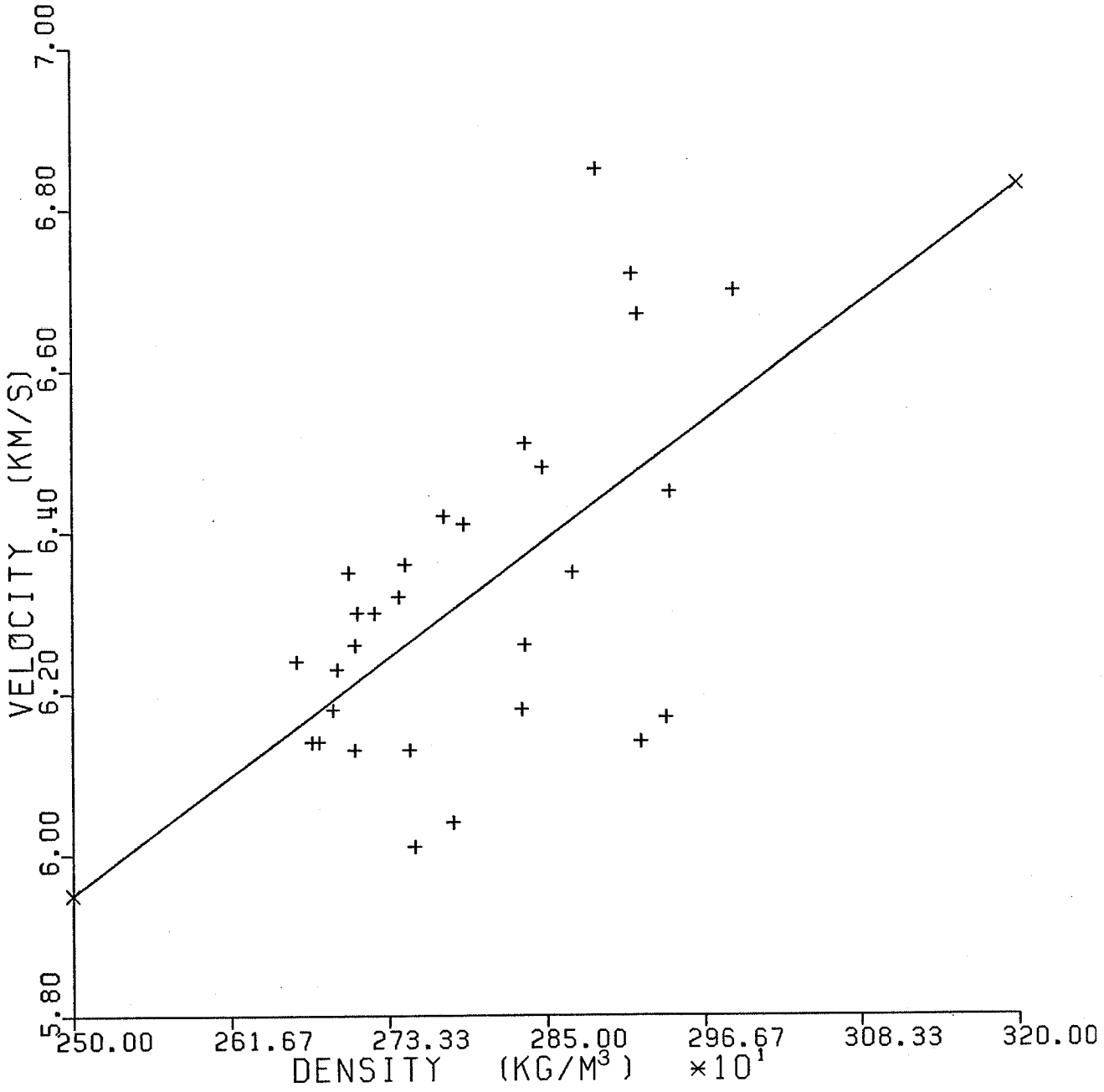


Figure 3.7. Least squares best fit straight line for the P-wave velocity measurement at 44.2 MPa (the velocity of massive sulphide was not included).

volume of the sample. These changes are generally small, however, less than 1% for velocity and 3% for density at 1000 MPa (Birch, 1961). Hence the effect at 44.2 MPa was considered relatively negligible and no correction was applied for the measured data.

The above result demonstrates that the linear law is not appropriate for predicting velocity from density (or vice versa) for the pressure range considered in the present experiment. Consequently, another empirical law of the form $\rho=0.31V^{0.25}$ (Anstey, 1977) was tested for the observed data. The error in estimating the density from the velocity using this expression is about 2.5%, well within experimental error. Hence, this empirical law was taken as the appropriate expression for the velocity-density relationship in this study.

In the S-wave measurements (Figure 3.8 - 3.10), the observed values reflect more or less the same relative importance of porosity, density, and chemical composition as the P-wave velocities. It is to be noted, however, that the S-wave velocities are less sensitive to applied pressure, especially in the low pressure regions. Almost all rock units appear to have an S-wave velocity that is linearly correlated with applied pressure.

In summary, it appears that at depths of less than 2 km ( 50 MPa of pressure) the most important factors in determining the dry P-wave velocity are likely to be low crack aspect ratio pores and chemical composition. Beyond 10 MPa of pressure, however, the measured velocity is less sensitive to the applied pressure, which implies a significant decline in the effect of porosity and a correspondingly high effect of chemical composition in this region.

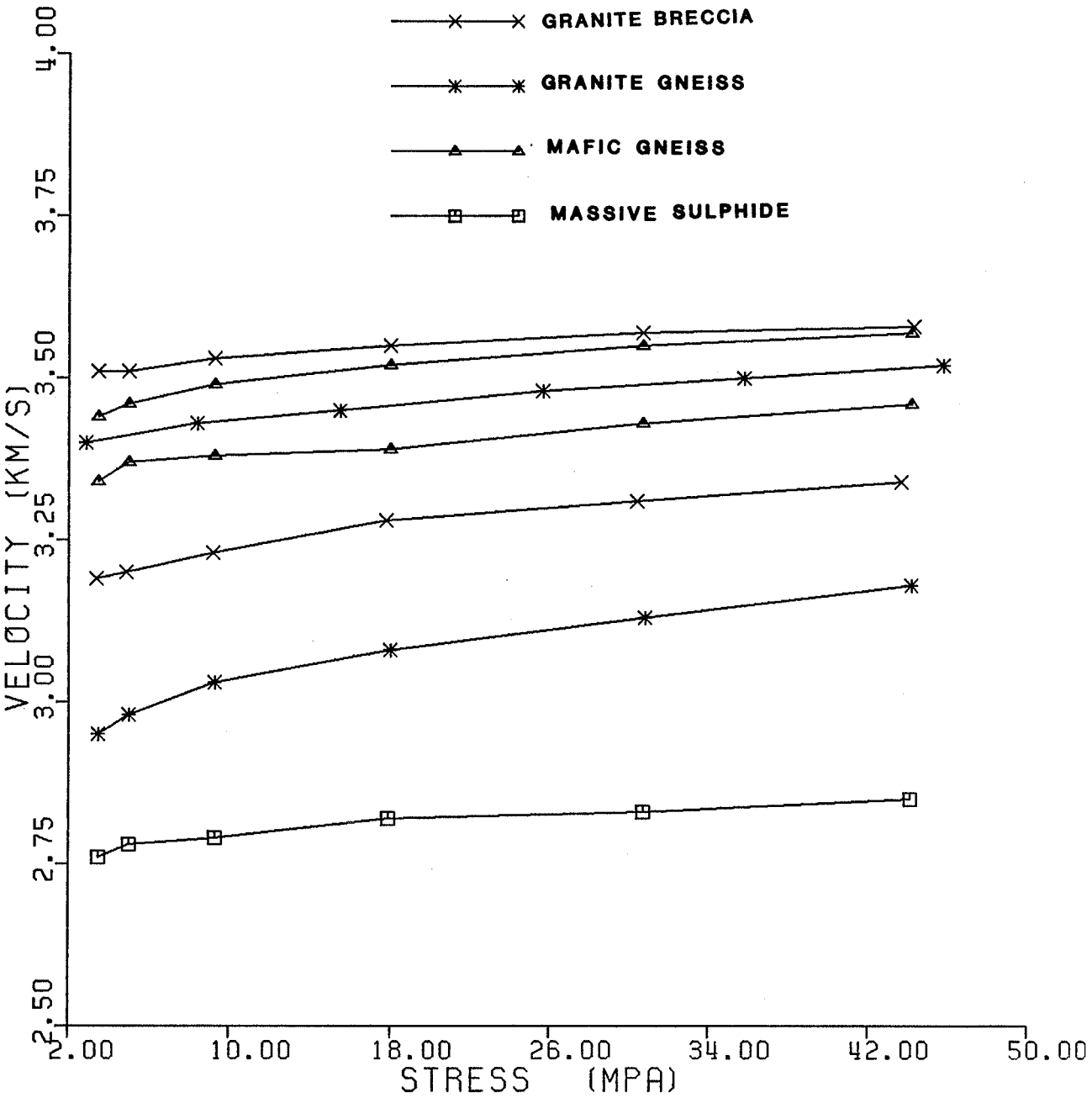


Figure 3.8. Dry S-wave velocity measurements (plotting scheme as in Figure 3.2).

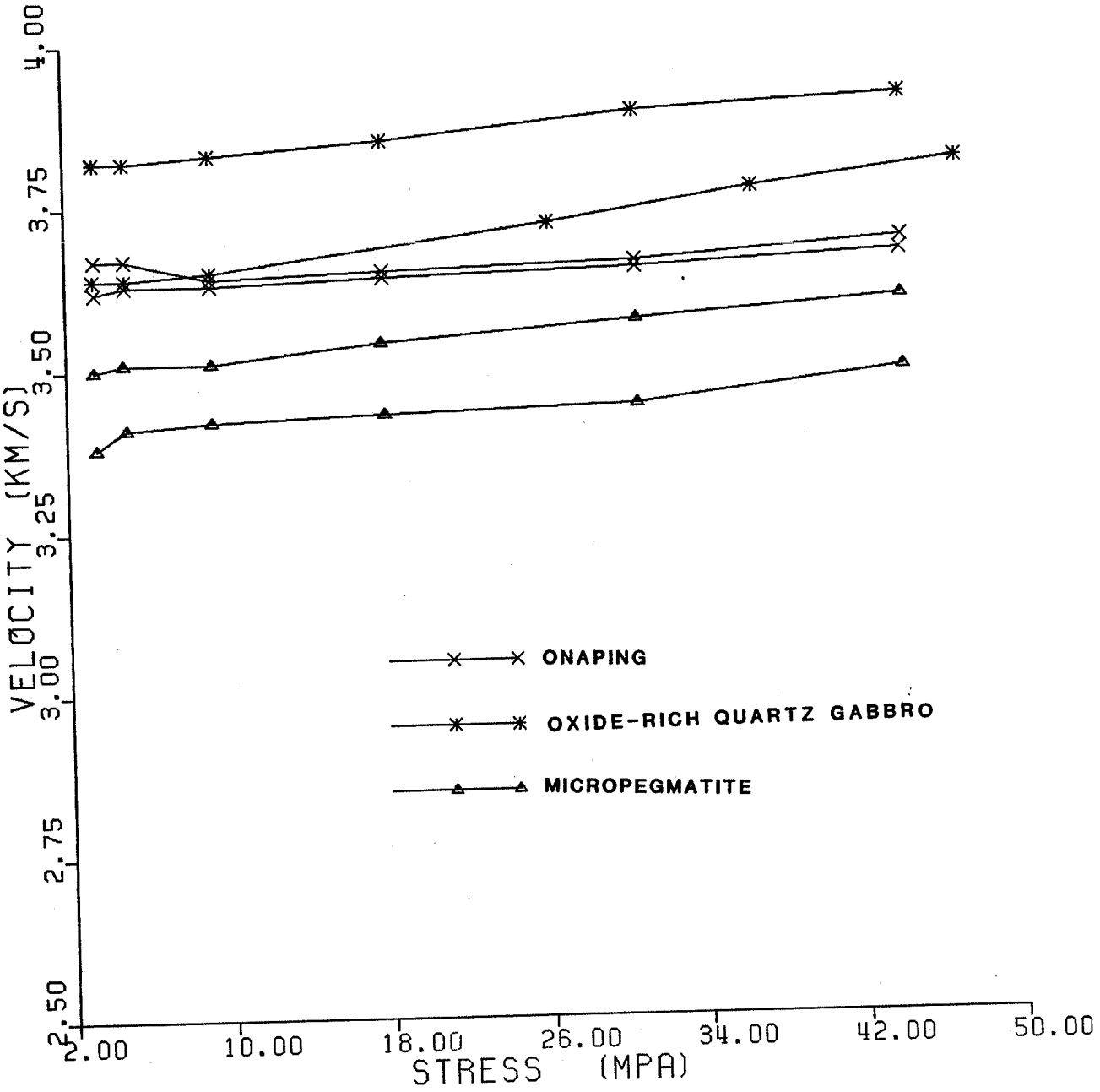


Figure 3.9. Dry S-wave velocity measurements (plotting scheme as in Figure 3.2). The oxide-rich quartz gabbro was repeated for explanation purposes.

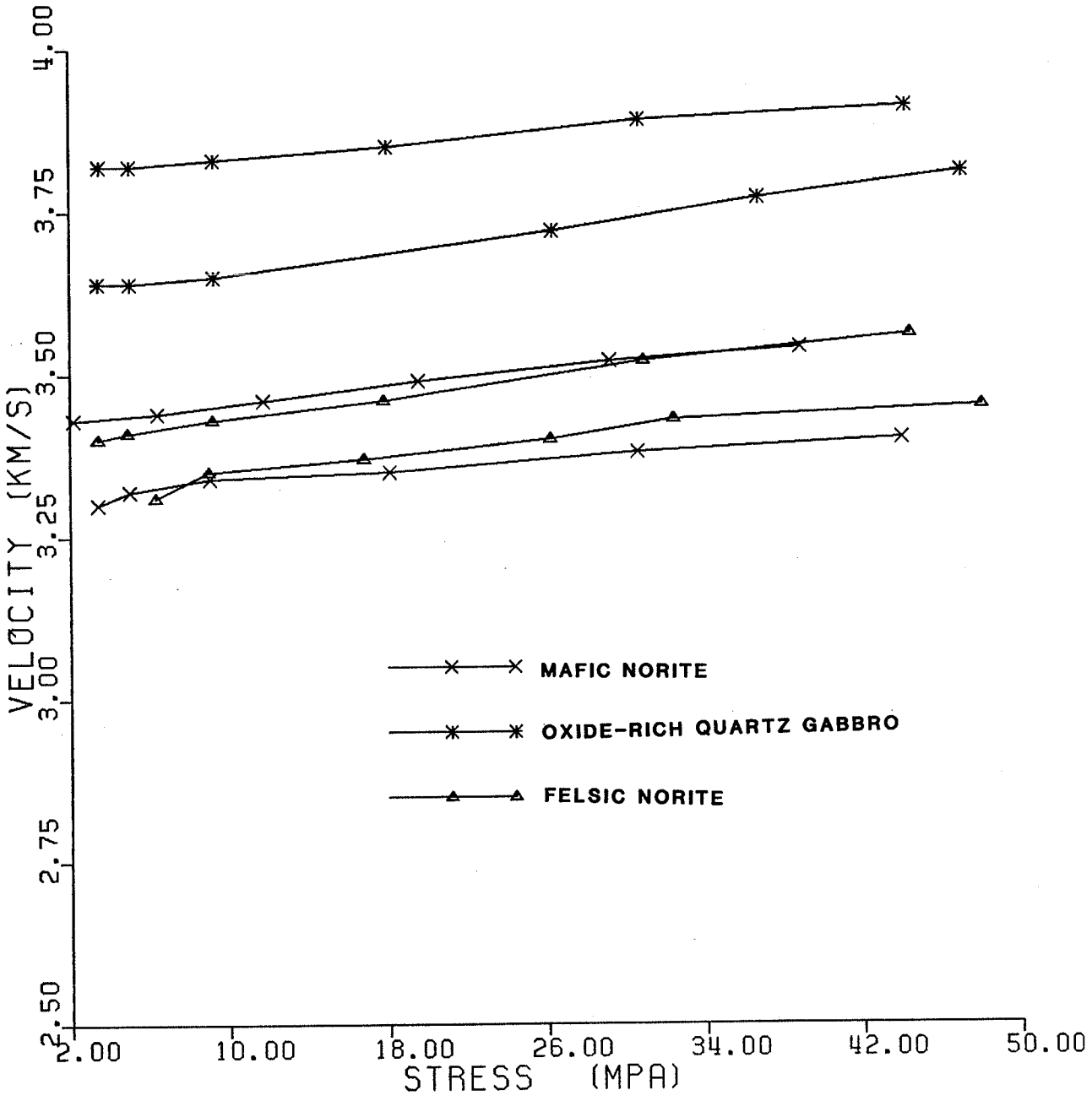


Figure 3.10. Dry S-wave velocity measurements (plotting scheme as in Figure 3.2).

The velocity measurement was not initially designed to provide an adequate explanation of some of the most important geophysical questions, such as the effect of anisotropy on seismic velocity. A velocity difference of up to 44 % at 0.1 MPa and 7.6 % at 1000 MPa has been observed for chlorite schist (Birch, 1961) when the measurement was made in two mutually perpendicular directions, one in the direction of the schistocity and another one normal to the schistocity. Thus, in view of the wide occurrence of metamorphic rocks in the Sudbury Basin, it would have been more useful if the measurements were made in such a way that they will also indicate the effect of anisotropy in the seismic velocity of Precambrian rocks. This could be done by noting the direction of foliation in the sample preparation of the metamorphic rock samples, and taking measurements both normal and parallel to the foliation.

The compressional wave velocities determined in this experiment will be used to construct the seismic models of different geological sections typically found in Sudbury. The underlying principles for the construction of such theoretical seismic models will be thoroughly dealt with in the following chapter.

# Chapter 4

## THEORETICAL BASIS OF THE SEISMIC MODELLING

Since the main objective of this thesis is seismic modelling of geological structures of exploration interest, it will be appropriate to deal with the underlying principles of the seismic method to be employed. Accordingly, the present chapter will be concerned with the theoretical and computational aspects of the seismic modelling to be accomplished in the next chapter.

The ultimate objective of any seismic survey is to provide a geological model of the subsurface structure. To do so, most of the seismic interpretation in the past merely used the travel time data to determine the velocity versus depth of the area, i.e., only the kinematic aspect of the seismic data was utilized. Since the early seventies, however, the introduction of synthetic seismograms as an interpretation tool has enabled us to make full use of a seismic signal. This opened a new dimension to seismic data interpretation whereby the dynamic characteristics, amplitude and phase, of a seismic record can be fully investigated.

At present, there are a number of theoretical methods of generating synthetic seismograms. The most popular ones are the reflectivity method (Fuchs and Muller, 1971), the generalized ray method (Helmberger, 1968; Gilbert and Helmberger, 1972; Wiggins and Helmberger, 1974), asymptotic ray theory (Cerveny and Ravindra, 1971; Cerveny et al., 1977; Cerveny, 1979; Hron and Kanassewich, 1971), and the WKBJ method (Chapman, 1978). All of the above mentioned methods were developed for

whole earth or crustal seismological applications and some of them have been adapted to exploration seismology in recent years. Although the methods of calculation are substantially different, the theory is the same for any given earth model with a given source. After a set of synthetic seismograms are obtained using any of the above methods, a comparison is made between theory and observation. Since we are making use of the whole waveforms present in the data to judge whether a particular geological model and seismic source are acceptable or not, synthetic seismograms are a major advance over the use merely of ray theoretical travel time curves.

Most of the algorithms currently used for computing synthetic seismograms are valid only for laterally homogeneous media. More recently, methods applicable to laterally inhomogeneous media have been reported (Hong and Helmberger, 1978; Frazer and Phinney, 1980). Though an approximate method with a number of restrictions, asymptotic ray theory is the only other method presently available that can compete in the study of body wave propagation in laterally inhomogeneous media. Another advantage of asymptotic ray theory method over other methods is that it is fast and flexible. This makes the method more versatile to use not only for research purposes but also for routine interpretations. All these features make the asymptotic ray method more suitable to use under the geological conditions of the Sudbury Basin.

## 4.1 Asymptotic ray theory

The linearized elastodynamic equation of motion in an inhomogeneous perfectly elastic and isotropic medium is given by

$$\rho \frac{\partial^2 \bar{u}}{\partial t^2} = (\lambda+\mu)\bar{\nabla}(\bar{\nabla}\cdot\bar{u}) + \mu(\bar{\nabla}^2\bar{u} + \bar{\nabla}\lambda(\bar{\nabla}\cdot\bar{u}) + \bar{\nabla}\mu\times(\bar{\nabla}\times\bar{u}) + 2(\bar{\nabla}\mu\cdot\bar{\nabla})\bar{u} \quad \ldots (4.1)$$

where $\bar{u}$ is particle displacement vector, t is time, $\rho$ is density, and $\lambda$ and $\mu$ are Lame's constants (symbols with horizontal bar on top represent vector quantities). For a homogeneous, elastic and isotropic medium, equation (4.1) reduces to

$$\rho \frac{\partial^2 \bar{u}}{\partial t^2} = (\lambda+2\mu)\bar{\nabla}(\bar{\nabla}\cdot\bar{u}) - \mu\bar{\nabla}\times(\bar{\nabla}\cdot\bar{u}) \quad \ldots\ldots\ldots (4.2)$$

In asymptotic ray theory, we assume a time harmonic solution for the elastodynamic equation in inverse powers of the frequency, $\omega$ ;

$$\bar{u} = \exp\left[i\omega(t-\tau)\right]\sum_{K=0}^{\infty}(i\omega)^{-K}\bar{u}_K \quad \ldots\ldots\ldots (4.3)$$

This is the ray series expansion, with phase function $\tau$ and amplitude coefficients $\bar{u}_K$, which are independent of $\omega$ and t . Both $\tau$ and $\bar{u}_K$ are unknown functions of x,y,z which can be determined by inserting equation (4.3) into equation (4.1). Equation (4.3) yields the kinematic and dynamic characteristics which are asymptotic to the wave solution. The moving surfaces of constant phase, $t = \tau(x,y,z)$, are called wave fronts and the orthogonal trajectories of these surfaces are known as rays.

The ray series solution requires that the phase function be analytic. In the neighbourhood of points where the phase function $\tau$ is not

analytic, solution(4.3) is not valid. Thus in the vicinity of points where the time-distance curve of the wave has end points, cusps, tangent points with the travel time curve of another wave, asymptotic ray theory loses its applicability. This happens for example in the vicinity of caustics and critical regions(where the time-distance curves of reflected and head waves are tangent to one another). A recent modification of the method by Cerveny et al.,(1977) improves the accuracy in these regions. In general, the asymptotic expansion yields best results if :

a) The frequency content of the wavefield is very high

b) Velocity gradients are always smaller with respect to the predominant frequency.

c) The radii of curvature of the interfaces are substantially larger than the wavelength.

It is to be noted that the error which arises in keeping only the first few terms in the ray series tends to diminish as the frequency becomes higher, except in the close neighbourhood of singular points. In many cases it is sufficient to work with the leading term of equation(4.3), i.e.,

$$\bar{u} = exp\left[i\omega(t-\tau)\right]\bar{u}_0 \qquad \ldots\ldots\ldots (4.4)$$

This solution is known as the zero-order solution or zeroth approximation. This is the solution which can be obtained according to the principles of geometrical optics. The remaining terms correspond to the corrections of the geometrical solution. To determine the behavior of head waves, however, we need to consider the first two terms of the series (the first order solution),

$$\bar{u} = \exp[i\omega(t-\tau)][\bar{u}_0 + (i\omega)^{-1}\bar{u}_1] \qquad \ldots\ldots\ldots (4.5)$$

## 4.2 Fundamental equations of ray theory.

The first step in applying asymptotic ray theory to investigate subsurface geology is to find an appropriate formula for the phase function and the amplitude coefficients of the ray series. This is done by inserting the ray series solution, equation (4.3) into the elastodynamic equation (4.1), which gives

$$\sum_{K=0}^{\infty} (i\omega)^{-K} \left\{ (i\omega)^2 \bar{N}(\bar{u}_K) - i\omega \bar{M}(\bar{u}_K) + \bar{L}(\bar{u}_K) = 0 \right. \qquad \ldots (4.6)$$

where

$$\bar{N}(\bar{u}_K) = \rho \bar{u}_K + (\lambda+\mu)(\bar{u}_K \cdot \bar{\nabla}\tau)\,\bar{\nabla}\tau + \mu(\bar{\nabla}\tau)^2 \bar{u}_K$$

$$\begin{aligned} \bar{M}(\bar{u}_K) = {} & (\lambda+\mu)\{\bar{\nabla}(\bar{u}_K \cdot \bar{\nabla}\tau) + \bar{\nabla}\tau(\bar{\nabla}\cdot\bar{u}_K)\} \\ & + \mu\{2(\bar{\nabla}\tau\cdot\bar{\nabla})\bar{u}_K + (\bar{\nabla}^2\tau)\bar{u}_K + \bar{\nabla}\lambda(\bar{u}_K\cdot\bar{\nabla}\tau) \\ & + \bar{\nabla}\mu \times (\bar{\nabla}\tau \times \bar{u}_K) + 2(\bar{\nabla}\mu\cdot\bar{\nabla}\tau)\bar{u}_K \end{aligned}$$

$$\begin{aligned} \bar{L}(\bar{u}_K) = {} & (\lambda+\mu)\bar{\nabla}(\bar{\nabla}\cdot\bar{u}_K) + \mu\bar{\nabla}^2\bar{u}_K + \bar{\nabla}\lambda(\bar{\nabla}\cdot\bar{u}_K) \\ & + \bar{\nabla}\mu\times(\bar{\nabla}\times\bar{u}_K) + 2(\bar{\nabla}\mu\cdot\bar{\nabla})\bar{u}_K \end{aligned}$$

For equation (4.6) to be true for any value of the frequency $\omega$, the coefficient of each power of $\bar{u}$ must vanish. Thus we have

$$\bar{N}(\bar{u}_0) = 0 \qquad \ldots\ldots\ldots (4.7a)$$

$$\bar{N}(\bar{u}_1) - \bar{M}(\bar{u}_0) = 0 \qquad \ldots\ldots\ldots (4.7b)$$

$$\bar{N}(\bar{u}_K) - \bar{M}(\bar{u}_{K-1}) + \bar{L}(\bar{u}_{K-2}) = 0 \qquad \ldots\ldots\ldots (4.7c)$$

This system of partial differential equations are very important in asymptotic ray theory and enable us to determine $\tau$ and successively all $\bar{U}_K$.

## 4.3 The phase function and ray tracing systems.

The phase function $\tau$ can be determined by taking

a) the scalar product of equation (4.7a) with $\bar{\nabla}\tau$,

$$\left[-\rho + (\lambda+2\mu)(\bar{\nabla}\tau)^2\right](\bar{U}_0 \cdot \bar{\nabla}\tau) = 0 \qquad \ldots\ldots\ldots (4.8)$$

b) the cross product of equation (4.7a) with $\bar{\nabla}\tau$,

$$\left[-\rho + \mu(\bar{\nabla}\tau)^2\right](\bar{U}_0 \times \bar{\nabla}\tau) = 0 \qquad \ldots\ldots\ldots (4.9)$$

When we require that $\bar{U}_0 \neq 0$ and $\bar{\nabla}\tau \neq 0$, we arrive at the following system of solution :

$$-\rho + (\lambda+2\mu)(\bar{\nabla}\tau) = 0 \quad , \quad \bar{U}_0 \times \nabla\bar{\tau} = 0 \qquad \ldots\ldots\ldots (4.10)$$

then, $\bar{U}_0 \cdot \bar{\nabla}\tau \neq 0$ ;

$$-\rho + \mu(\bar{\nabla}\tau)^2 \neq 0 \quad , \quad \bar{U}_0 \cdot \bar{\nabla}\tau = 0 \qquad \ldots\ldots\ldots (4.11)$$

then $\bar{U}_0 \times \bar{\nabla}\tau \neq 0$

From these solutions, we can derive the well known Eikonal Equation as

$$(\bar{\nabla}\tau)^2 = 1/\alpha^2 \quad , \text{ where } \quad \alpha = \left(\frac{\lambda+2\mu}{\rho}\right)^{1/2} \ldots\ldots (4.12)$$

for P-wave (compressional wave) motion

$$(\bar{\nabla}\tau)^2 = 1/\beta^2 \quad , \text{ where } \quad \beta = \left(\frac{\mu}{\rho}\right)^{1/2} \ldots\ldots\ldots (4.13)$$

for S-wave (shear wave) motion.

Equation (4.12) and (4.13) determine the phase function $\tau$ in terms of its value at some initial surface. The right-hand side of the Eikonal Equation is the inverse of the square of the velocity of propagation of the wave front along a ray. It is the Eikonal equation that determines the kinematic properties of waves such as wave fronts, rays, and times of arrival.

One of the most frequently used techniques for solving the Eikonal Equation is the method of characterstic curves (Cerveny and Hron, 1980), a method that enables us to solve partial differential equations by means of a system of ordinary differential equations. The characteristic curves of the Eikonal Equation represent rays and are determined by the system of six ordinary differential equations of the first order. Using $p_1, p_2, p_3$ instead of $\overline{\nabla}\tau$ (i.e., $p_i = \frac{\partial \tau}{\partial x_i}$), we can write the characteristics of the Eikonal Equation as :

$$\frac{\partial x_i}{\partial \tau} = v^2 p_i \quad , \quad \frac{\partial p_i}{\partial \tau} = -\frac{\partial \ln v}{\partial x_i} \quad , \quad i = 1, 2, 3 \qquad \ldots\ldots\ldots (4.14)$$

where $p_i$ = components of the wave slowness vector, with

$$p_1^2 + p_2^2 + p_3^2 = v^{-2} ,$$

and $v$ = P-wave or S-wave velocity.

Thus, if we specify a given ray by its initial values at

$$\tau = \tau_0 \quad \text{as} \quad x_i = (x_i)_0 , \quad p_i = (p_i)_0 , \; i = 1, 2, 3 \qquad \ldots\ldots\ldots (4.15)$$

where $(p_i)_0$ satisfy the relation $(p_i)_0 (p_i)_0 = v^{-2}((x_k)_0)$, we can compute the coordinates of points along the ray $(x = x_i(\tau))$ and the components of the slowness vector along the ray $(p_i = p_i(\tau))$.

A more useful way of writing the above system of differential equations is to express them in terms of polar angles. The direction of

the ray can be characterized by polar angles $\varphi$ and $\delta$ $(0 < \varphi \leq 2\pi,\ 0 \leq \delta \leq \pi)$ such that :

$$p_1 = v^{-1}\cos\varphi \sin\delta, \quad p_2 = v^{-1}\sin\varphi\sin\delta, \quad p_3 = v^{-1}\cos\delta. \quad \ldots (4.16)$$

consequently, the ray tracing system can be expressed as

$$\frac{dx_1}{d\tau} = v\cos\varphi\sin\delta$$

$$\frac{dx_2}{d\tau} = v\sin\varphi\sin\delta$$

$$\frac{dx_3}{d\tau} = v\cos\delta \qquad \ldots\ldots (4.17)$$

$$\frac{d\varphi}{d\tau} = -(v_1\cos\varphi + v_2\sin\varphi)\cos\delta + v_3\sin\delta$$

$$\frac{d\delta}{d\tau} = -(v_1\cos\varphi + v_2\sin\varphi)\cos\delta + v_3\sin\delta$$

where $v_i = \dfrac{\partial v}{\partial x_i}$

Thus the ray tracing system (equation (4.17)) is composed of five equations of the first order. The corresponding initial conditions are obviously given as :

$$\text{at} \quad \tau = \tau_0 \ ; \ x_i = (x_i)_0 \ , \ \varphi = \varphi_0, \ \delta = \delta_0 \quad \ldots. \ (4.18)$$

The values of $(x_i)_0$ specify the initial point of the ray, $\varphi_0$ and $\delta_0$ the initial direction of the ray at $(x_i)_0$.

The ray tracing system given above can be used only as long as $v(x_i)$ is a smooth function of spatial coordinates, up to the point of intersection of the ray with an interface of the first order (Cerveny, et al., 1977). When a ray strikes an interface, certain quantities of the ray tracing system change discontinuously. At such a point, it will be

necessary to derive new initial conditions for the rays of reflected/ transmitted waves.

Most of the structural problems in exploration seismology can be successfully handled by assuming an inhomogeneous earth whose velocity depends on two coordinates only, i.e., using an earth model with lateral and vertical inhomogeneity. This reduces the ray tracing system of equations to three equations. Thus equation (4.17) simplifies to :

$$\frac{dx}{d\tau} = v \sin\delta$$

$$\frac{dz}{d\tau} = v \cos\delta \qquad \ldots\ldots\ldots (4.19)$$

$$\frac{d\delta}{d\tau} = -v_x \cos\delta + v_z \sin\delta$$

where $v_x = \frac{dv}{dx}$, $v_z = \frac{dv}{dz}$ and $-\pi \leq \delta \leq \pi$. The corresponding initial conditions can be stated as :

for $\tau = \tau_0$ ; $x = x_0$ , $z = z_0$ , $\delta = \delta_0$

The ray tracing system and the associated initial conditions enable us to compute rays, travel times and wave fronts in an inhomogeneous media with curved interfaces. The system of ordinary differential equations can be numerically solved using well known methods such as the Runge-Kutta method. The computer program, TRACE ( Appendix A ), which is extensively used in this thesis, is based on the theoretical principles described so far. In the following chapter, this computer program will be used to trace rays in inhomogeneous 2-Dimensional seismic models, which are simple imitations of real geological conditions in Sudbury.

## 4.4 Amplitude coefficients of the ray series.

An expression for the amplitude coefficients of the ray series can be obtained by solving the transport equations that follow from the basic system of differential equations in ray theory (Cerveny and Ravindra, 1971). The general solution is quite involved, but we are interested in the zeroth approximation (leading term) for P-wave motion which can be expressed as :

$$U_0(\tau) = U_0(\tau_0)\left[\frac{\alpha(\tau_0)\rho(\tau_0)\mathcal{F}(\tau_0)}{\alpha(\tau)\rho(\tau)\mathcal{F}(\tau)}\right] \qquad \ldots\ldots\ldots (4.20)$$

where $\alpha$ and $\rho$ are P-wave velocity and density respectively, $\mathcal{F}$ is a function that plays a basic role in the evaluation of dynamic properties of seismic waves due to its close relation to the geometrical expansion of the ray tube. According to equation (4.20), we can compute $U_0$ at any point of the ray when we know $U_0(\tau_0)$ at another point $\tau = \tau_0$.

The formula for the amplitude of the leading term has a simple physical interpretation. It tells us that the amplitude varies in accordance with the law of the conservation of energy within a narrow ray tube. This is based on the assumption that the energy of seismic waves flows only along the rays, and does not penetrate through the walls of the ray tube. This is not generally true, and the formula can be applied only in the zeroth approximation.

The expression for the amplitude of the leading term can be useful as long as there is no interface of any kind in the model under consideration. When the earth model contains one or more interfaces, then we have to determine the amplitude at a given point using interface conditions and other relevant formula. For this, we need to know the elas-

tic and geometric parameters of both media in the neighbourhood of the point of incidence and the properties of the incident waves.

Since P-waves are the most important types of waves used in exploration seismology, we restrict ourselves to the investigation of these waves in a stratified earth.

When a P-wave impinges on an interface of the first order, only P and SV reflected and transmitted waves are generated. The reflection/transmission coefficients generally depend on the angle of incidence and on the velocities and densities on both sides of the interface at the point of incidence. Referring to Figure (4.1), and denoting the reflection transmission cofficient at the point $A_1$ by $R$, we can write:

$$U^R(A_1) = R\,U^I(A_1) \qquad \ldots\ldots\ldots (4.21)$$

where $U^I(A_1)$ is the incident wave at the point $A_1$, and $U^R(A_1)$ is the reflected/transmitted wave at the point $A_1$.

If we assume that $U^I$ is known at any point of the incident ray such as $B_0$ in Figure (4.1), then we can compute $U^R$ at the point $B$, lying on the reflected/transmitted ray. Applying equation (4.20) for both incident and reflected(transmitted) wave, we can write :

$$U^R(B) = \left[\frac{\rho(B_0)\,\alpha(B_0)\,\mathcal{F}(B_0)}{\rho(B)\,\alpha(B)\,\mathcal{F}(B)}\right]^{1/2} R \left[\frac{\rho'(A_1)\,\alpha'(A_1)\,\mathcal{F}'(A_1)}{\rho(A_1)\,\alpha(A_1)\,\mathcal{F}(A_1)}\right]^{1/2} U^I_{(B_0)} \qquad (4.22)$$

In this equation, $\rho'(A_1)$, $\alpha'(A_1)$, and $\mathcal{F}'(A_1)$ represent $\rho$, $\alpha$ and $\mathcal{F}$ at the

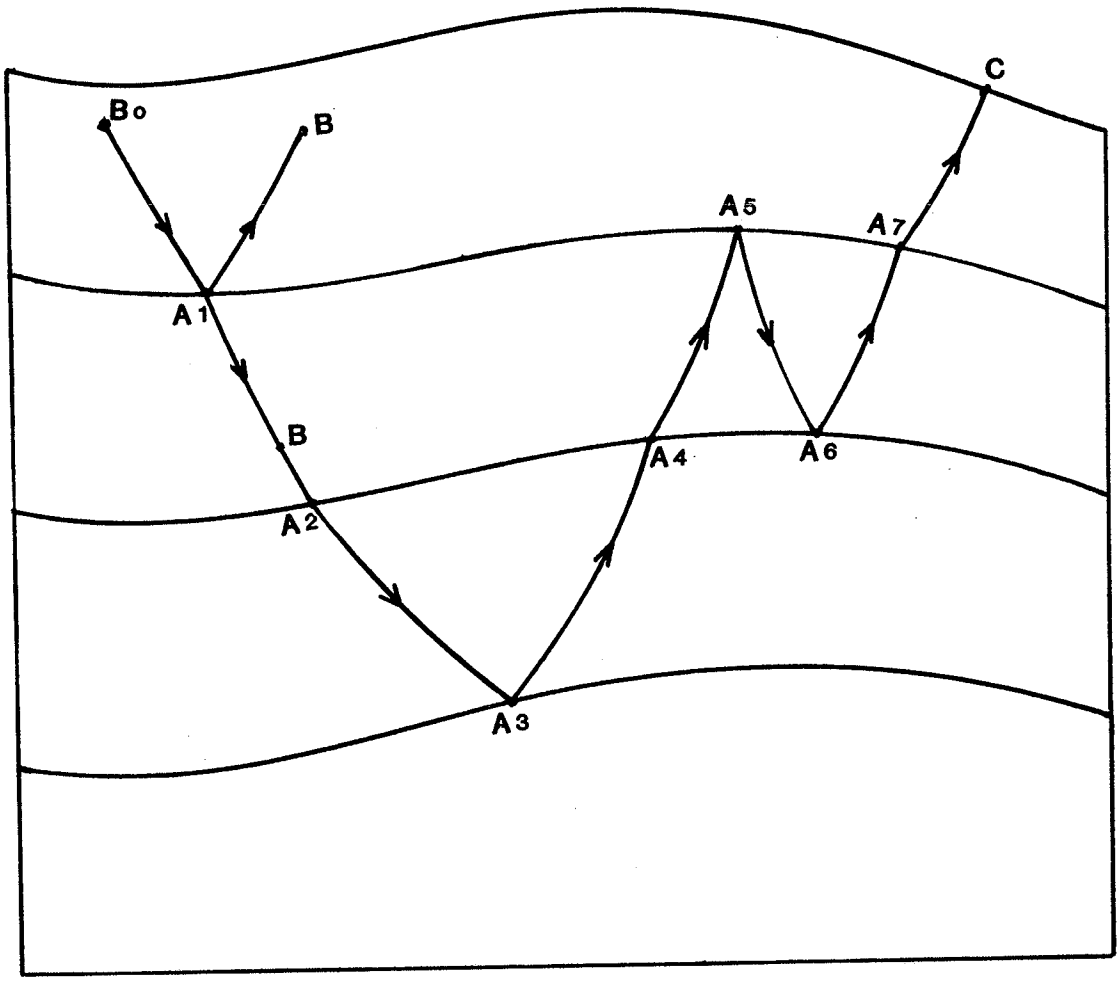


Figure 4.1. Reflected and transmitted waves in a multilayered medium with curved interfaces.

point $A_1$ on the side of the generated wave. For the ray that originates at $B_0$ (Figure 4.1), and traverses points $A_1$ through $A_I$ to point $C$, the reflected/transmitted wave is given by :

$$U^R_{(C)} = U^I_{(B_0)} \left[\frac{\rho(B_0)\alpha(B_0)\mathcal{J}(B_0)}{\rho(C)\alpha(C)\mathcal{J}(C)}\right]^{\frac{1}{2}} \prod_{j=1}^{N} R_j \left[\frac{\rho'(A_j)\alpha'(A_j)\mathcal{J}'(A_j)}{\rho(A_j)\alpha(A_j)\mathcal{J}(A_j)}\right]^{\frac{1}{2}} \quad \ldots (4.23)$$

This final expression for the amplitude of a reflected/transmitted wave can be modified to include a source term. The most commonly assumed source, the point source, is generally described by two take-off angles of the ray under consideration (ray parameters) and the directional characteristics.

All the quantities in equation (4.23) except $\mathcal{J}$ can easily be determined from an assumed seismic model. The quantity $\mathcal{J}$ and the associated geometrical spreading, on the other hand, are considerably complicated and require substantial computing time. Various methods of computation for these quantities (both exact and approximate) have been developed recently (Cerveny et al., 1977) and incorporated in most ray tracing computer programs.

## 4.5 Synthetic seismograms and their applications

The advent of electronic computers has created new dimensions for a better comparison of theory and observation. Modern computers have become so vital in the interpretation of massive geophysical data, which frequently involves massive data processing and the generation of synthetic seismograms.

At present there seem to be three major uses for synthetic seismograms :

a). The construction of a more refined model. This is best illustrated by the work of Helmberger (1968) to study the crust and mantle in the Bering Sea, and his investigation of the lateral variations in Western United States and Northern Mexico (Helmberger, 1972). The basic principle is to vary the geological layer properties until good agreement with observation is obtained.

b). The determination of the relative importance of various phases resulting from a complicated model. This lies in the realm of exploration seismology and it is one of the main concerns of this thesis. Here we are interested in the identification of reliable reflections which can be followed over several kilometers and also be correlated with particular reflecting horizons (May and Hron, 1978; Hilterman, 1970; Tucker and Yorston, 1973).

c). The last application of synthetic seismograms is to geometries that cannot be solved exactly (Pilant, 1979), such as the interaction of waves with edges, corners, and points. By comparing a synthetic seismogram with a record section obtained from a physical model, the nature and importance of the diffraction effects can be measured (Hong and Helmberger, 1977; Langston, 1977).

The first step in the construction of synthetic seismograms is to generate numerical codes of the most important elementary waves. Then the kinematic and dynamic parameters of these waves are computed and the waves with large enough amplitudes are selected. The criteria for the selection of such waves for a given number of plane parallel layers has been developed by (Hron, 1971). For curved interfaces, the method

of ray generation and selection is slightly different. However, the general criteria is to realize :

1) the most important rays(rays with large amplitude contributions) are the rays with a minimal (or near-minimal) number of reflections and therefore a maximal (or near-maximal) number of transmissions (Ben-Menham and Singh, 1981), for example, primary reflections in exploration seismology, and 2) contributions from converted rays can be significant when the conversion takes place at a reflection but are usually negligible when converted at transmission. Finally, elementary seismograms corresponding to the elementary waves are determined and summed up to give the desired synthetic seismogram.

In the next chapter, the computer program, TRACE (see appendix) which is based on the ray tracing principles of section 4.3 will be used to trace seismic rays in typical geological sections of the Sudbury Basin. This same program also computes the amplitude of the reflected wave (as outlined in section 4.4), the arrival time, and surface position with respect to the source. This information, i.e., the output of program TRACE will be fed to another program which computes synthetic seismograms to obtain the seismic response of the particular model. Thus, the next chapter incorporates the P-wave velocity data of chapter 3 and the theoretical principles of the present chapter.

# Chapter 5

## THE SEISMIC MODELLING

Seismic modelling is the construction of the seismic response of a proposed geological set-up which is either structural or stratigraphic, or both. The computation requires a knoweledge of the model parameters such as velocity distribution, physical dimension, and model structure. If an observed seismic data is already at hand, then one can vary these parameters until the seismic response shows a good match with the observed seismic section. The model so obtained will be considered to be a representative of the true subsurface geology.

In this chapter, the ray theoretical principles outlined in the previous chapter and the laboratory seismic velocity measurements of chapter 3 will be combined to construct various models of the Sudbury Basin.

### 5.1 Model parameters

The most essential step in the formulation of a seismic model is to specify the physical and geometrical parameters of each medium in the model. Under geometrical parameters we have the shape and position of seismic interfaces. The geometrical parameters of the seismic modelling are derived from the two geological sections of the North Range environment of Sudbury (Figures 5.1a and 5.1b). This is a section of the area from which the core samples for the velocity measurement were

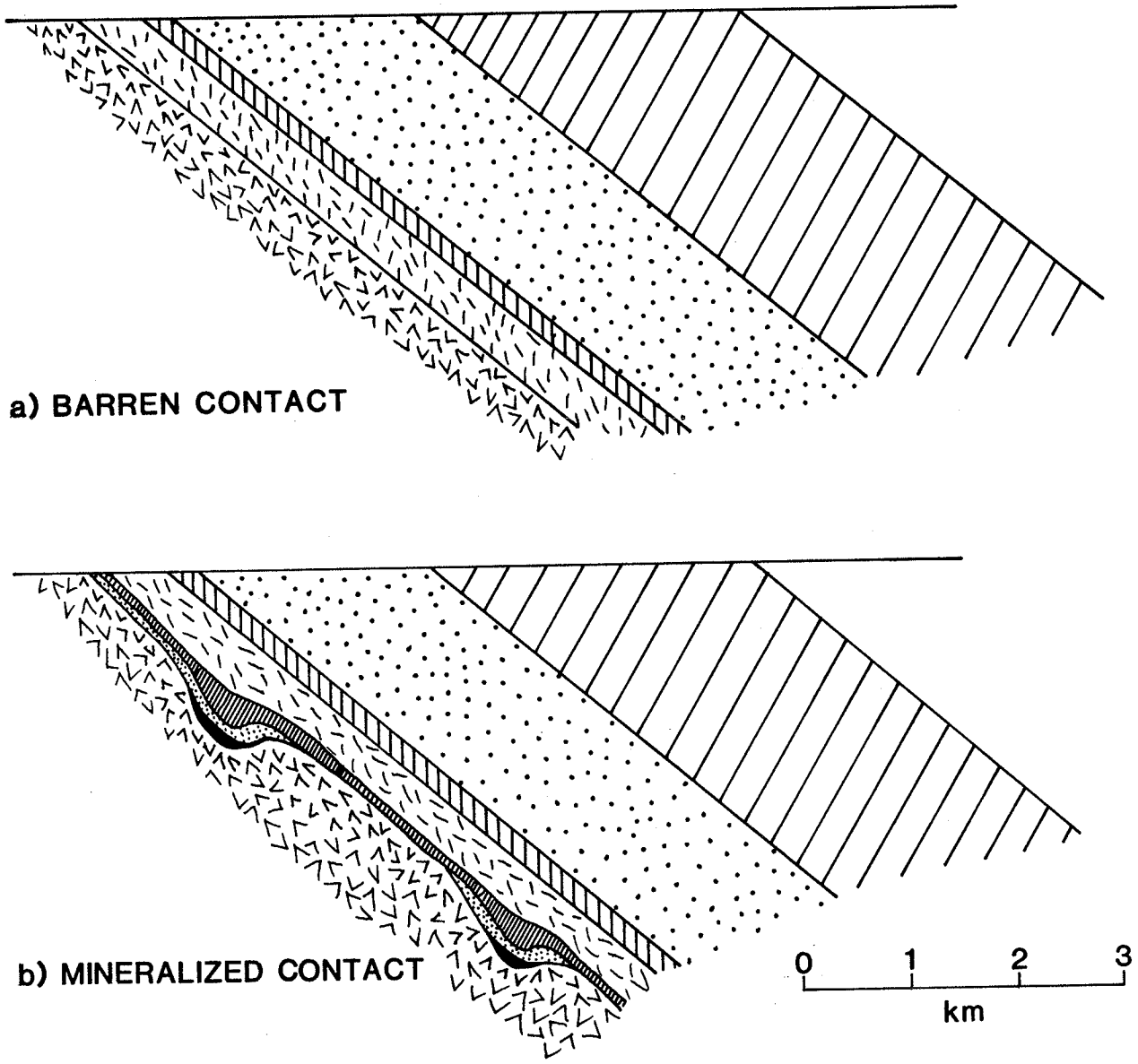


Figure 5.1. (a) Diagramatic section of a barren contact in the North Range environment.
(b) Diagramatic section of a mineralized contact in the North Range environment.

obtained. The Figure shows the contact relationships and the thicknesses of the different rock units. Part(a) is a diagrammatic section of a barren contact, whereas part(b) corresponds to a diagrammatic section of a typical mineralized contact in the North Range environment. Additional geological models other than the ones shown in Figure 5.1 will also be considered.

By physical parameters of a medium we mean P-wave velocity and S-wave velocity, and density. It should be emphasized, however, that velocity is the most critical parameter playing a major role in any seismic modelling. In this thesis, P-wave velocities and rock densities as determined in chapter 3 will serve as prescribed.

## 5.2 Acoustic impedance and reflection coefficient in Sudbury

Knowing both the physical and geometrical parameters, there are two main problems that should be considered before we embark on applying reflection seismics to map the boundaries of crystalline rocks. The first is whether, at the contacts between the different types of rocks, the acoustic contrasts are sufficient to generate reflections observable at the surface. The second problem is the difficulty encountered in interpreting observations caused by the irregularity of the rock boundaries in an area of interest.

When we talk of the detectability of the seismic response, we are concerned primarily with the variation in reflection amplitudes imposed by the subsurface geology. Consequently we exclude amplitude considerations due to such factors as instrument sensitivity, source energy,

geophone-ground coupling etc,. Then we are left with the major factors that affect the variation of amplitude; spherical divergence, interface transmission losses, and multiple reflection effects. In this section, however, only the nature of interface reflection coefficients of the intended seismic model will be considered.

In the light of the geological conditions of the Sudbury Basin, we have the necessary background information to investigate the detectability of the reflected enery. Using the laboratory measured P-wave velocities and densities, the acoustic impedance of the major rock units have been computed (Figure 5.2). The impedance was computed by taking the product of the density and the average velocity (Table 2) at a given pressure, i.e., $Z = \rho V$ ( where Z = acoustic impedance, $\rho$ = density, and V = velocity ) assuming vertical reflection.

It is clear from Figure 5.2 and Table 3 that the massive sulphide has an exceptionally high acoustic impedance, followed by the oxide-rich quartz gabbro and mafic norite. The two felsic rocks, granite gneiss and micropegmatite have the lowest and second lowest impedance respectively. The remaining four rock units (granite breccia, mafic gneiss, Onaping and felsic norite ) appear to have values that are not very much different from one another, specially in the low pressure regions. Another important point to be learned from this data is the presence of a uniform impedance contrast all the way from the lowest to the highest pressure. This suggests that for the pressure values considered, the impedance contrast appears to be independent of the applied pressure, or the depth from the surface.

Table 2. Average P-wave velocity, density, and porosity to 44.2 MPa of stress.

| ROCK TYPE | S T R E S S ( M P a ) | | | | | | DENSITY | DENSITY | POROSITY |
|---|---|---|---|---|---|---|---|---|---|
| | 3.5 | 5.0 | 9.3 | 18.0 | 30.7 | 44.2 | ($kg/m^3$) (DRY) | ($kg/m^3$) (WET) | (PERCENT) |
| ONAPING | 6.157 | 6.243 | 6.266 | 6.309 | 6.309 | 6.328 | 2734.6 | 2735.6 | 0.07 |
| MICROPEGMATITE | 5.905 | 5.993 | 6.067 | 6.143 | 6.194 | 6.252 | 2694.2 | 2697.8 | 0.36 |
| OXIDE-RICH QUARTZ GABBRO | 6.335 | 6.418 | 6.477 | 6.512 | 6.622 | 6.633 | 2889.1 | 2890.6 | 0.15 |
| FELSIC NORITE | 5.851 | 5.950 | 6.003 | 6.041 | 6.123 | 6.227 | 2791.9 | 2795.5 | 0.36 |
| MAFIC NORITE | 6.077 | 6.084 | 6.139 | 6.256 | 6.284 | 6.366 | 2909.3 | 2912.0 | 0.27 |
| GRANITE BRECCIA | 5.829 | 5.889 | 5.975 | 6.078 | 6.110 | 6.123 | 2739.6 | 2791.4 | 0.37 |
| MASSIVE SULPHIDE | 4.914 | 4.979 | 5.046 | 5.069 | 5.185 | 5.209 | 4153.4 | 4160.8 | 0.74 |
| MAFIC GNEISS | 5.918 | 5.959 | 6.068 | 6.182 | 6.271 | 6.299 | 2797.8 | 2799.8 | 0.20 |
| GRANITE GNEISS | 5.701 | 5.721 | 5.827 | 5.925 | 5.991 | 6.038 | 2684.1 | 2688.2 | 0.40 |
| SUDBURY BRECCIA | 5.845 | 5.924 | 5.965 | 6.047 | 6.090 | 6.176 | 2831.8 | 2832.9 | 0.11 |
| OLIVINE DIABASE | 6.300 | 6.320 | 6.380 | 6.580 | 6.670 | 6.670 | 2989.2 | 2992.0 | 0.28 |

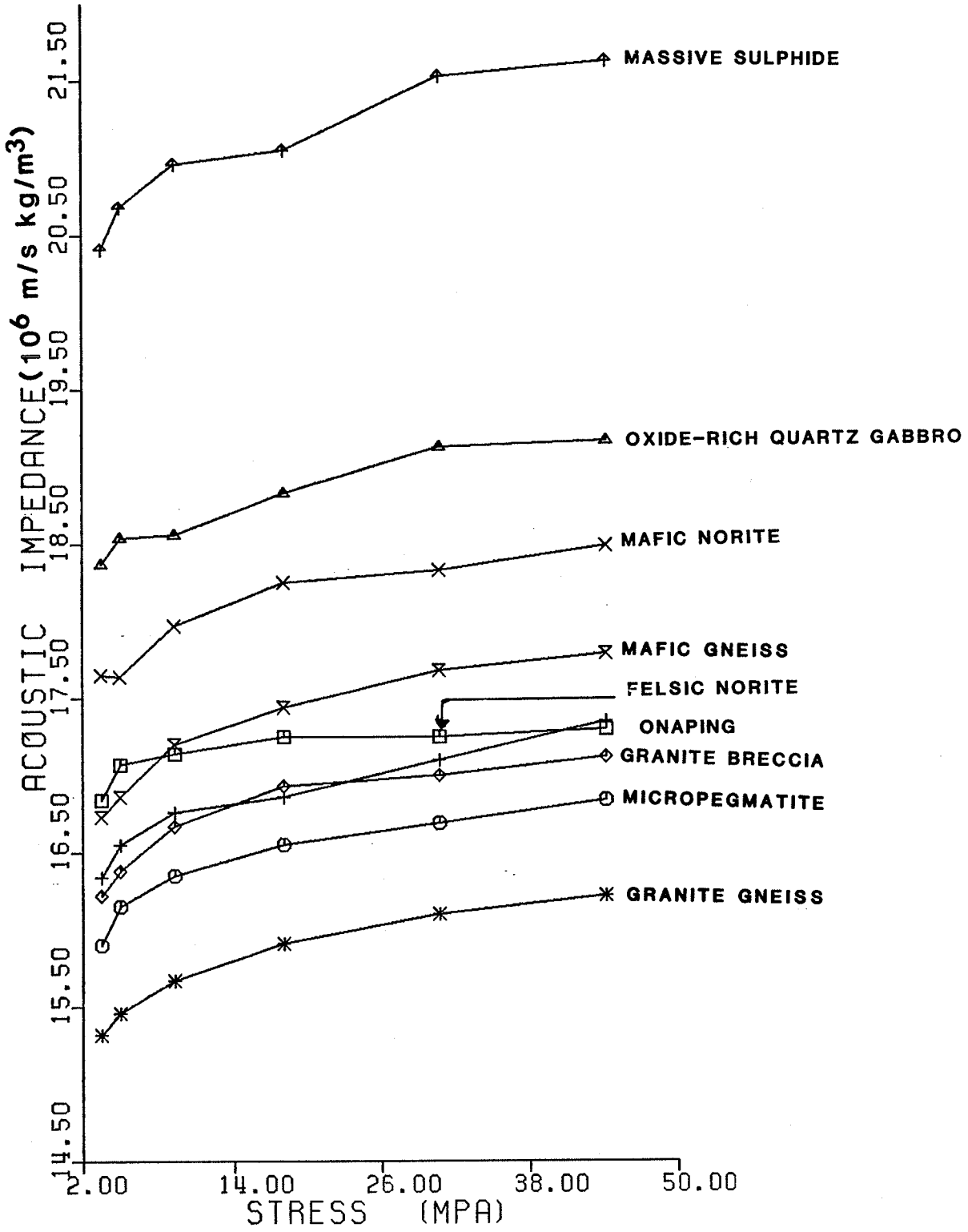


Figure 5.2. Acoustic impedance of the major rock units in the North Range environment.

Table 3. Acoustic impedance (in millions m/s kg/m³ ) to 44.2 MPa of stress of the major rock units in Sudbury.

| ROCK TYPE | STRESS (MPa) | | | | | |
|---|---|---|---|---|---|---|
| | 3.5 | 5.0 | 9.3 | 18.0 | 30.7 | 44.2 |
| ONAPING | 16.84 | 17.07 | 17.14 | 17.25 | 17.25 | 17.30 |
| MICROPEGMATITE | 15.90 | 16.15 | 16.35 | 16.55 | 16.69 | 16.84 |
| OXIDE-RICH QUARTZ GABBRO | 18.30 | 18.54 | 18.71 | 18.81 | 19.13 | 19.16 |
| FELSIC NORITE | 16.36 | 16.61 | 16.76 | 16.87 | 17.10 | 17.39 |
| MAFIC NORITE | 17.68 | 17.70 | 17.86 | 18.20 | 18.28 | 18.52 |
| GRANITE BRECCIA | 16.25 | 16.41 | 16.66 | 16.94 | 17.03 | 17.07 |
| MASSIVE SULPHIDE | 20.41 | 20.68 | 20.96 | 21.05 | 21.53 | 21.63 |
| MAFIC GNEISS | 16.56 | 16.67 | 16.98 | 17.23 | 17.55 | 17.62 |
| GRANITE GNEISS | 15.32 | 15.36 | 15.64 | 15.90 | 16.08 | 16.21 |
| SUDBURY BRECCIA | 16.55 | 16.77 | 16.89 | 17.12 | 17.24 | 17.49 |
| OLIVINE DIABASE | 18.83 | 18.89 | 19.07 | 19.67 | 19.94 | 19.94 |

More insight about the seismic response of the Sudbury Basin can be gained by computing the reflection coefficient at the boundaries of the different rock units in the geological section. Consequently, the plane wave reflection coefficient for normal incidence was calculated for each of the contacts in Figure 5.1 using the equation,

$$R = \frac{Z2-Z1}{Z2+Z1} \qquad \ldots\ldots\ldots\ldots\ldots\ldots \quad (5.1)$$

Where R = reflection coefficient, Z1 = acoustic impedance of medium 1, and Z2 = acoustic impedance of medium 2.

The computation was accomplished by assuming a stack of homogeneous layers corresponding to the rock units in the geological section. Accordingly, the Onaping is taken as the top-most layer, and the gneissic rocks as the lower-most layer or infinite half space. On the basis of the contact relationships depicted in Figures 5.1a and 5.1b, there are fourteen possible interfaces, assuming the footwall rock to be either a mafic gneiss or a granite gneiss (Table 4 ). It is also known (from the core logs), that the footwall can have zones of Sudbury breccia. This might raise the number of possible seismic interfaces to eighteen. Nevertheless, considering the limited occurrence of the rock unit and an acoustic impedance very similar to mafic gneiss, the additional interfaces can be safely ignored in this study.

The reflection coefficient of each of these interfaces is displayed in Figure 5.3. Of course, some of these interfaces may not have any geological significance due to their limited size and/or occurrence. Nine of the fourteen possible interfaces (Table 4) have negative

Table 4. Reflection coefficient to 44.2 MPa of stress for possible interfaces in Sudbury.

| ROCK TYPE | STRESS (MPa) | | | | | |
|---|---|---|---|---|---|---|
| | 3.5 | 5.0 | 9.3 | 18.0 | 30.7 | 44.2 |
| ONAPING AND MICROPEGMATITE | -0.029 | -0.028 | -0.024 | -0.021 | -0.016 | -0.013 |
| MICROPEGMATITE AND OXIDE-RICH QUARTZ GABBRO | 0.072 | 0.069 | 0.063 | 0.064 | 0.068 | 0.065 |
| OXIDE-RICH QUARTZ GABBRO AND FELSIC NORITE | -0.058 | -0.057 | -0.051 | -0.055 | -0.056 | -0.050 |
| FELSIC NORITE AND MAFIC NORITE | 0.038 | 0.032 | 0.035 | 0.040 | 0.036 | 0.032 |
| FELSIC NORITE AND MAFIC GNEISS | 0.012 | 0.009 | 0.013 | 0.017 | 0.017 | 0.013 |
| FELSIC NORITE AND GRANITE GNEISS | -0.032 | -0.034 | -0.034 | -0.029 | -0.030 | -0.034 |
| MAFIC NORITE AND GRANITE BRECCIA | -0.042 | -0.037 | -0.038 | -0.036 | -0.038 | -0.038 |
| MAFIC NORITE AND MAFIC GNEISS | -0.027 | -0.023 | -0.022 | -0.023 | -0.018 | -0.019 |
| MAFIC NORITE AND GRANITE GNEISS | -0.071 | -0.066 | -0.068 | -0.069 | -0.065 | -0.065 |
| GRANITE BRECCIA AND MASSIVE SULPHIDE | 0.114 | 0.116 | 0.114 | 0.108 | 0.118 | 0.116 |
| GRANITE BRECCIA AND MAFIC GNEISS | 0.015 | 0.014 | 0.016 | 0.015 | 0.020 | 0.019 |
| GRANITE BRECCIA AND GRANITE GNEISS | -0.026 | -0.029 | -0.031 | -0.031 | -0.027 | -0.027 |
| MASSIVE SULPHIDE AND MAFIC GNEISS | -0.099 | -0.102 | -0.099 | -0.094 | -0.098 | -0.097 |
| MASSIVE SULPHIDE AND GRANITE GNEISS | -0.142 | -0.144 | -0.144 | -0.139 | -0.144 | -0.143 |

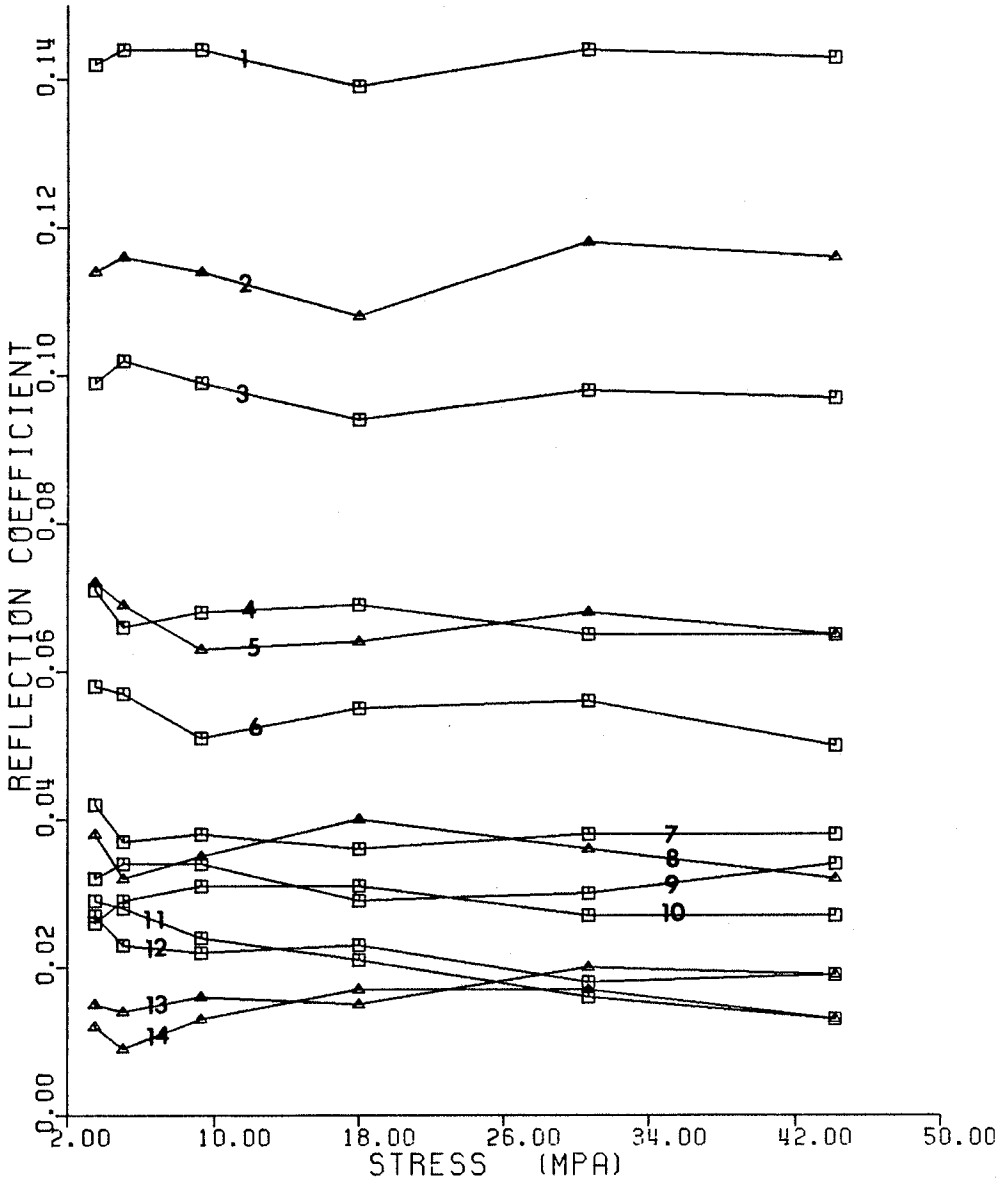


Figure 5.3. Reflection coefficient of possible interfaces in the North Range environment. The interfaces are: 1=massive sulphide/granite gneiss, 2=granite breccia/massive sulphide, 3=massive sulphide/mafic gneiss, 4=mafic norite/granite gneiss, 5=micropegmatite/oxide-rich quartz gabbro, 6=oxide-rich quartz gabbro/felsic norite, 7=mafic norite/granite breccia, 8=felsic norite/mafic norite, 9=felsic norite/granite gneiss, 10=granite breccia/granite gneiss, 11=Onaping/micropegmatite, 12=mafic norite/mafic gneiss, 13=granite breccia/mafic gneiss, 14=felsic norite/mafic gneiss. (Triangles stand for negative values and squares for positive values).

reflection coefficients, and the magnitude of the reflection coefficients ranges from 0.009 for a felsic norite/mafic gneiss interface to 0.144 for a massive sulphide/granite gneiss interface. Only three interfaces, all formed with massive sulphide and an adjacent rock unit, have magnitudes that are comparable to the reflection coefficient of young sedimentary rocks (O'Doherty and Anstey, 1971). These interfaces could be suitable targets of a reflection seismic survey provided they also meet the geometric requirement.

Three other interfaces, namely, micropegmatite/oxide-rich quartz gabbro, oxide-rich quartz gabbro/felsic norite, and mafic norite/granite gneiss have moderately high reflection coefficients and may have considerable importance from an exploration point of view. The other interfaces have low coefficients, indicating that they may not return seismic energy strong enough to be detected by most available seismic equipment.

All the interfaces shown in Figure 5.3 may not be geologically meaningful in all parts of Sudbury. For example, in the North Range environment, the footwall rock is made up of granitic rocks (see Map No 2170 Ontario Department of Mines (now Ontario Geological Survey)). In this case, all reflection coefficient computations that depend on the elastic parameters of mafic gneiss will be unrealistic for this part of the Basin. Some other interfaces may be of such a small scale to have any geophysical significance.

The most outstanding features of the reflection coefficients in Sudbury are: a) reasonably high reflection coefficients on either side of the massive sulphide layer, b) moderately high reflection coefficients

for micropegmatite/oxide-rich quartz gabbro and mafic norite/granite gneiss interfaces. These interfaces appear to possess features of a suitable target for future reflection seismic survey.

## 5.3 Geological and seismic boundaries

One of the most important reasons why the seismic method is not valid in many geological environments is the lack of correspondence between geological boundaries and seismic boundaries. Actual geological units are not generally homogeneous and geological boundaries are not expected to be sharp most of the time. They are always characterized by a zone of transition, the thickness of which may vary from a fraction of a centimeter to tens or even hundreds of meters. In exploration seismology, however, the subsurface geology is frequently assumed to be composed of homogeneous layers separated by sharp boundaries (first order discontinuities). Any significant deviation from this assumption reduces the amplitude of the seismic wave reflected at the boundary.

Whether a geological boundary with a transition zone is sharp or not depends on the thickness of the transition zone and the frequency of the seismic wave used. It has been shown (Noponen et al., 1979) that the amplitude of reflection will not be affected by the presence of a transition zone the thickness of which is less than 10% of the seismic wavelength used. For a frequency of 30 Hz (the predominant frequency in exploration seismology) and the average velocity in Sudbury (about 6.2 km/s), a transition zone with a thickness less than 20 m will not affect the amplitude of the reflected energy. This study assumes that

the above requirement is reasonably satisfied in the geological condition of the Sudbury Basin.

## 5.4 Seismic modelling of the North Range environment

The seismic modelling to be effected in the following sections assumes that the velocity measurement described in Chapter 3 represents the seismic velocity distribution of the Sudbury Basin to 2 km of depth. The primary interest, however, is to see what lies well below this depth, to a depth of 6 or 8 km. Consequently, the available velocity data was made to serve this purpose by applying a suitable extrapolation as shown in Figures 5.4a and 5.4b. The velocities of the two rock units (greenstones and leucocratic gneiss) included in the Figures were measured in conjunction with a crustal seismic survey in Northwestern Ontario (Young, 1979), in the Superior Structural Province of the Canadian Shield.

The first seismic model considered is the one that corresponds to the geological section of Figure 5.1a, i.e., a barren contact in the North Range environment. The geological contact is known to dip from 30° to 50° , so the dip of the layers in the models was made to lie in this range. Layer thickness corresponds to the thickness of the rock unit it represents, except in some regions of sharp corners. Layer properties are given by the average P-wave velocity specified at points having regular horizontal intervals but arbitrary depths. The velocity within a layer can change laterally or vertically, resulting in a two dimensional inhomogeneous medium. Also, all the layers considered are assumed to be perfectly elastic and isotropic media.

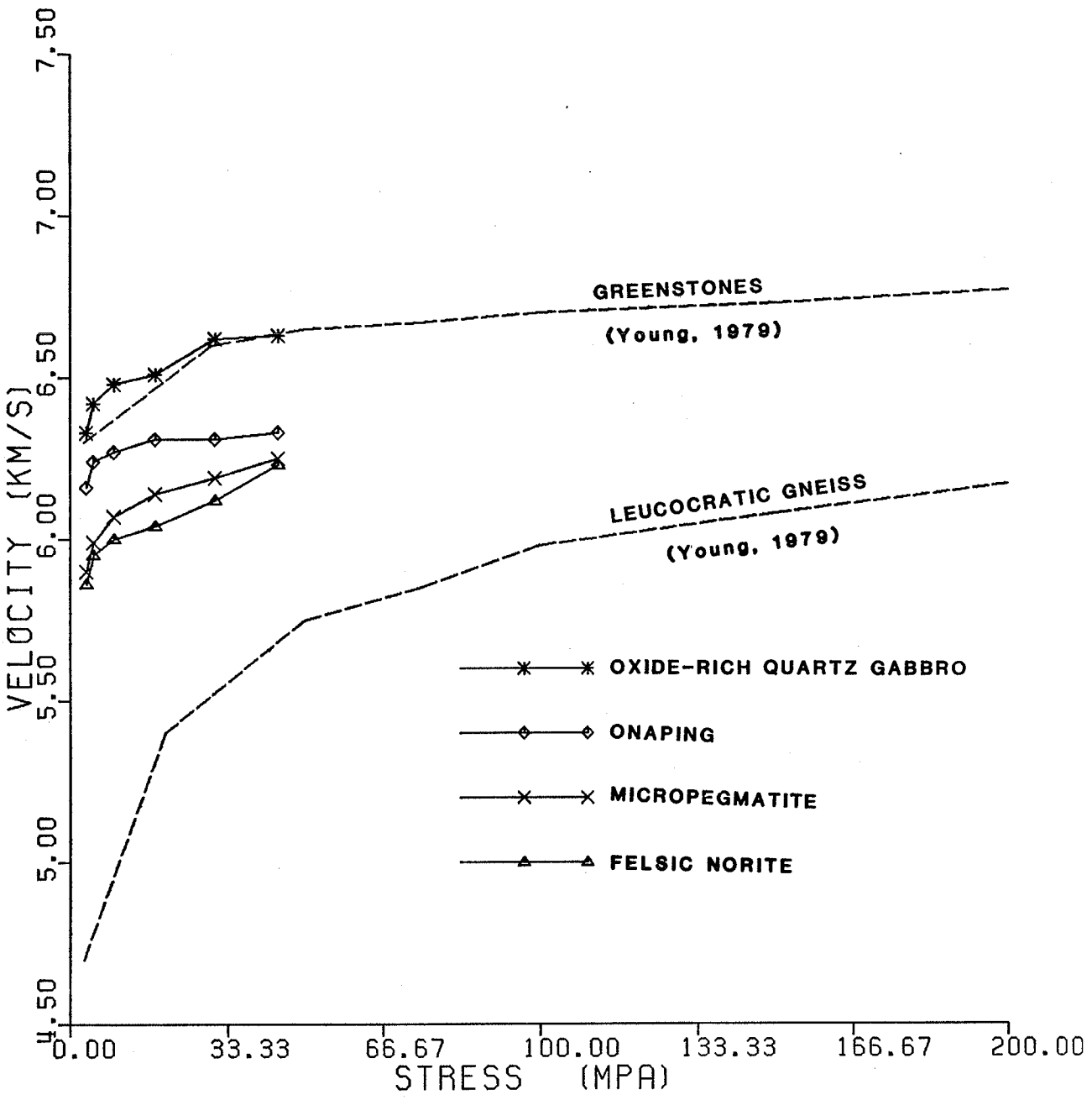


Figure 5.4. (a) Average P-wave velocity of the top four rock units and data from Young (1979). See text for explanation.

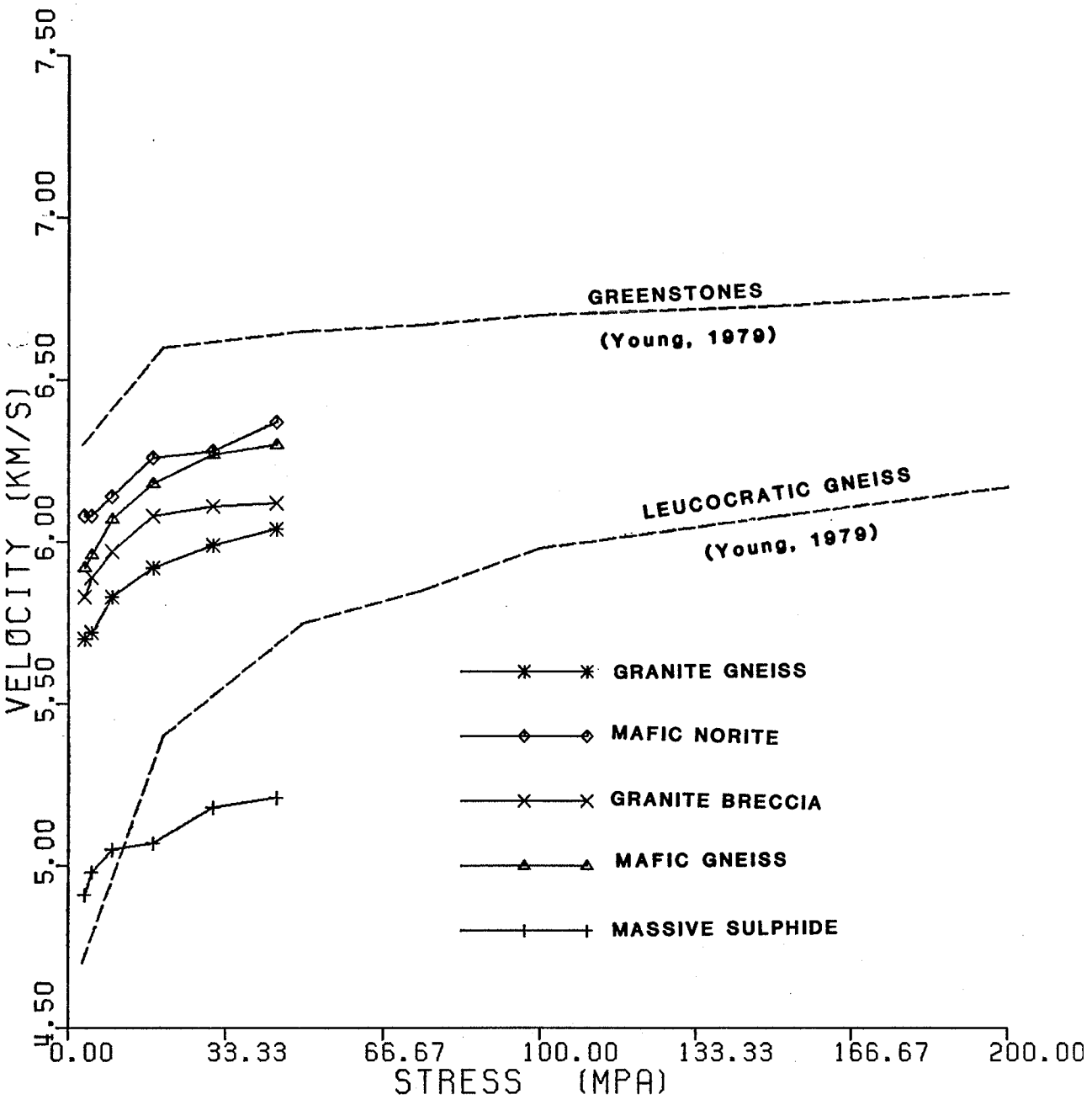


Figure 5.4 (b) Average P-wave velocity of the lower four rock units and massive sulphide, and data from Young (1979). See text for explanation.

In Figure 5.5a, the upper most layer stands for the top two formations (Chelmsford sandstone and Onwatin slate) of the Whitewater group, followed by the Onaping formation, micropegmatite, oxide-rich quartz gabbro, felsic norite and granite gneiss (footwall rock). The wide occurrence of granitic rocks in this part of Sudbury, (Figure 2.3) can justify the choice of granite gneiss as the footwall rock. In all the models constructed, the last interface was included simply to facilitate the computing work and bears no geological significance.

The vertical velocity model at 4 km distance from the origin for the seismic model shown in Figure 5.5a is given in Figure 5.6a. For reasonably thick layers such as the Onaping and micropegmatite, the velocity was allowed to change both laterally and vertically. But, for thin layers like oxide-rich quartz gabbro, the vertical variation was considered to be negligible, so only lateral velocity gradient was used.

The synthetic seismogram generated for the model of Figure 5.5a is shown in Figure 5.5b. The reflected arrivals from each of the irruptive rocks and the footwall rocks are plotted in real time scale. It can be seen that the reflected energy from all the interfaces reaches the recording device in less than 1.6 seconds. For this particular sampling interval(4 ms), all the arrivals are well separated in time. There doesn't seem to be any problem in identifying one interface from another, even for the thinnest layer in the structure.

Reflection amplitude generally follows the same pattern as the reflection coefficient of Figure 5.3, the high amplitude coming from the interface with the highest reflection coefficient. Despite the fact that the top of the oxide-rich quartz gabbro is 1.8 km deeper than the

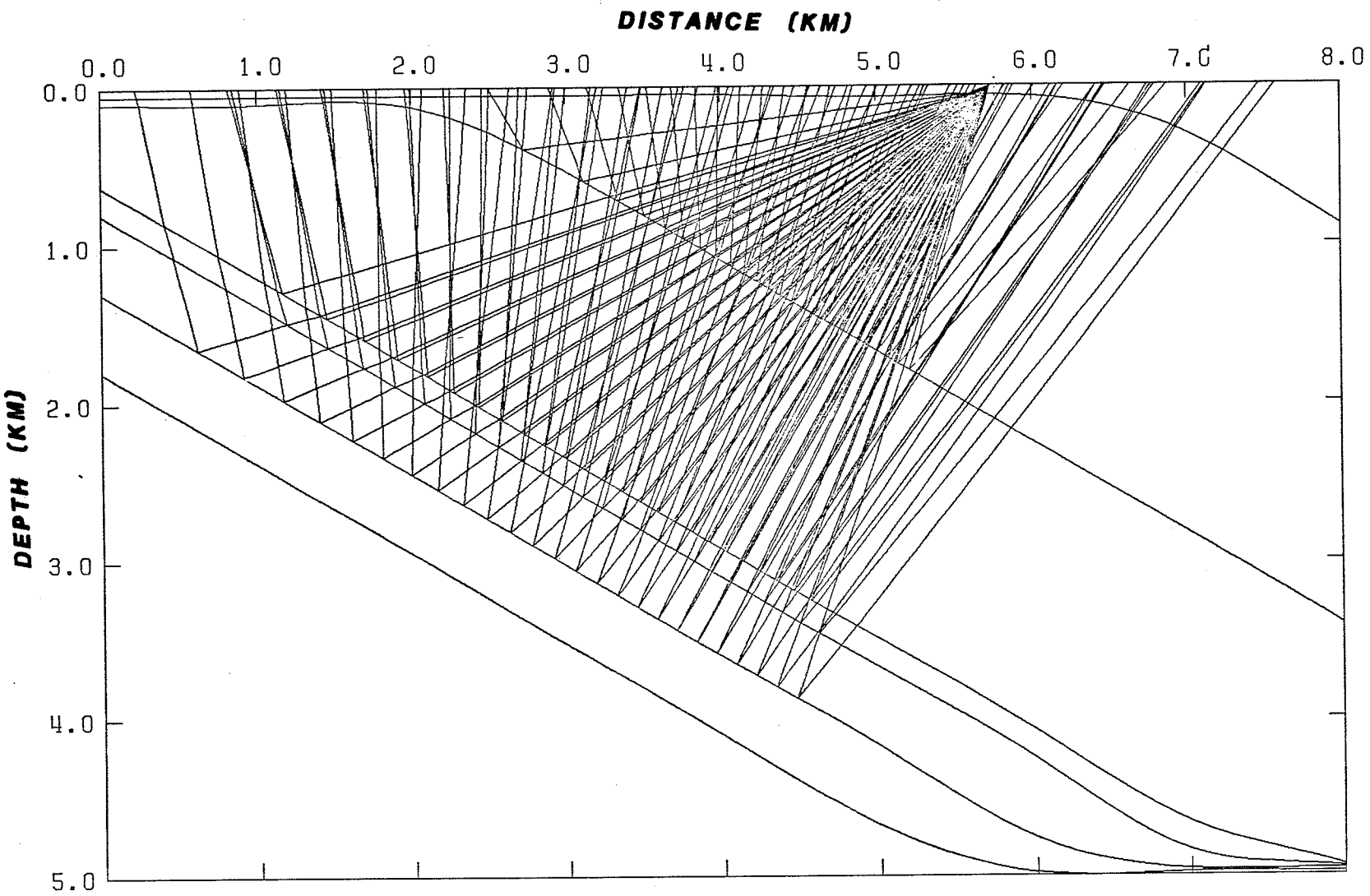


Figure 5.5. (a) Ray tracing of the North Range environment model.

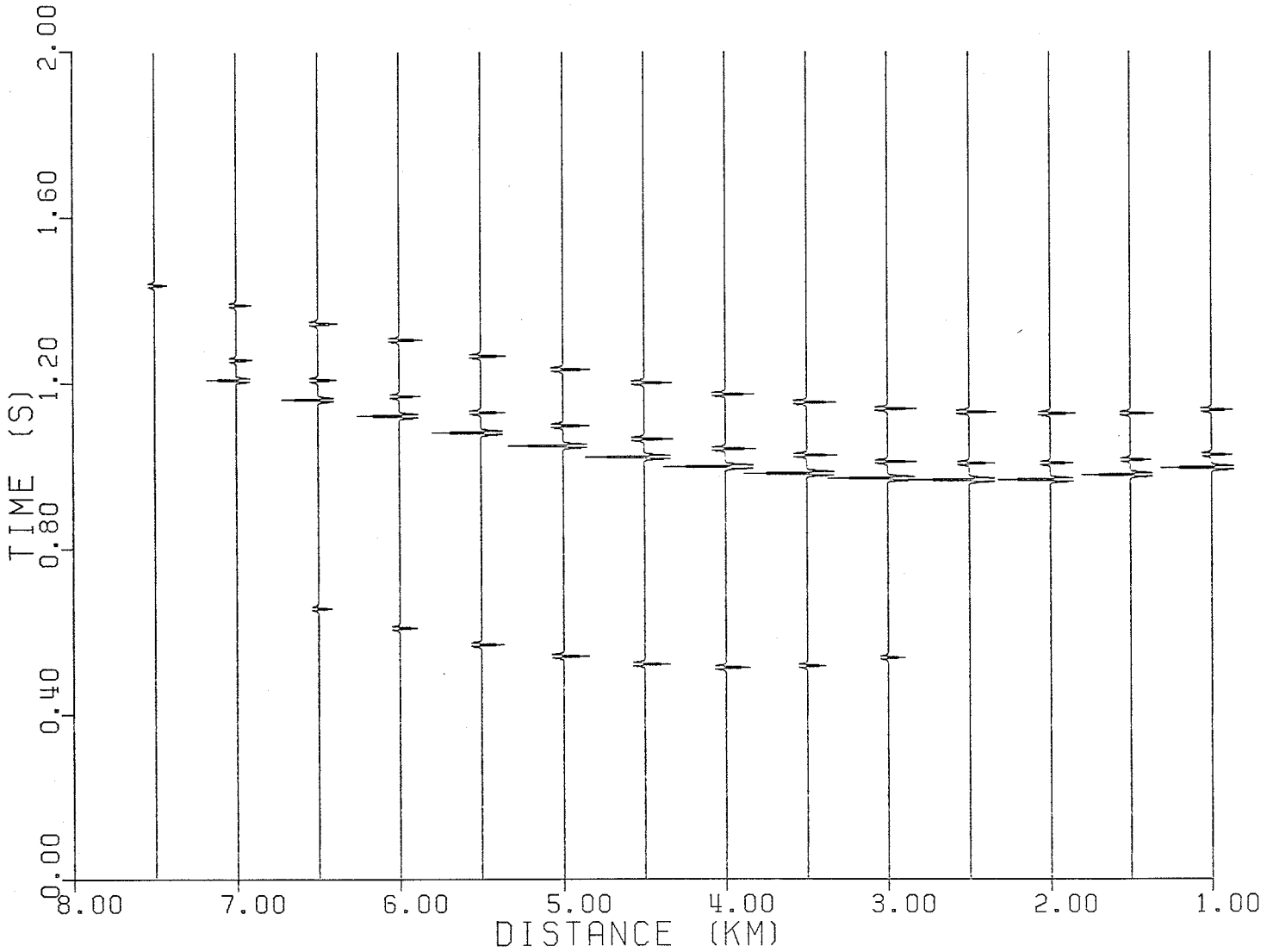


Figure 5.5. (b) Synthetic seismogram of the North Range environment model.

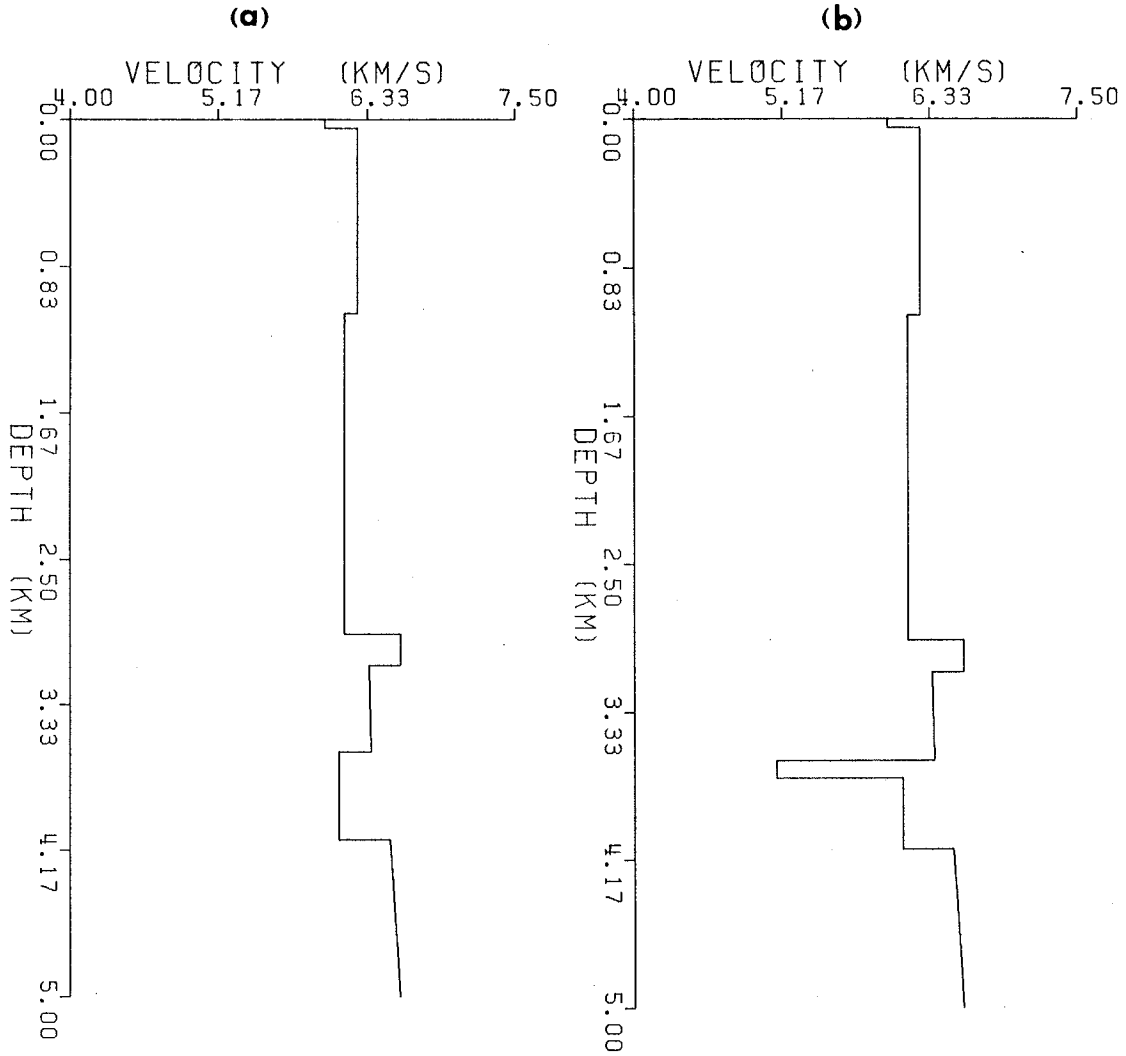


Figure 5.6. (a) Vertical velocity model of the North Range environment model at 4 km distance from the origin.
(b) Vertical velocity model at 4 km distance from the origin of the North Range environment model with a sulphide layer.

top of the micropegmatite, the amplitude of the reflection from the deeper interface is more than two and a half times as strong as the reflection above it. For up-dip arrivals, the amplitude appears to show a very weak dependence on offset distance.

The present model was modified by increasing the dip of the contacts from 30° to 40° (Figure 5.7a), an intermediate value for the geological dip in the area. The corresponding synthetic seismogram (using the same format as Figure 5.5b) is shown in Figure 5.7b. No major change, either in the subsurface coverage or the nature of the travel time could be observed, except for a difference in the time gap between the first arrival and the second arrival.

The amplitude picture is more or less the same for both models. To obtain a reasonable comparison of amplitudes, however, the source positions in both models were moved back and forth until a good match in the travel time of the prominent arrivals (second arrivals) was obtained. It was difficult to obtain a good match to all the arrivals, consequently, the partial match attained between offset distances 4.5 km and 6.0 km was considered satisfactory. For this region, we can assume that the path followed by the rays in both models has the same velocity structure. Any change in the amplitude observed can be attributed to the change in the dip angle. The comparison made on this ground shows no appreciable difference in amplitudes. This implies that no serious loss of amplitudes can be introduced in treating the 30° seismic model to represent the North Range environment. Besides, actual reflection data characterized by steeper dips usually creates serious problems of data processing, for example, migration. Hence the

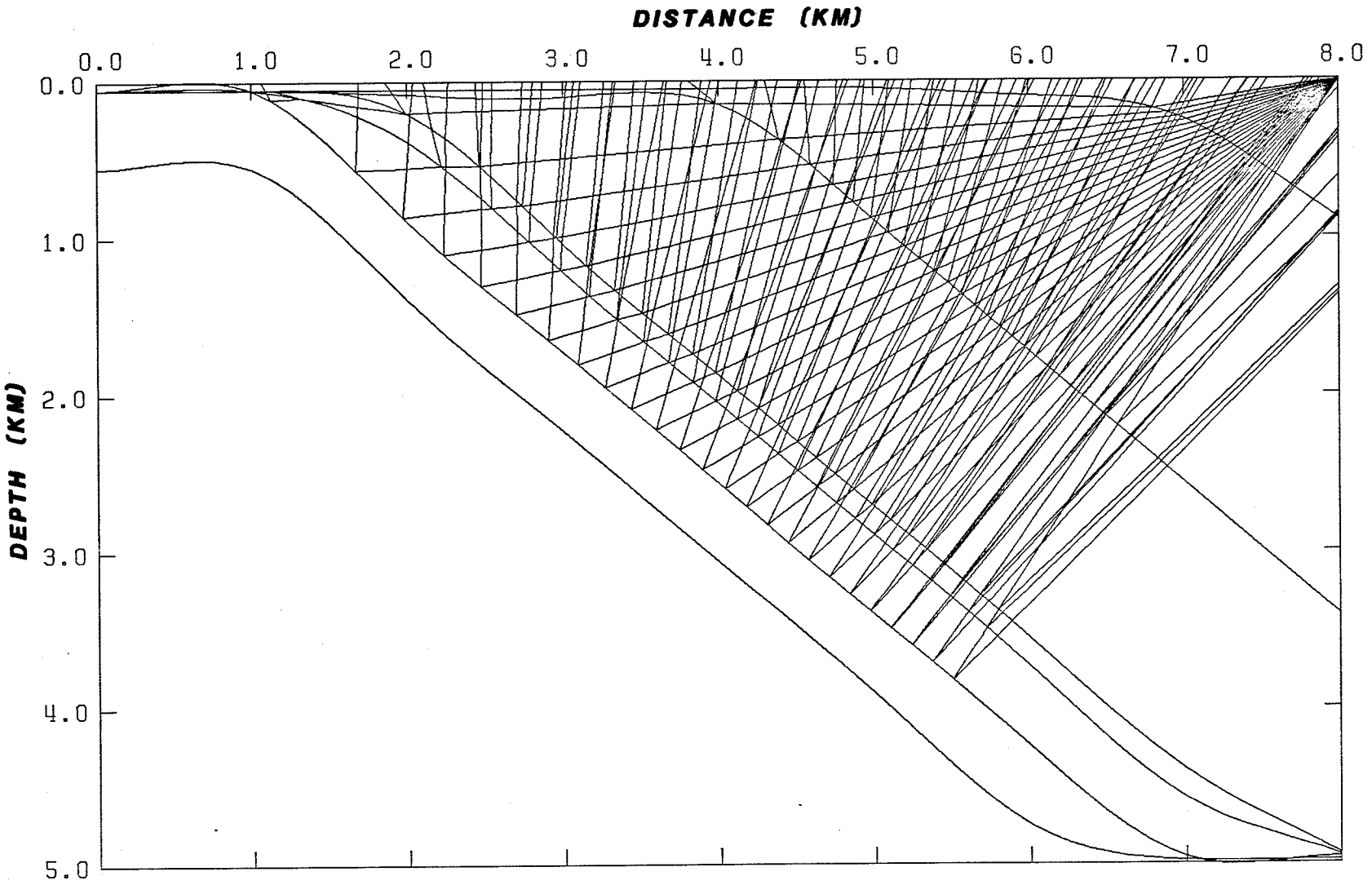


Figure 5.7. (a) Ray tracing of the North Range environment model with 40° dip.

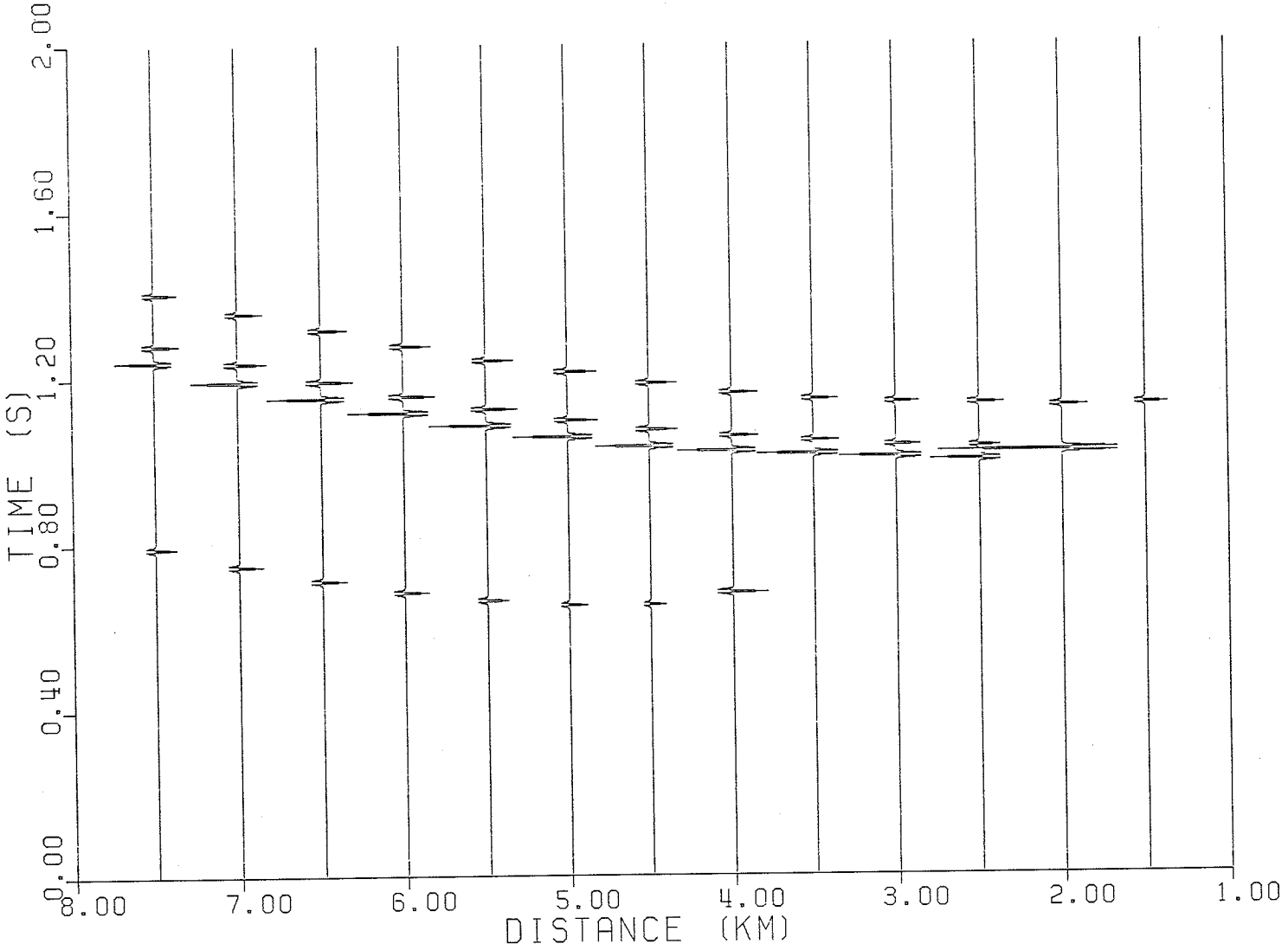


Figure 5.7. (b) Synthetic seismogram of the model shown in part (a).

dip of the layers in the North Range seismic models will be uniformly taken as 30° .

Once a seismic model for a barren geological structure is constructed, the next logical step will be to modify this model so that it can include a mineralized zone and obtain a seismic equivalent for the geological section of Figure 5.1b. Before attempting to make a seismic representation of the exact mineralized zones in the North Range environment, it will be useful to construct a model with a planar massive sulphide zone and see how much it affects the seismic response. This was done in Figure 5.8a, where a layer of massive sulphide is sandwitched between the felsic norite and the footwall rocks with a velocity model as shown in Figure 5.6b. In this model, it is possible to include two layers representing mafic norite and granite breccia, between the sulphide and the felsic norite. However, a close examination of Figures 5.2 and 5.3 shows that felsic norite and granite breccia have approximately identical acoustic impedance and the two interfaces above the massive sulphide (felsic norite/mafic norite and mafic norite/granite breccia) have very low reflection coefficients. The required impedance contrast at the top of the sulphide layer will not be affected by replacing the granite breccia with felsic norite. This avoids the possible computing error that might arise from including two thin layers with two weak interfaces. This arrangement also lowers the computing time by about 30 percent.

The synthetic section for the model of figure 5.8a is given in Figure 5.8b. The most pronounced picture of this section is the distinctly high reflection amplitude coming from the top and bottom of the sul-

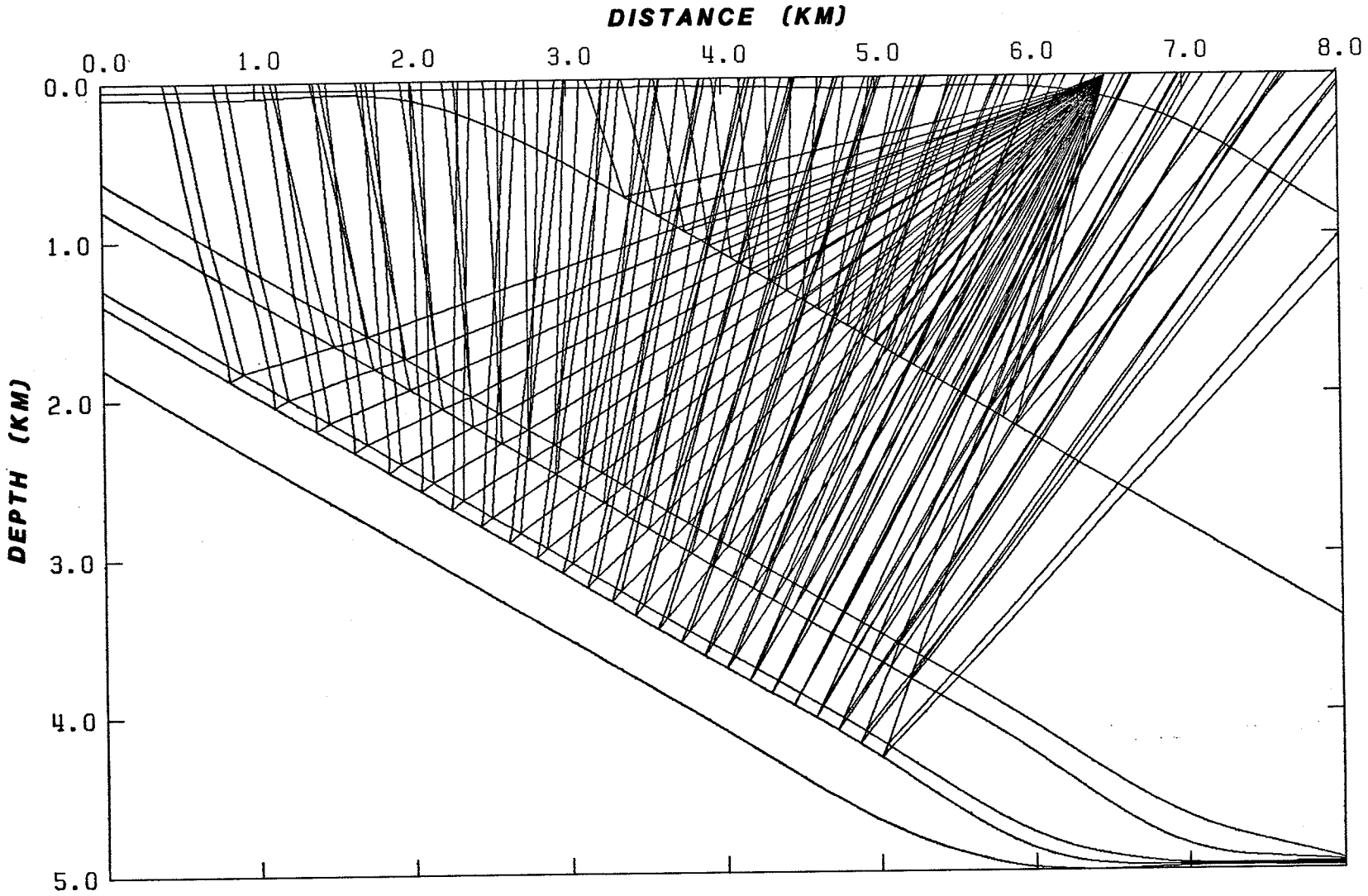


Figure 5.8. (a) Ray tracing of the North Range environment model with a sulphide layer inserted between the felsic norite and the footwall.

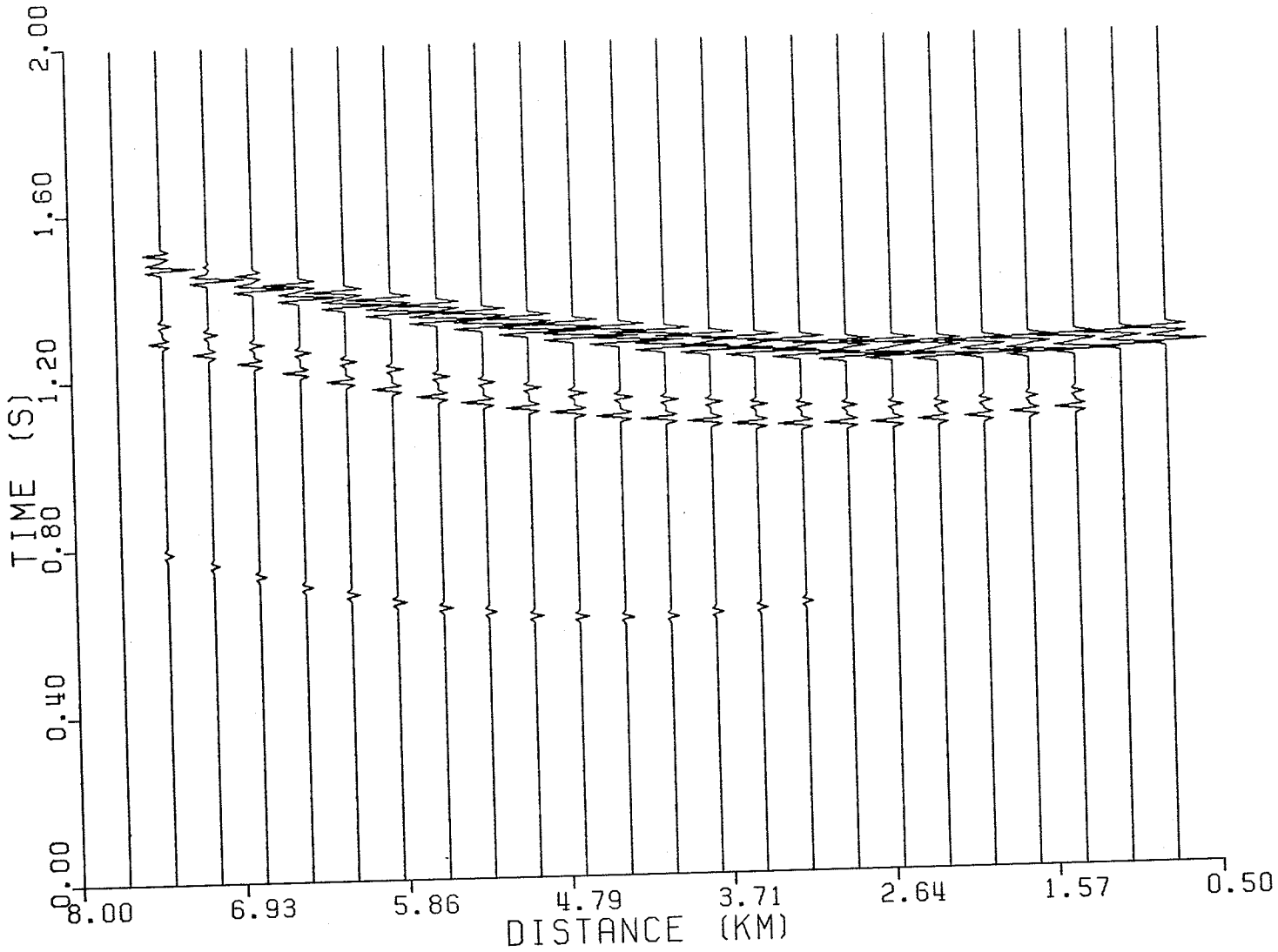


Figure 5.8. (b) Synthetic seismogram of the model shown in part (a).

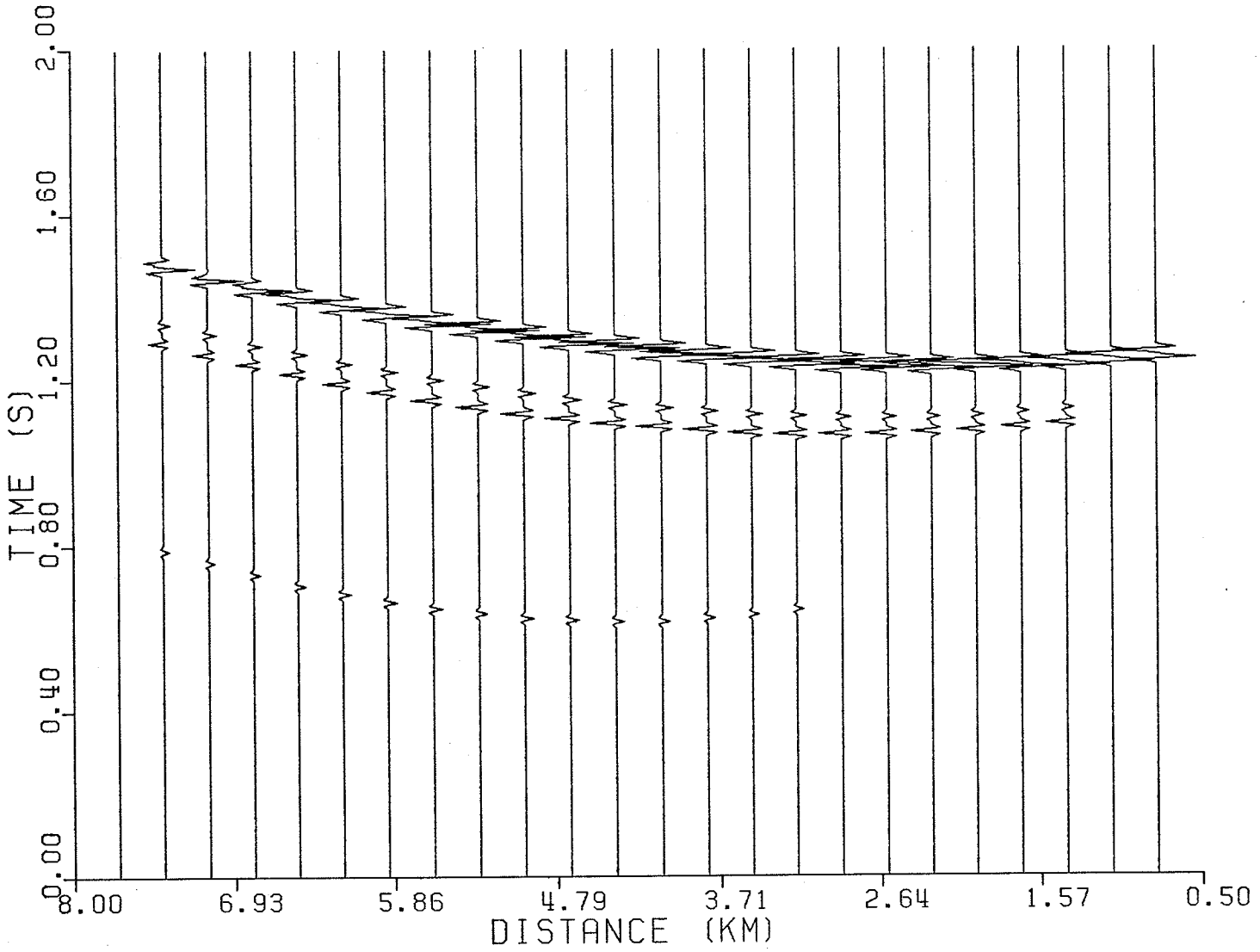


Figure 5.8. (c) Synthetic seismogram of the model shown in part (a), the sulphide body has a thickness of 45 m (the maximum thickness of massive sulphides in the North Range).

phide layer. There is also a phase reversal in the form of the signal reflected from the two interfaces, which will be manifested as long as the two arrivals are separated in time. This degree of resolution, however, may not be achieved in real geological conditions. The thickness of massive sulphide in the area is known to vary from a few meters to 45 m (N.L. Anderson, personnal communication), but the synthetic section of Figure 5.8b requires a thickness of 85 m for the sulphide layer. The maximum realistic thickness of the sulphide layer (45 m) results in the response shown in Figure 5.8c. There may be an uncertainity as to how thick the sulphide zone is, but the response is still strong enough to reveal the presence of the zone. Recently, however, the introduction of high resolution seismic techniques has greatly improved the limit of resolution. Thus, through the use of this new technique, it would be possible to map mineralized bodies of the type found in Sudbury.

The last model pertinent to the geology of the North Range environment is the one that has a greater depth extent and a correspondingly large lateral extent, Figure 5.9a. This model is very similar to the model of Figure 5.5a in many respects; the same attitude and thickness of layers, elastic parameters etc. The source-receiver position is arranged in such a way that the subsurface mapping will be twice as deep as the previous models. This is with the intention that a model of this scale can provide more valuable information for future structural studies of the Basin as a whole.

It can be observed from the synthetic section of this model (Figure 5.9b) that there are arrivals all the way from 1.3 seconds to about 3.0

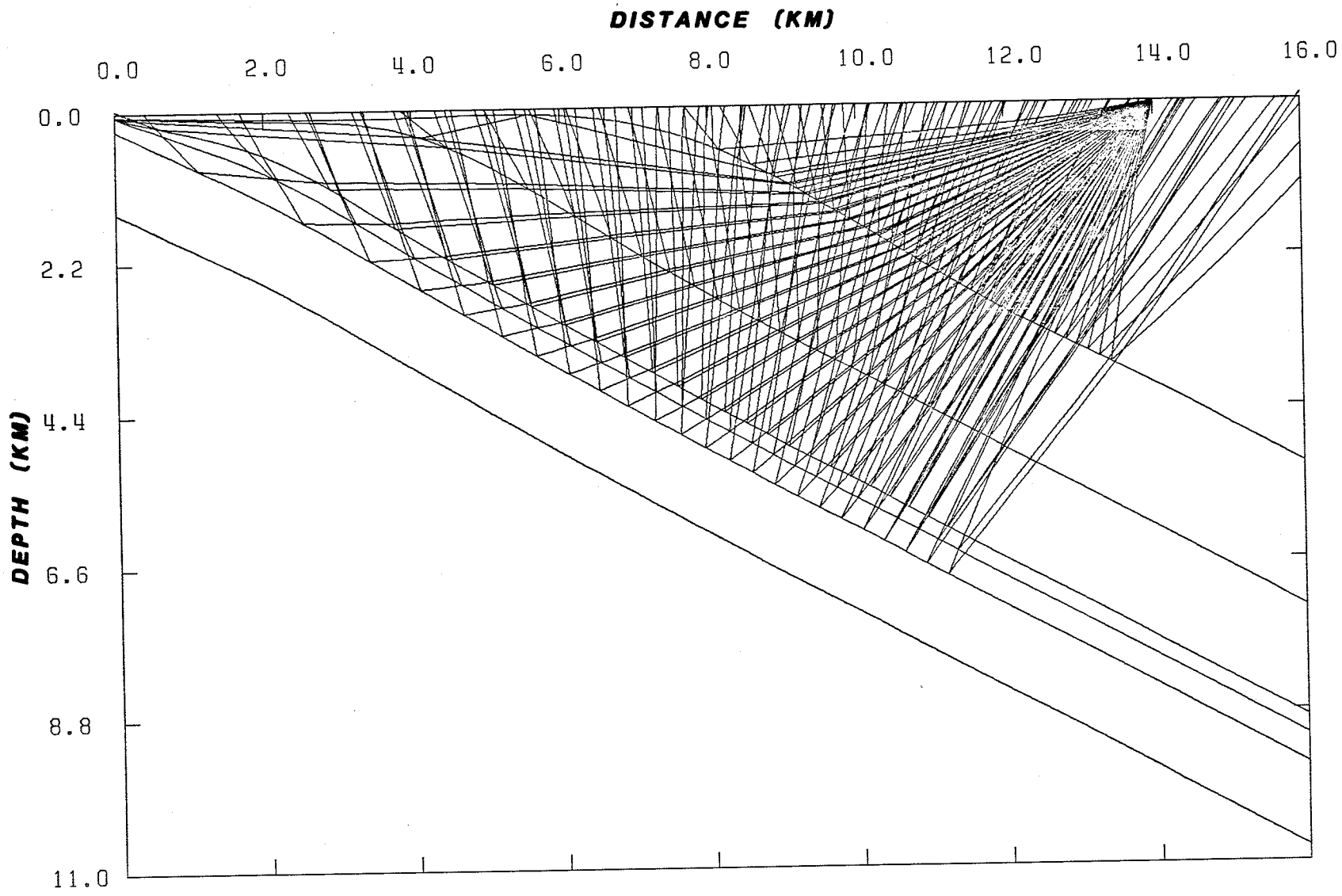


Figure 5.9. (a) Ray tracing of the deep North Range environment model

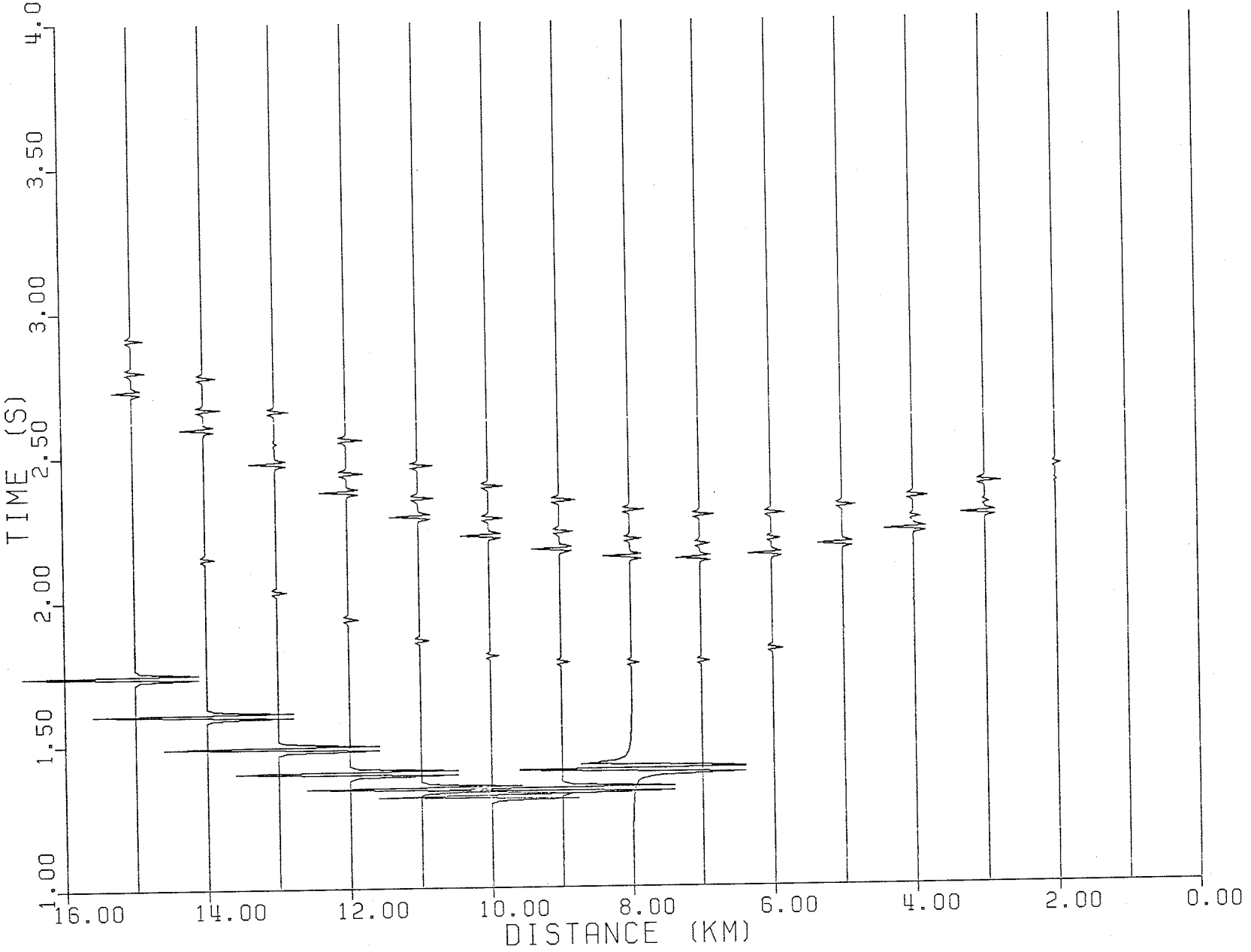


Figure 5.9. (b) Synthetic seismogram of the model shown in part (a).

seconds, approximately twice the arrival time for the shallow models. The reflection from the top of the Onaping layer has been included in the section, and shows up as a uniquely high amplitude arrival. This amplitude characteristic is the result of the low P-wave velocity assigned to the layer representing the sedimentary formations and the shallowness of the interface. For reflections coming below this interface, the temporal as well as the amplitude relationship is generally similar to the one obtained for the shallow models. The reflection from the oxide-rich quartz gabbro is still the most prominent arrival, and the arrival from the top of the micropegmatite layer is the weakest. Thus one can expect to obtain reliable reflections from the oxide-rich quartz gabbro even at such great depths.

More exploration significance can be attached to the present model if it can be modified so as to give some indication of the presence of a mineralized zone. On the other hand, all the available seismic techniques (with the exception of high resolution seismic techniques) can hardly detect a geological unit with a thickness less than 45 m (maximum thickness of massive sulphide) at a depth of 5 - 8 km. Thus it will be meaningless to put a sulphide layer below the felsic norite, as in Figure 5.8a. Consequently a different, but geologically more plausible approach was employed. On the North Range, the ore-bodies are typically associated with mafic sub-layer rocks (Dence, 1978: see also Figure 5.1b) that underlie the main body of norite and make a sharp contact with the underlying footwall rocks. This unit is reasonably thicker than a massive sulphide zone and has a much wider extent. Furthermore, the reflection coefficient obtained when the mafic sub-layer is in contact with granite gneiss is sufficiently high to warrant sub-

stantial reflections.

Thus the barren model of Figure 5.9a was modified by inserting a 200 m thick mafic sub-layer (maximum thickness for this unit is 300 m, N.L.Anderson, personnal communication) between the felsic norite and the footwall rocks (Figure 5.10a and 5.10b). The reflection from the bottom of the mafic sub-layer is as strong as the reflection from the top of the oxide-rich quartz gabbro. Hence, reflections of this magnitude, if correlated over large distances, can result in more diagnostic geophysical data which can be used to outline probable mineralized zones.

## 5.5 On the seismic model of the Sudbury Basin

One of the objectives of a future seismic survey in Sudbury would be to promote the present understanding of the whole Sudbury Structure. A large scale seismic survey covering the whole Basin may define the real shape of the structure, which in turn would provide valuable information regarding the origin of the entire structure. On the basis of the available geological as well as geophysical data, several authors have suggested a number of models for the Sudbury Basin (Peredery, 1972; Popelar, 1972; Patison, 1979). Recently, a model which provides a simple explanation for the field, petrographic and mineralogical data available to date has been suggested (Dence, 1978). Although some compositional differences are known to exist, rocks of the North and South Ranges are very similar. In this case the elastic properties of the core samples from the North Range environment, as determined in chapter 3, can be projected to represent the velocity distribution of the whole

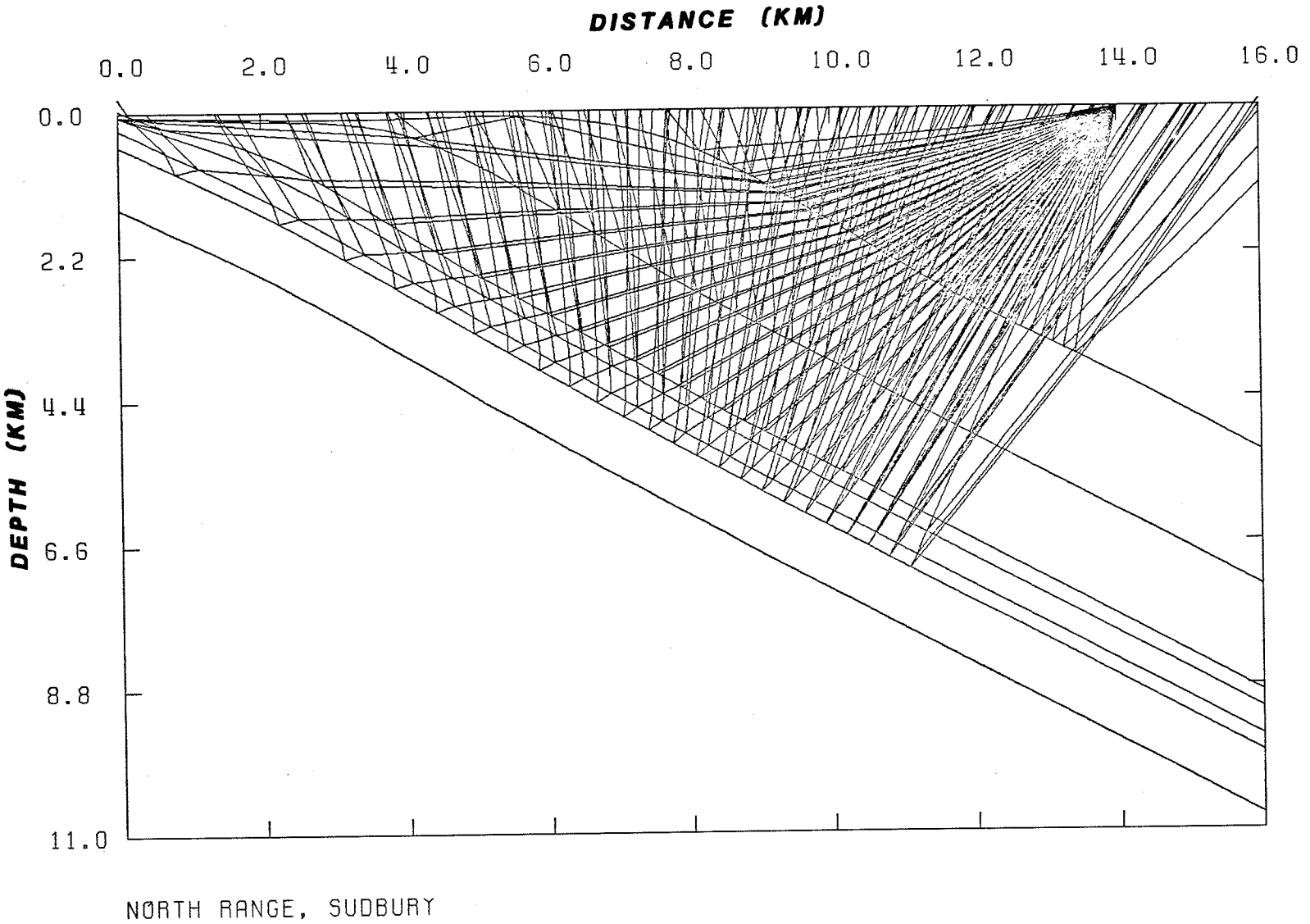


Figure 5.10. (a) Ray tracing of the deep North Range environment model with mafic norite sub-layer inserted between the felsic norite and footwall.

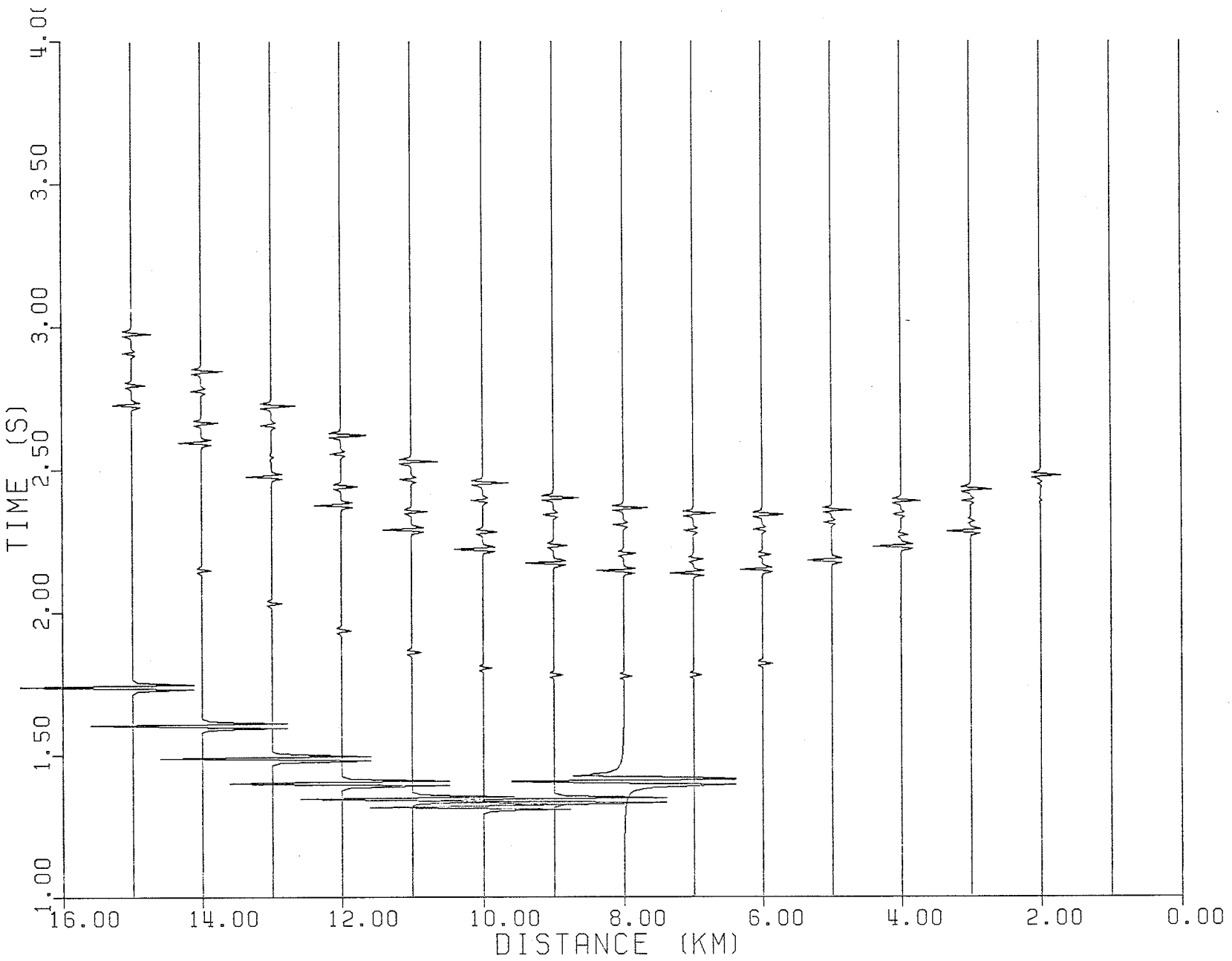


Figure 5.10. (b) Synthetic seismogram of the model shown in part (a).

Sudbury Basin. The velocity data combined with the postulated geological models can result in a simplified seismic model for the Basin, (Figures 5.11a and 5.11b).

The horizontal extent of the model is taken to be the same as the width of the Sudbury Basin and the maximum depth is within the range of values predicted by most geological models. The North Range contacts are dipping at 30° , whereas the South Range contacts have an average dip of 47° (the true geological dip is between 50° and 70° ). Layer thicknesses and velocity distribution are approximately the same as the model of Figure 5.9a. The rock unit that served as a marker horizon in the models of the North Range environment, oxide-rich quartz gabbro and its south range equivalent, upper gabbro, are represented by one unit in this model. Similarly, mafic norite and its South Range counterpart quartz-rich norite are taken to be identical.

The travel time of the model with the source located in the center of the Basin is relatively complicated. Nevertheless, the relative importance of the different arrivals is generally maintained. Actual seismic surveys of this nature may result in a more complicated travel-time picture which might create some problems of phase identification. Contributing factors to this kind of problem may be changes in the attitude of formations within each limb of the Basin, lack of continuity of reflections due to irregularity of contacts, and diffractions from faults, terminating beds, etc.

The synthetic seismogram obtained by including a mafic norite layer between the felsic norite and the footwll rocks (Figures 5.12a and 5.12b) has the same degree of travel time complication as the previous

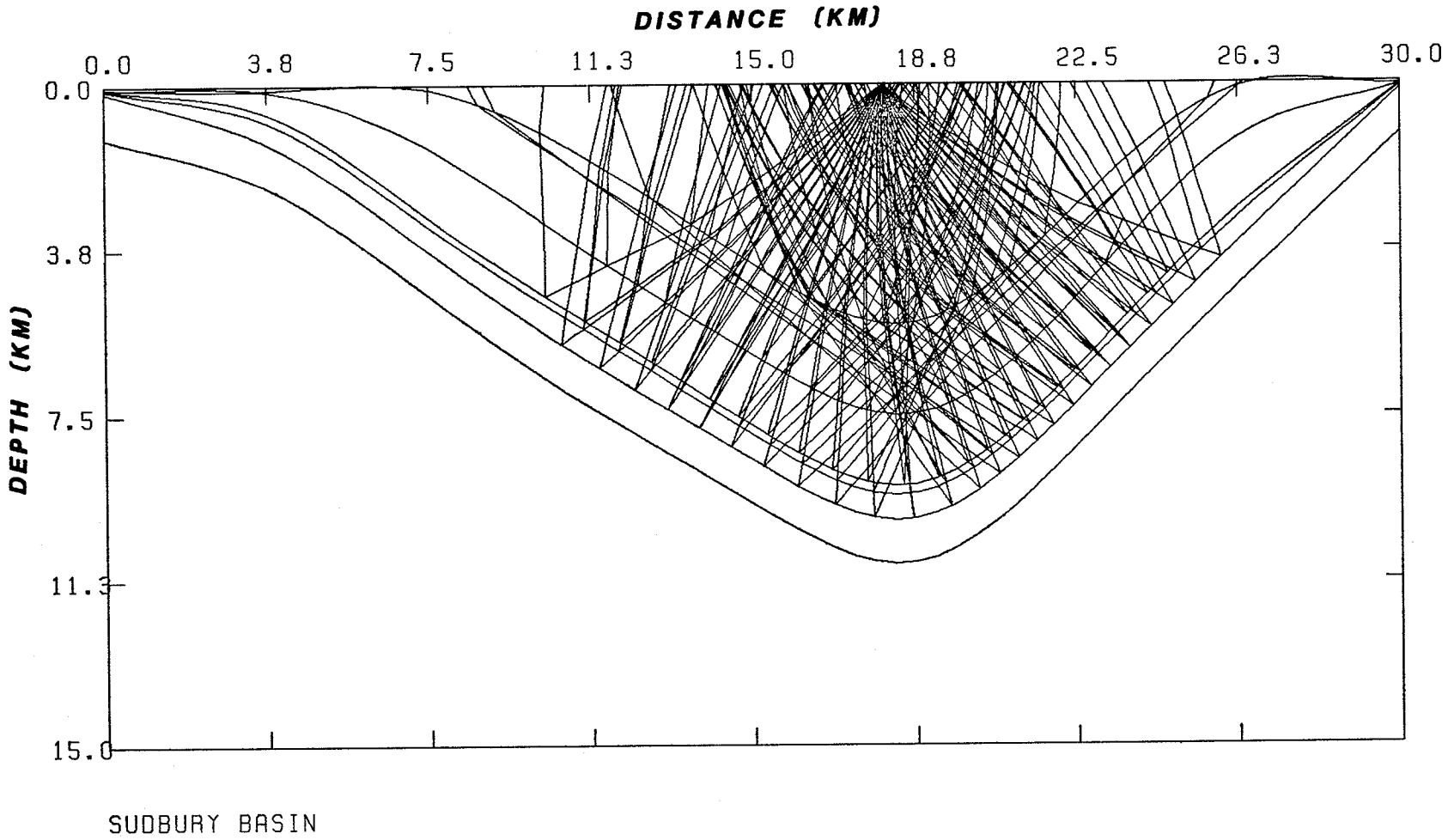


Figure 5.11. (a) Ray tracing of the Sudbury Basin model; source located at 18 km distance from the origin.

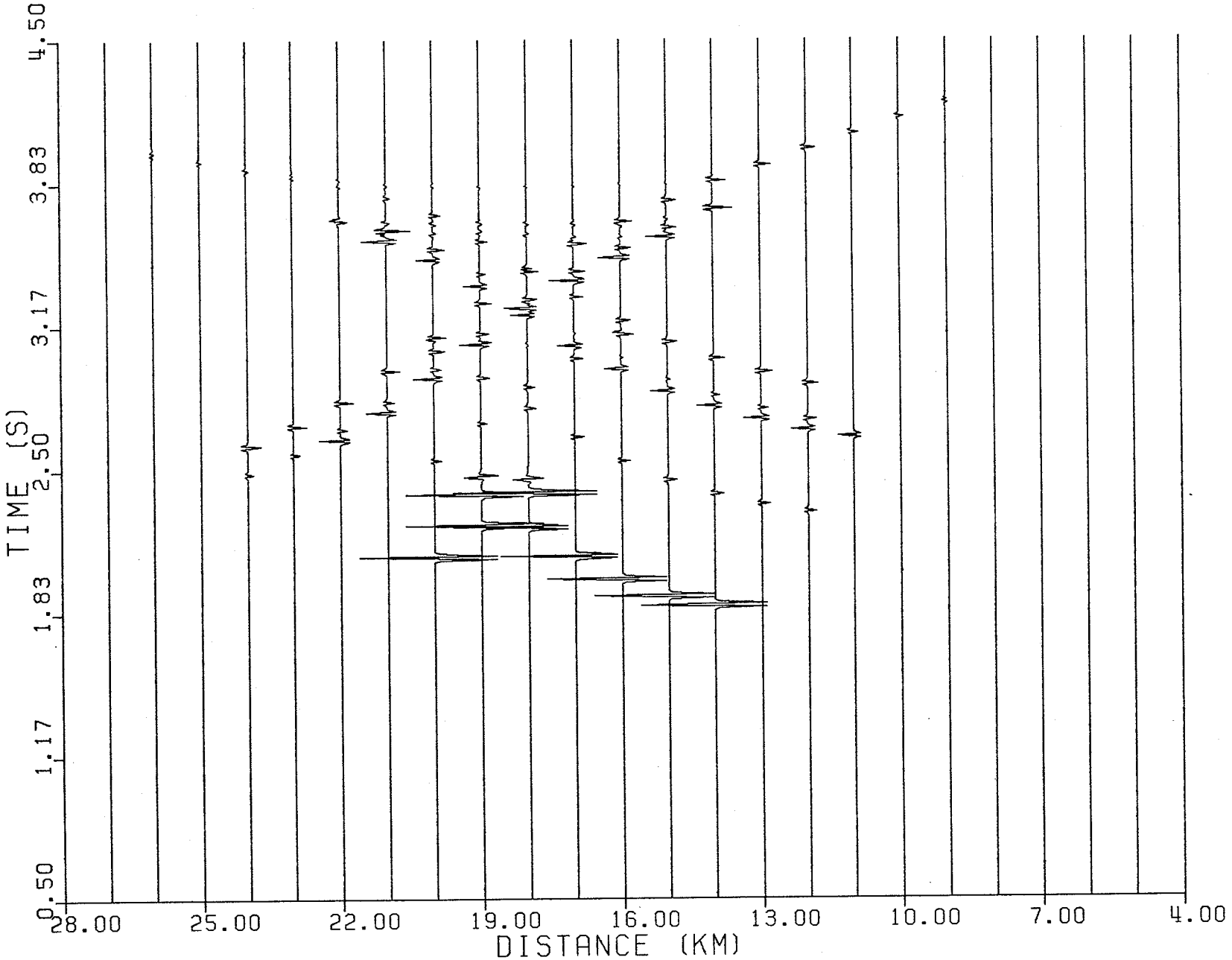


Figure 5.11. (b) Synthetic seismogram of the Sudbury Basin model.

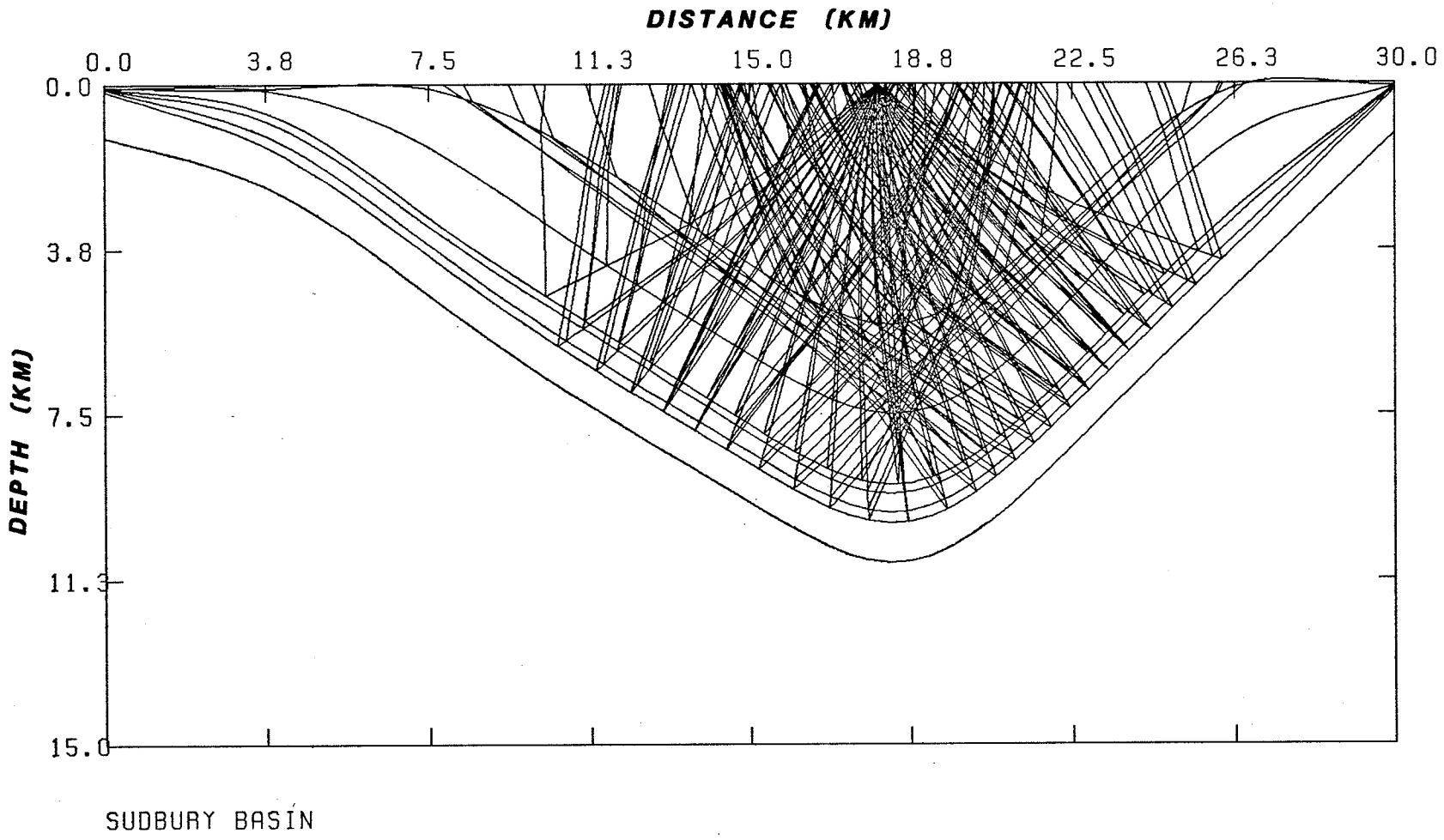


Figure 5.12. (a) Ray tracing of the Sudbury Basin model with mafic norite sub-layer inserted between the felsic norite and the footwall.

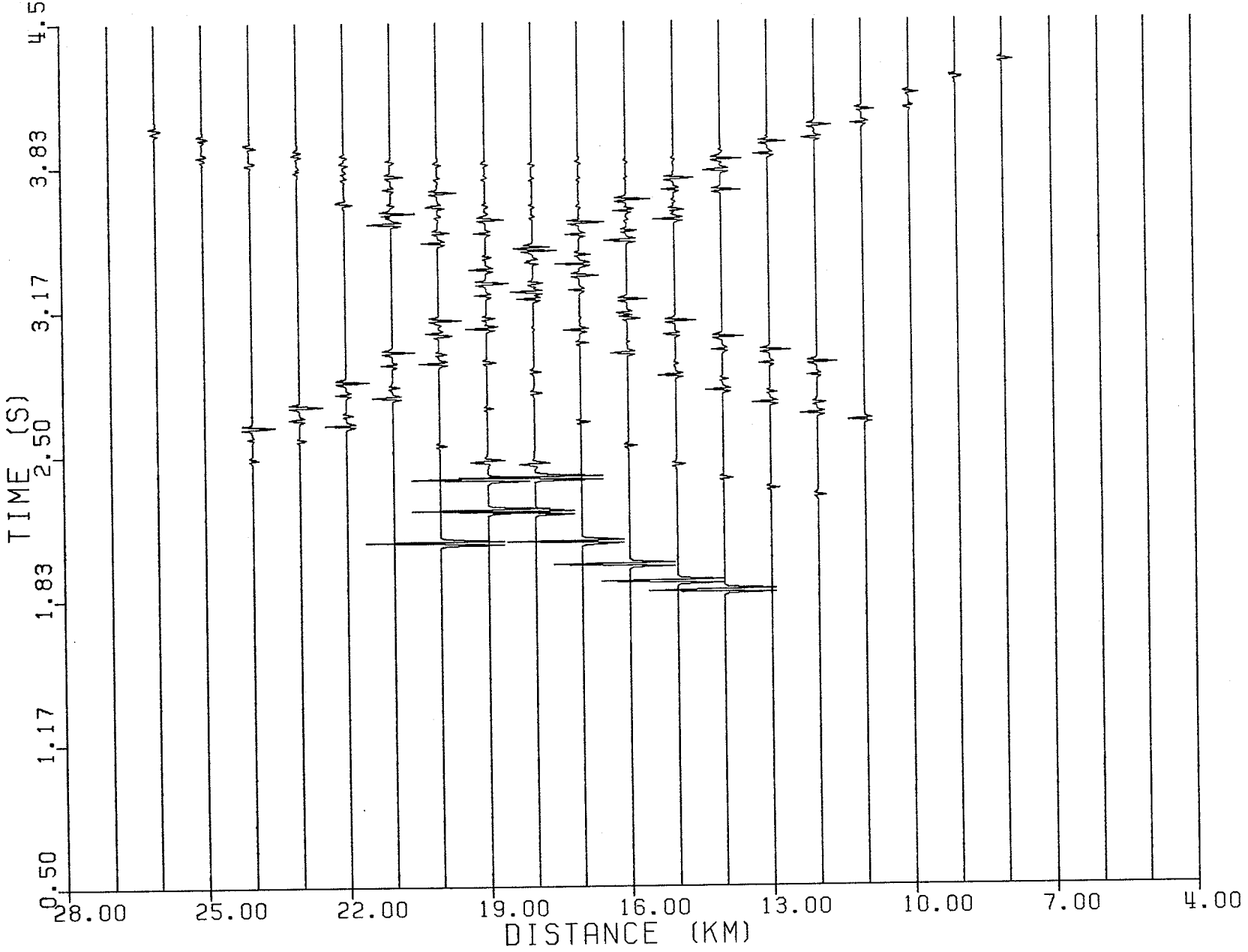


Figure 5.12. (b) Synthetic seismogram of the model shown in part (a).

model. However, the presence of another strong late arrival originating from the bottom of the mafic norite will obviously have a positive contribution to phase identification.

At this stage, it will be more instructive to see the seismic response of the Basin when the source is moved from the present position(18 km from the origin). For this purpose, two more seismic responses, one by moving the source position 4 km towards the North Range (Figures 5.13a and 5.13b) and another by moving the source 4 km towards the South Range (Figure 5.14a and 5.14b), were obtained. The first thing to be noticed from these results is that the kind of symmetry observed in the travel time of the previous response is very much distorted. Also, there appears to be a reduction in the amplitude of the reflections below the micropegmatite when the source is moved towards the South Range. The most probable source of this reduction could be the relatively steep dip of the interfaces on this side of the Basin.

There is one more interesting lesson we can learn from the comparison of Figures 5.13b and 5.10b. Both seismograms were generated by putting the source at a distance of 14 km from the origin. Any feature that is absent in figure 5.10b, but present in figure 5.13b is caused by the presence of the South Range limb of the structure. Thus, late arrivals similar to the ones observed in figure 5.13b will be commomly observed in all real seismic surveys carried out in the North Range environment.

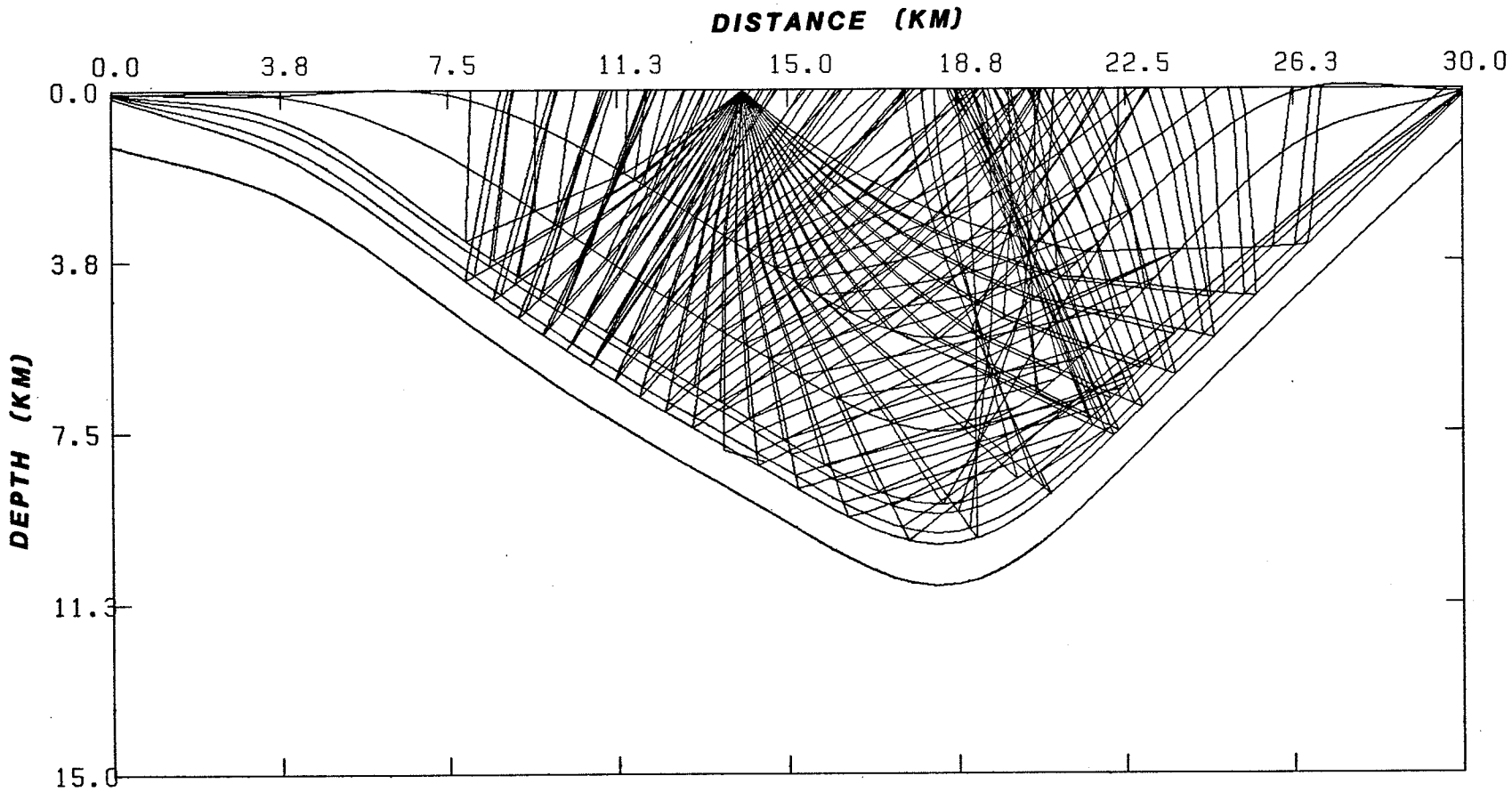


Figure 5.13. (a) Ray tracing of the Sudbury Basin model with the source loated at 14 km distance from the origin.

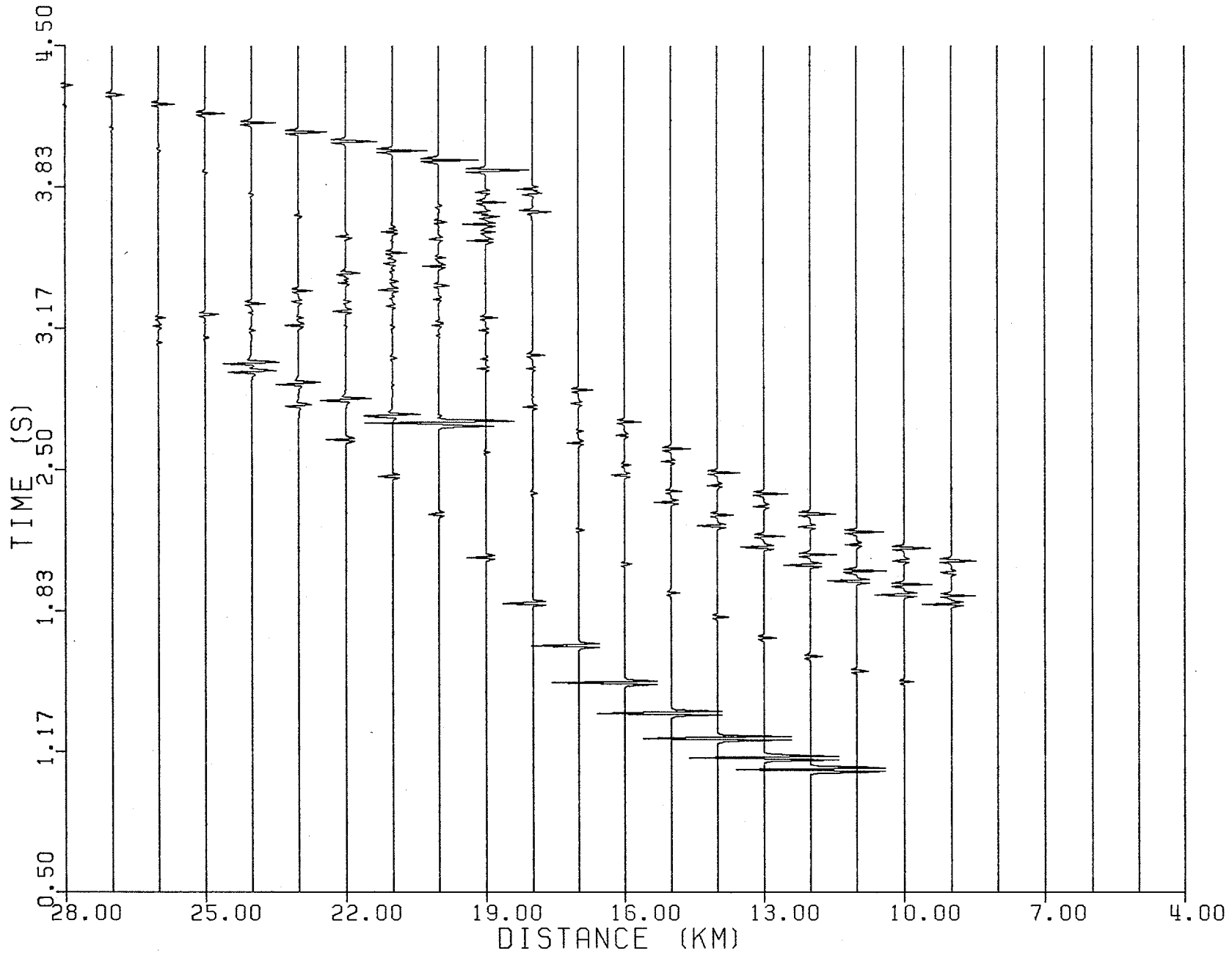


Figure 5.13. (b) Synthetic seismogram of the model shown in part (a).

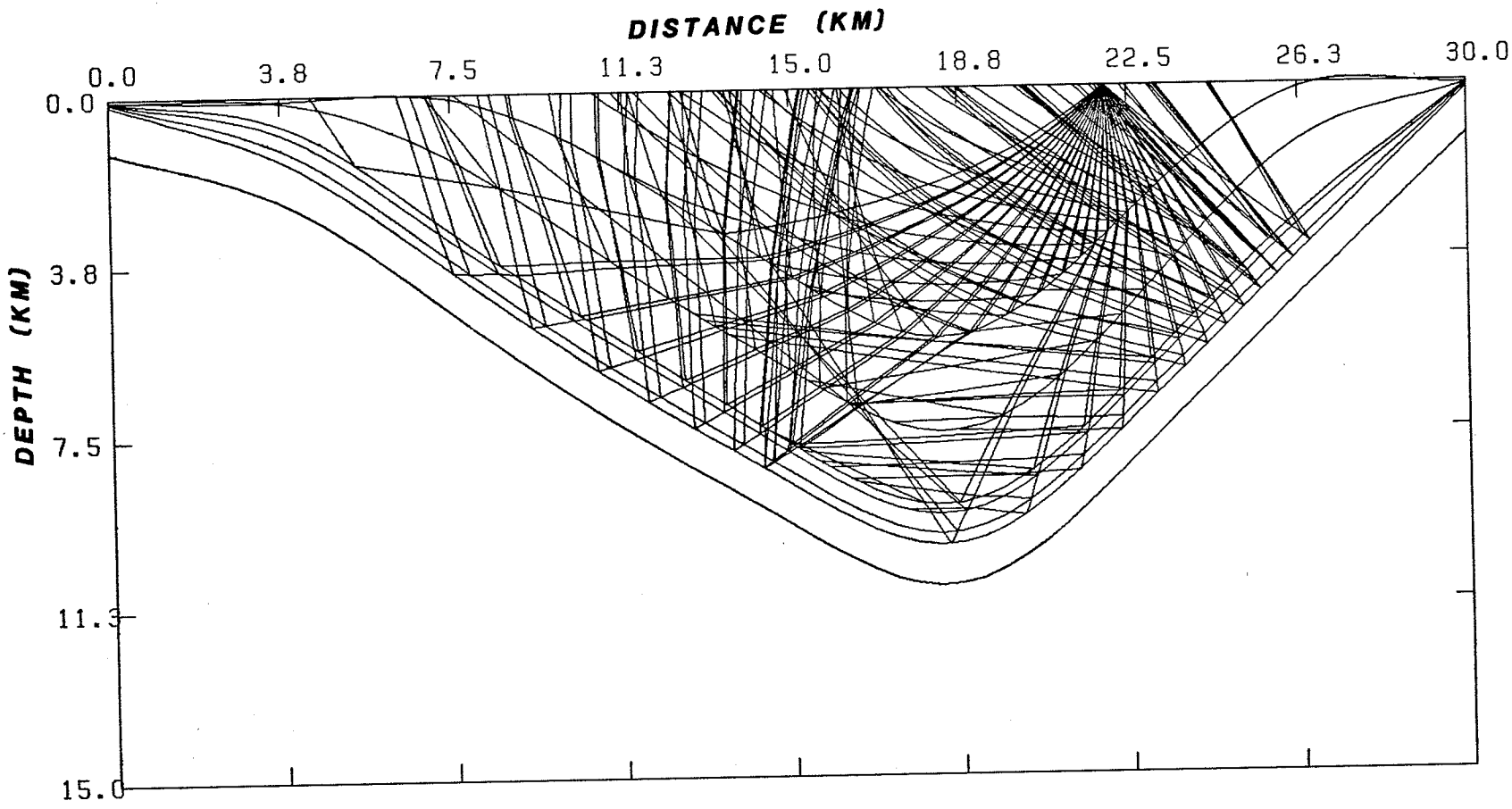


Figure 5.14. (a) Ray tracing of the Sudbury Basin model with the source located at 22 km from the origin.

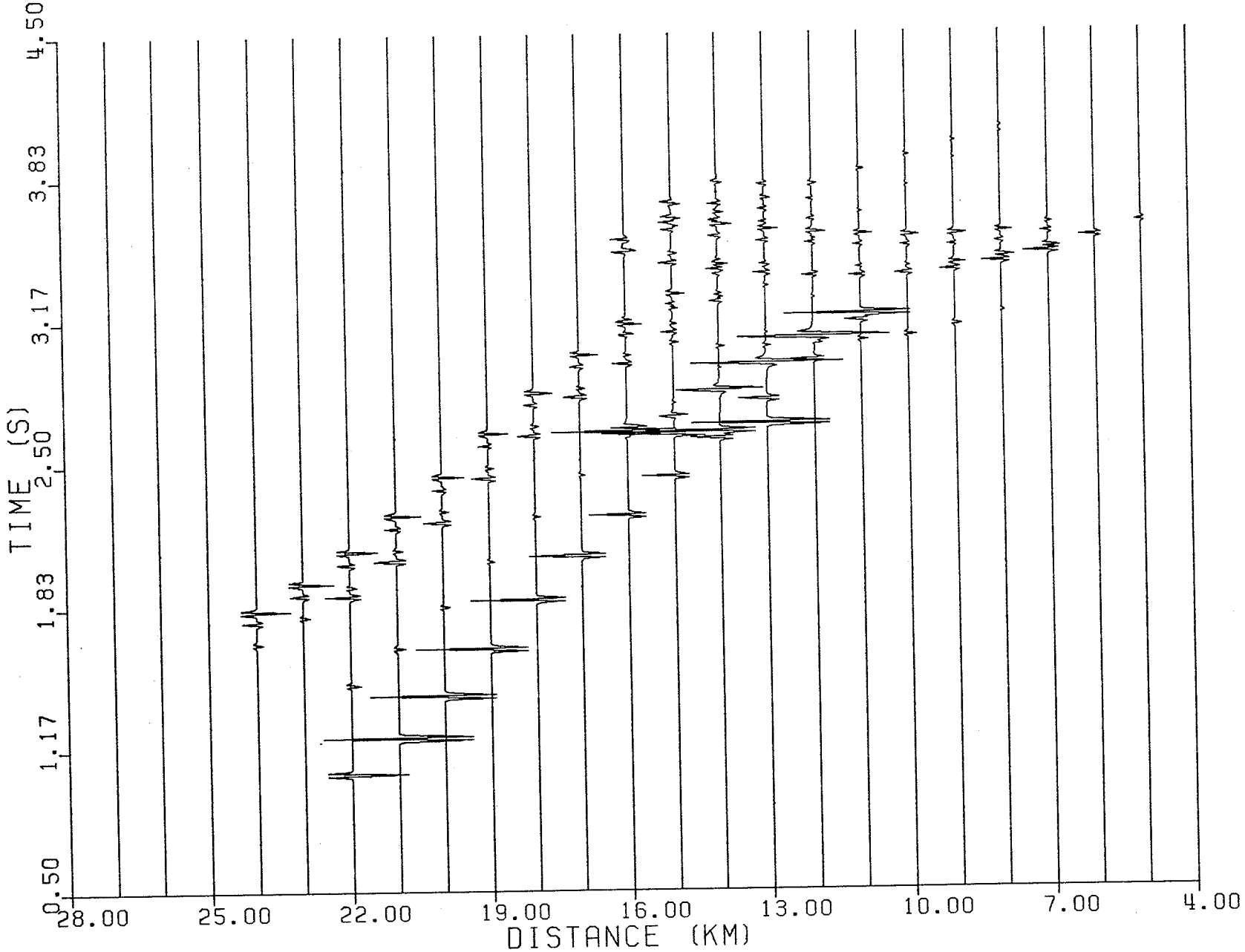


Figure 5.14. (b) Synthetic seismogram of the model shown in part (a).

## 5.6 Models of fine structures

The seismic modelling was so far directed towards investigating the contact relationships of major rock units in order to promote our understanding of the Sudbury Structure. This in turn may have a significant contribution to the ongoing search for a better explanation of the origin of the Sudbury Structure. However, the ultimate objective of a seismic survey in the area is to delineate zones of mineralization that have economic viability. This may assume an indirect approach, where one looks for structures favourable for the accumulation of the target material (the classical example is petroleum exploration), or a direct approach whereby the target material can be recognized by its seismic properties alone. In mineral exploration, it appears that both approaches are equally valid. In Sudbury, for example, the approximately planar-to-lenticular ore-bodies of the South Range can be handled by the direct approach, and the embayment structures of the North Range by the indirect approach.

One of the fundamental differences between prospecting for petroleum as opposed to ore deposits is that petroleum normally occurs in structures wherein the largest dimensions are in the horizontal plane presenting a fairly large target for both geophysical methods and drilling. In contrast, most ore deposits have large vertical dimensions with relatively small horizontal extent, resulting in a horizontally narrow target. Also, the compexity of ore-bearing structures and the diversity of associated rock types have demanded more precise methods of identifying them (Hobson, 1967).

A first step in implementing seismic techniques to search for ore deposits will be to simulate typical mineralized zones and generate their seismic response. This will be accomplished in the present section.

The first two seismic models will be devoted to generate the seismic responses of typical ore-bodies in the North and South Ranges, as portrayed in the diagramatic sections of Figures 2.4a and 2.4b. South Range ore-bodies as in Creighton and Murray, can be considered infinite in two dimensions, therefore they can be approximated by a lenticular sulphide body with vertical dimensions of about 0.5 km. Hanging wall rocks are represented by main irruptive norite (upper most layer, Figure 5.15a), contaminated norite and the gabbro-peridotite inclusion sulphide zone. The last two rock units are typically found in the South Range and no measured P-wave velocity was available. It was assumed, however, that the rock next to the felsic norite will have a velocity similar to mafic norite. The gabbro-peridotite zone, on the other hand, has relatively more sulphide content and it was felt more appropriate to assign it a velocity even lower than felsic norite. Due to the wide occurrence of mafic metavolcanic rocks in the Proterozoic rocks of the South Range, the velocity of the footwall rocks was taken to be that of mafic gneiss.

The resulting synthetic section is given in Figure 5.15b. The sulphide body is outlined by a uniquely high amplitude reflection but appears relatively thicker in the time section because of the velocity pull-down arising from the low velocity of the sulphide. In this case, the velocity pull-down will have a positive contribution to the resolv-

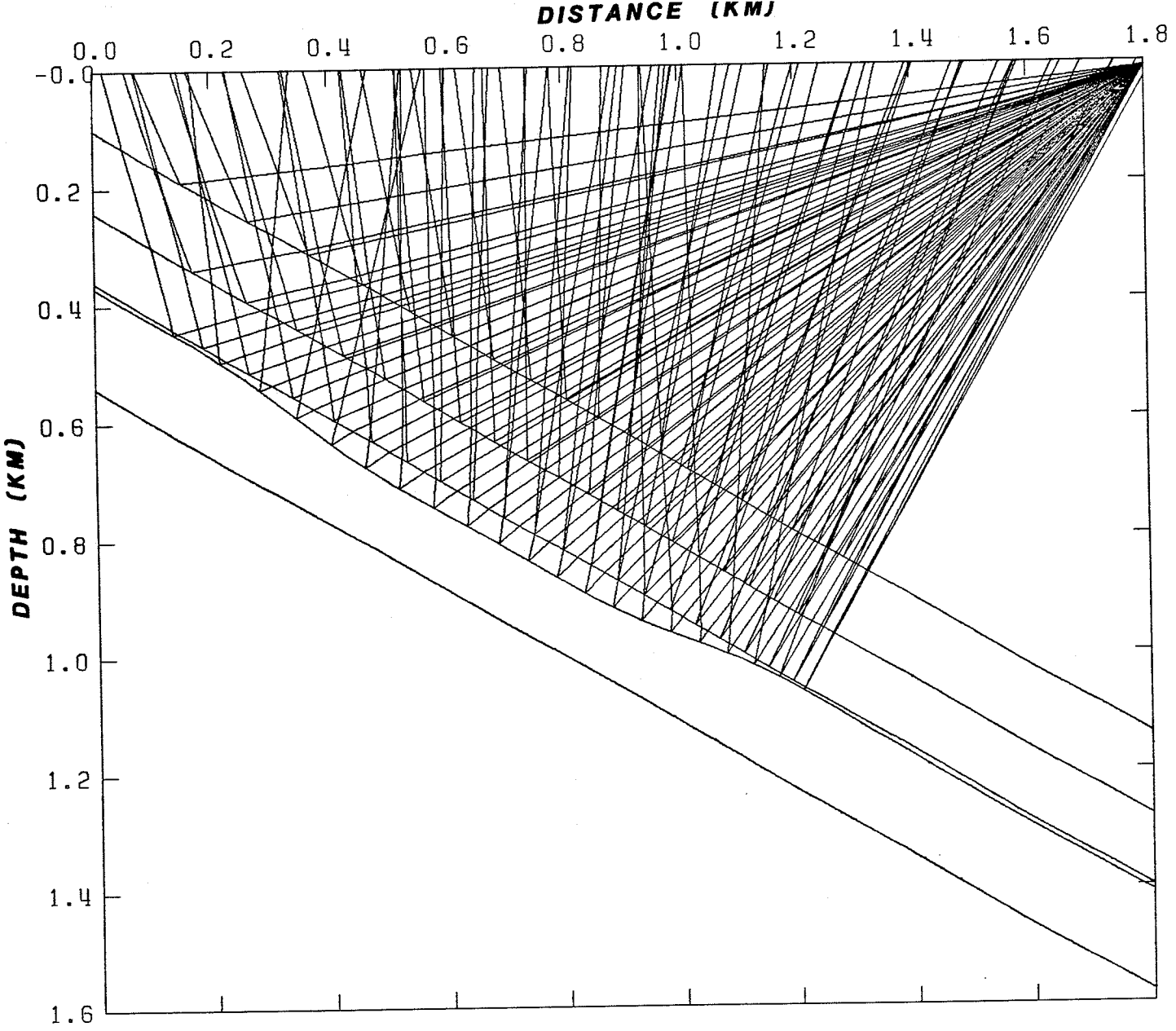


Figure 5.15. (a) ray tracing of a mineralized zone in the South Range environment.

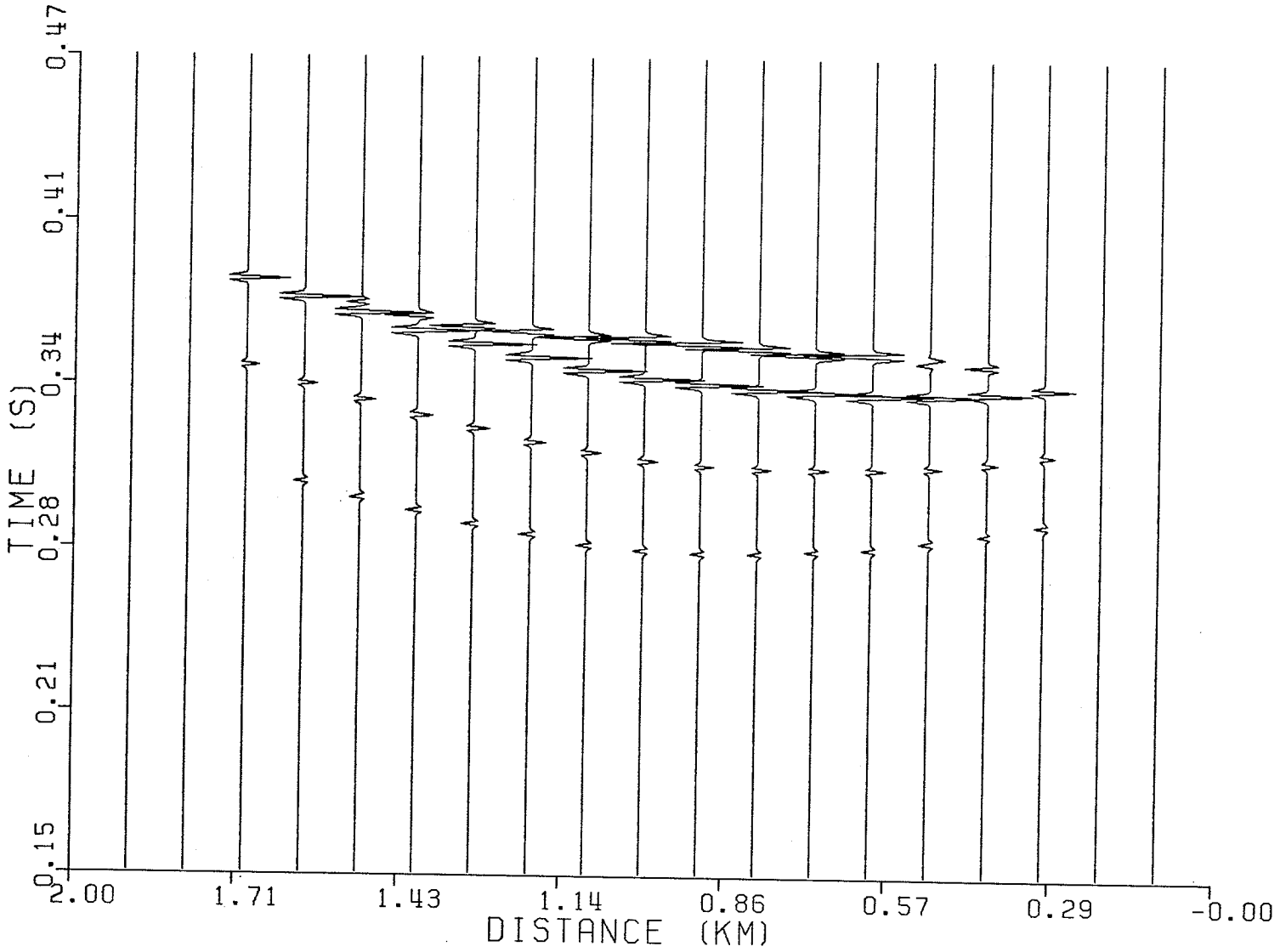


Figure 5.15. (b) Synthetic seismogram of the model shown in part (a).

ing power of the method. This model may not adequately represent actual South Range mineralized zones. Nevertheless, subsequent inferrences from models of this nature can provide us with some basic information. The construction of more realistic models for this type of mineralization obviously requires a careful assessment of the seismic velocity distribution based on further laboratory-measured velocity data, and the available geological information.

A mineralized zone in the North Range environment can be simulated by replicating the upper half of the mineralized contact in Figure 5.1b. The modelling was further simplified by assuming the seismic source to be located within the felsic norite so that the overall picture resembles the idealized embayment structure of Figure 2.4b. Accordingly, the constituent formations are, from top to bottom, felsic norite, mafic norite, granite breccia, massive sulphide, and granite gneiss(footwall) (Figure 5.16a). Outside the depression, the breccia and the sulphide are made as thin as possible and they are no longer specified by their own velocities. Instead, they will have the same velocity as the footwall rock for distances 0.00 to 0.75 km and 1.25 to 2.00 km. The specification for the rest of the velocity structure is similar to the previous models.

The response as shown in Figure 5.16b is similar to what can be expected from a relatively shallow seismic survey, all the prominent arrivals being recorded within a time span of less than half a second. At the bottom of the depression the breccia and the sulphide are 86 m and 65 m thick, respectively, yet the reflections from the three interfaces are not sufficiently separated in time. The three arrivals have

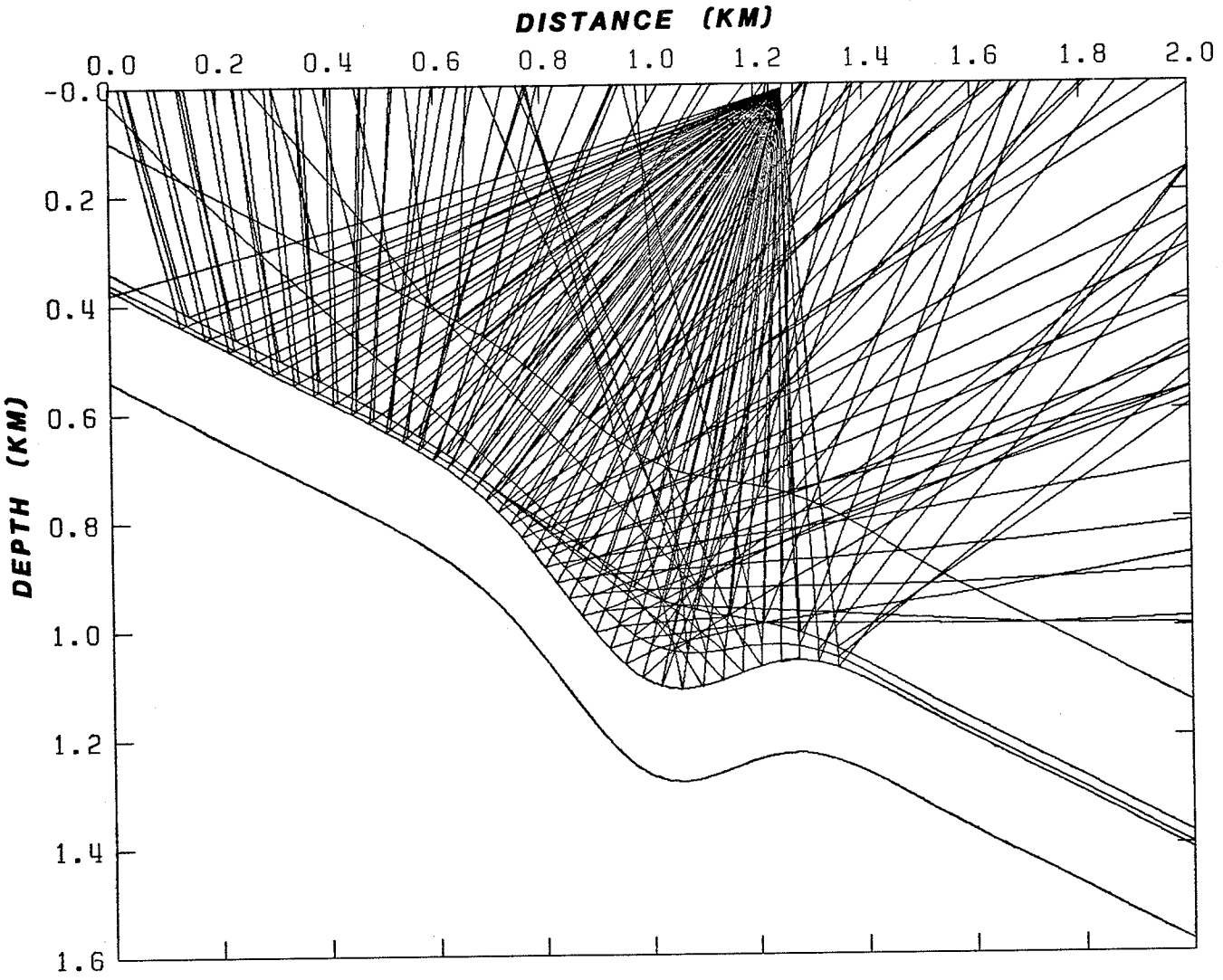


Figure 5.16. (a) Ray tracing of an idealized embayment structure.

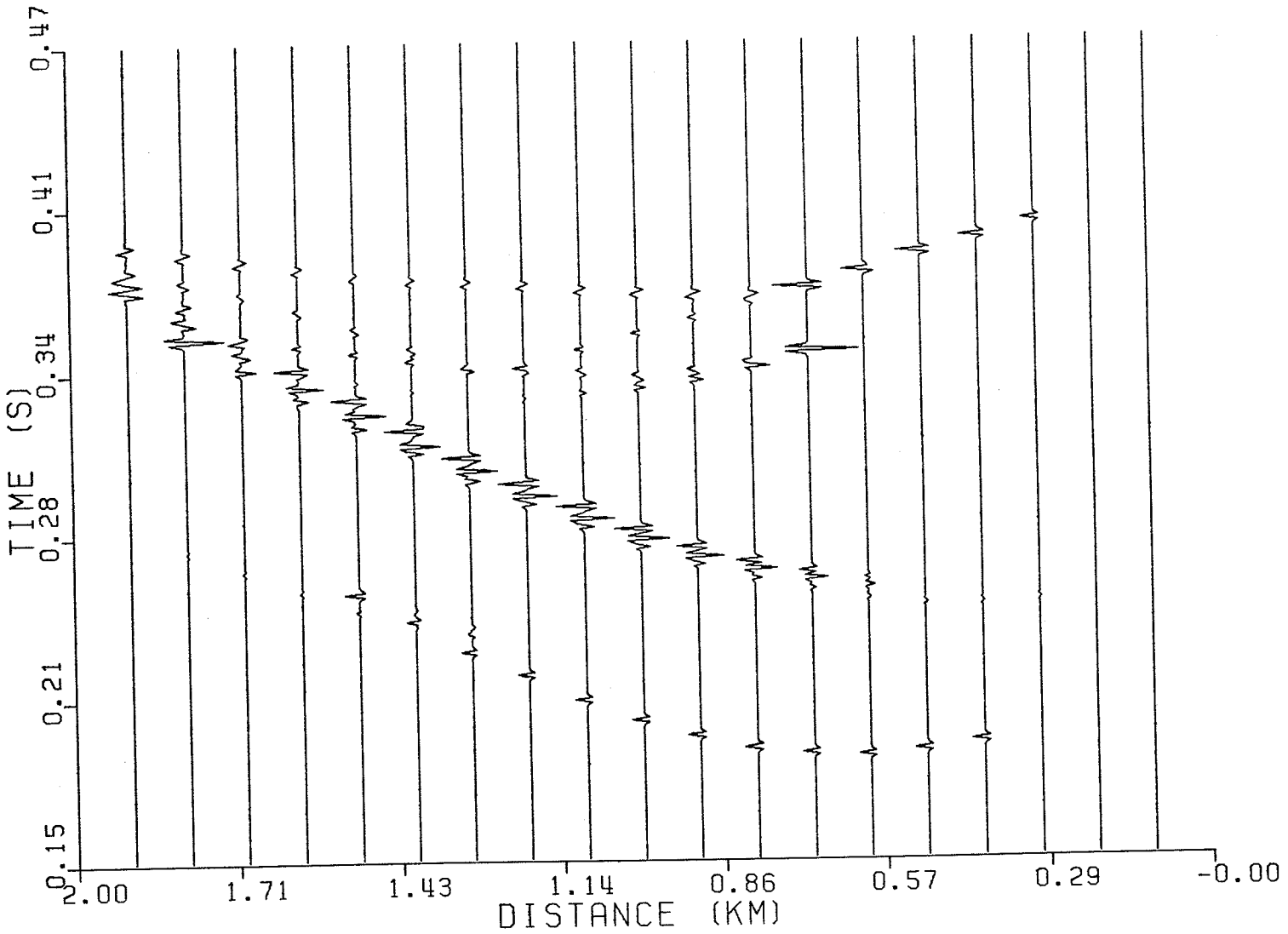


Figure 5.16. (b) Synthetic seismogram of the model shown in part (a).

merged to form one main envelope. In addition to the main arrivals that make up the envelope, there are late arrivals coming from the edges of the depression with amplitudes that diminish rapidly. If properly identified, these features, i.e., the strong envelope and the associated edge scattering, can be good indicaters of the presence of a mineralized embayment structure.

The last seismic model of a mineralzed structure is the one constructed by imitating the mineralized contact of the North Range environment. All rock units, except mafic norite and granite breccia, are included in this model (Figure 5.17a). The thin lenticular medium imbeded between the felsic norite and the footwall rocks (below 2 km and 4 km distance) represents massive sulphide. It has a maximum thickness of 75 m and the velocity of massive sulphide in the indicated regions.

It is to be noted that the sulphide zone in this model can be shaped to have more curvature than the one shown in the figure by supplying more dense input data, but this gives rise to more scattered energy where at one stage becomes too weak to be detected on the surface. The associated scattering may result in a more complicated travel time curve which makes phase identification more difficult.

The reflection from the top and bottom of the depression is generally difficult to recognize, primarily because of the focusing of the rays by the curvature. The amplitude characteristics is also significantly affected (Figure 5.17b). Some arrivals from the sulphide zone have amplitudes which are more or less comparable to the arrivals from the oxide-rich quartz gabbro, which has not been the case when we have a smooth sulphide layer (see Figure 5.8). Nevertheless, the role of

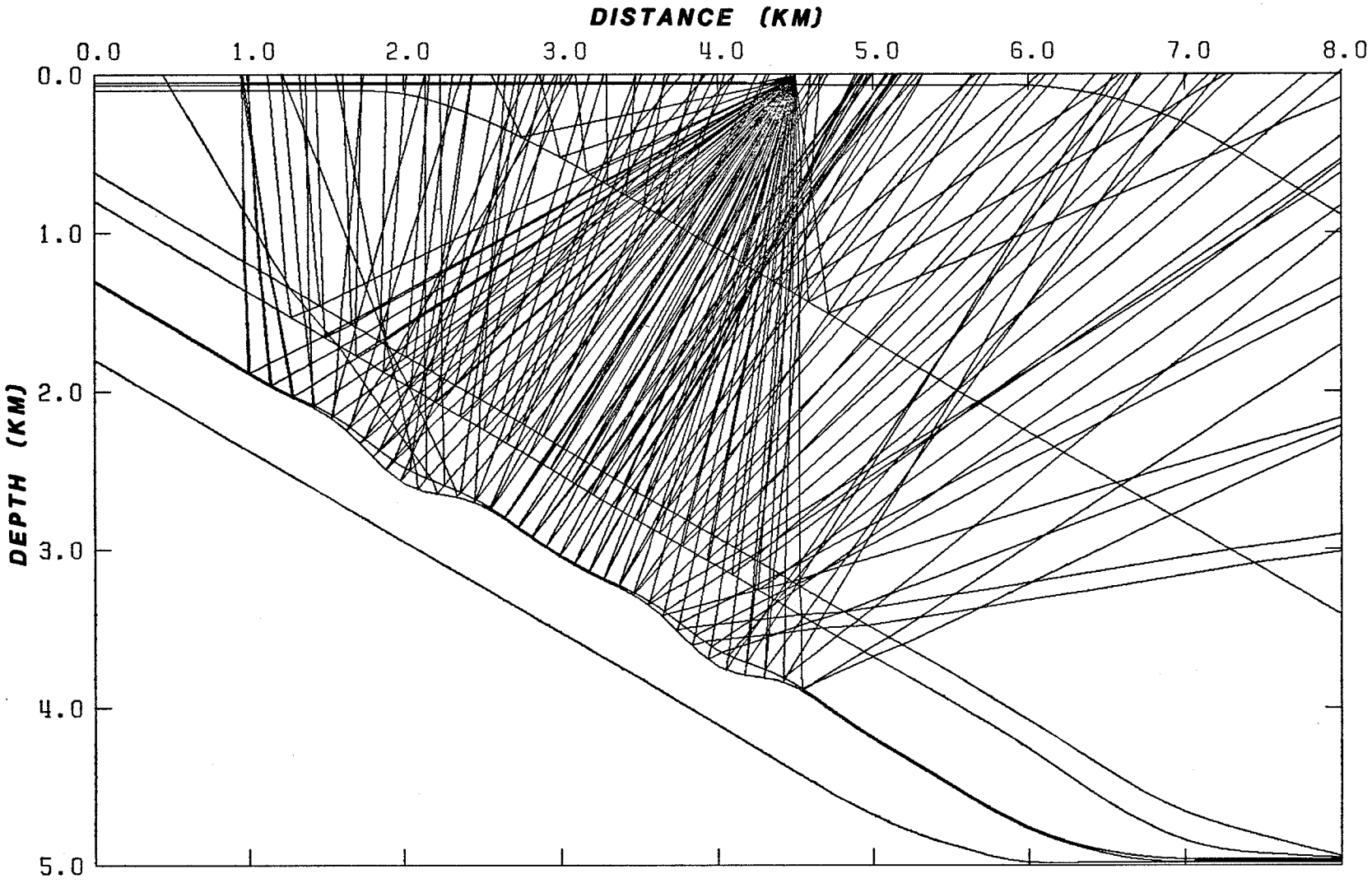


Figure 5.17. (a) Ray tracing of a mineralized contact in the North Range environment with a sulphide mass embeded between felsic norite and footwall rock below 2 km and 4 km distance.

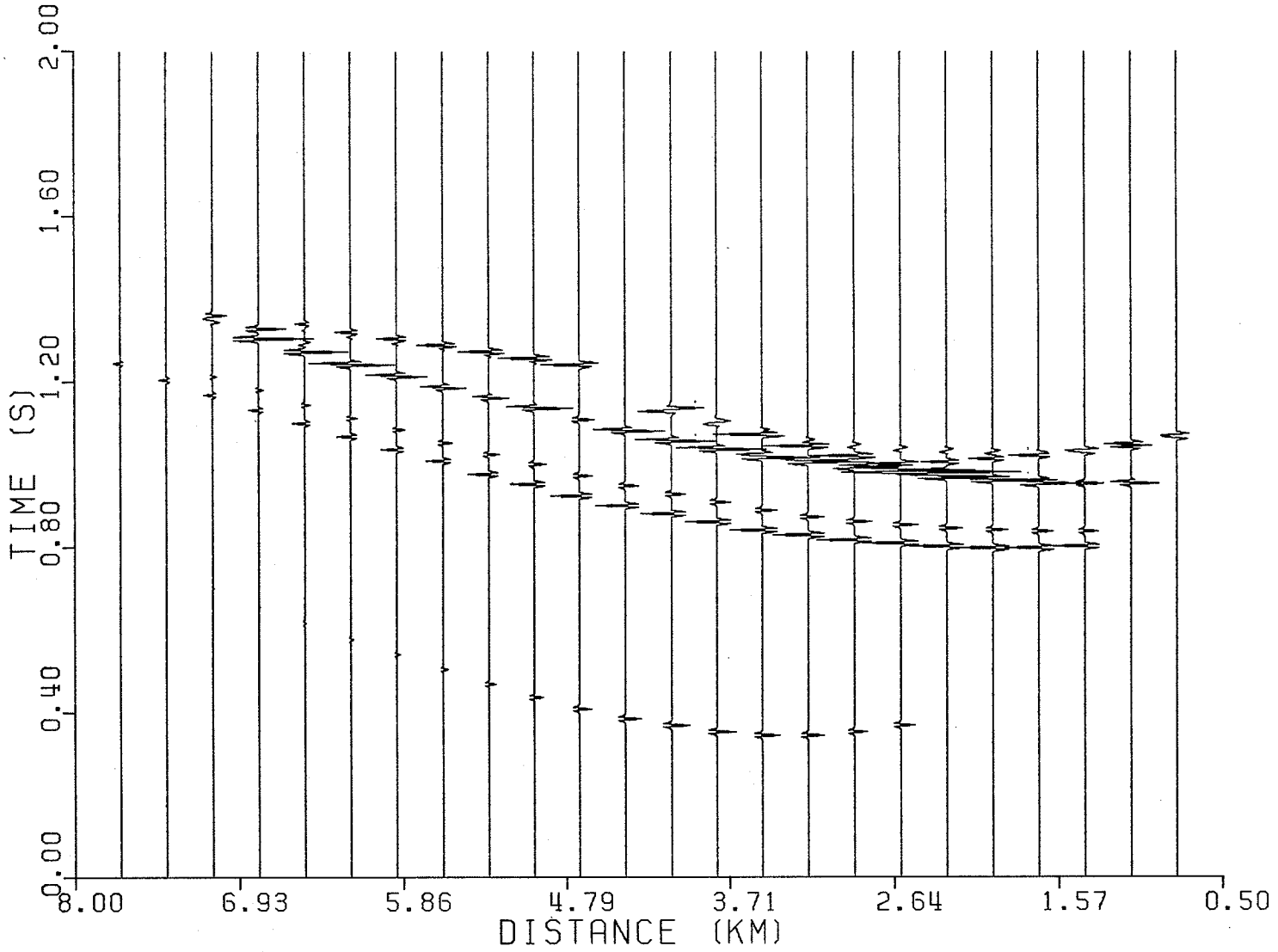


Figure 5.17. (b) Synthetic seismogram of the model shown in part (a).

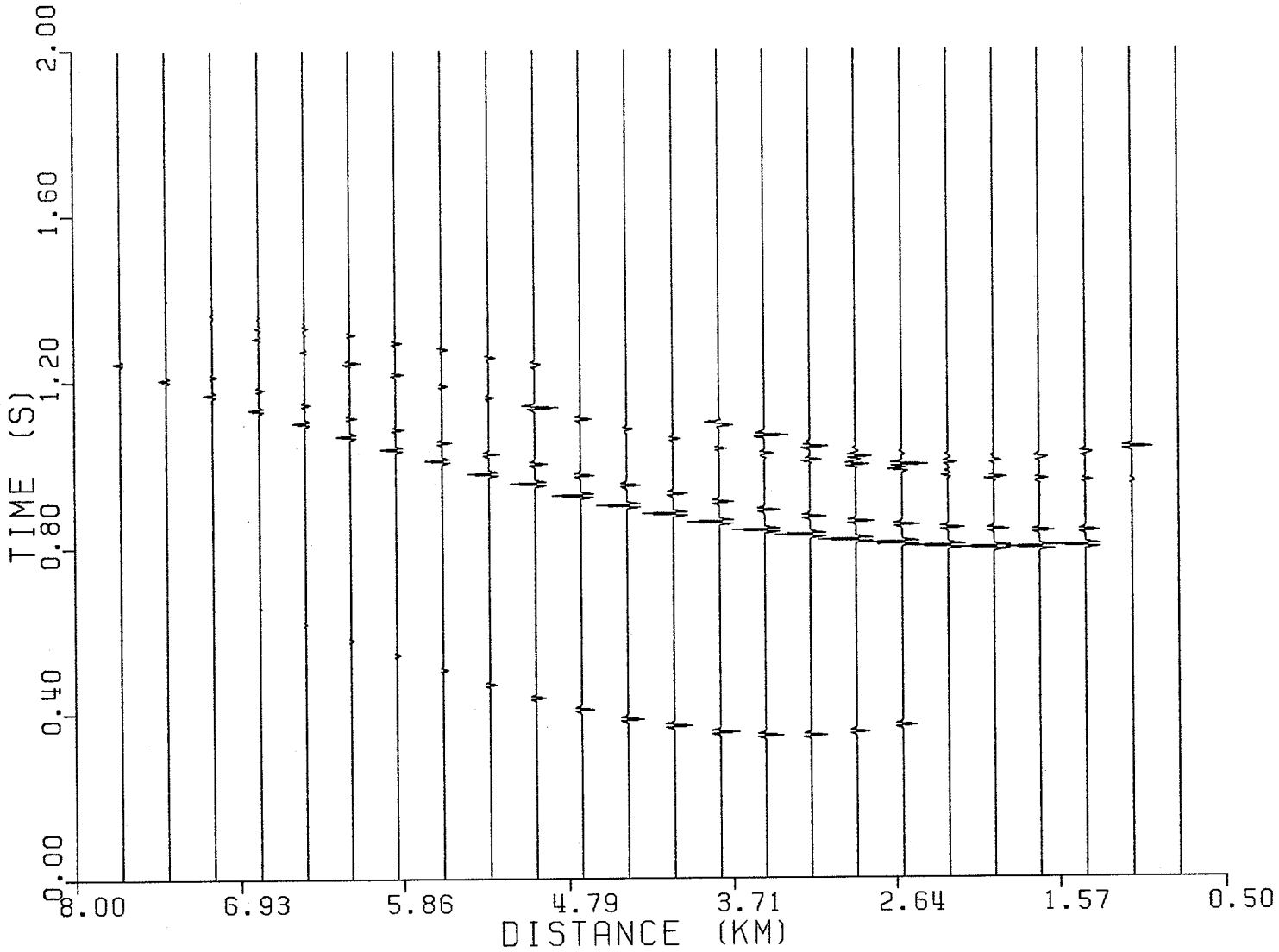


Figure 5.17. (c) Synthetic seismogram of the model shown in part (a) with the massive sulphide body replaced by an ordinary crystalline rock (mafic norite).

the high impedance contrast emanating from the presence of the sulphide body is appreciable. This was more elucidated by modifying the present model as shown in Figure 5.17c. This synthetic section was obtained by putting an ordinary crystalline rock (in this case mafic norite) inside the depression instead of massive sulphide. The travel time pattern in both figures (5.17b and 5.17c) is roughly the same except for the difference in the time gap between the last two reflections. The arrivals from the mineralized depressions (Figure 5.17b) have a wider time separation than the arrivals from the barren depression. Very dramatic differences can be seen in the amplitudes of the seismograms in the two figures, where there is a 75 percent reduction of amplitude when the sulphide is replaced by the ordinary rock. Therefore, the strong reflection amplitude caused by the sulphide, supplemented by the unique travel time originating from the structure may provide substantial information for the presence of a mineralized zone.

In summary, this chapter has incorporated the laboratory-measured P-wave velocities with ray theoretical principles to obtain a seismic expression of known and assumed geological structures. The oxide-rich quartz gabbro of the North Range environment consistently shows up as a marker horizon in all the models simulated. A similar response was obtained when a mafic norite sub-layer is in contact with a granite gneiss footwall. Finally, it was shown that the presence of a massive sulphide layer has a dramatic effect in the amplitude of the seismic response, which can be an extremely valuable criterion in deep seismic exploration for ore minerals.

# Chapter 6

## SOME ASPECTS OF DATA PROCESSING IN MINERAL EXPLORATION

Reflection seismology is a method that maps the subsurface structure of the earth from knowledge of the arrival times and wave forms of seismic events returned from subsurface interfaces. To do so, one should convert the received seismic traces which were recorded as a function of time into a function of depth, i.e., transforming the time series into a depth section of the earth.

In conventional reflection seismics, there are three main processing operations, namely, deconvolution, stacking, and migration. The first operation shifts the energy in the observed time series to the proper place with respect to the time axis, the second to the proper place with respect to the half-offset axis, and the third to the proper places with respect to the mid-point axis (Robinson, 1982) to increase the horizontal resolution. The contribution of the first two operations is the attenuation of multiple reflections, reverberations, and various types of noise. Then the application of migration transforms seismic energy to its proper spatial position.

### 6.1 Multiples in Sudbury

The most common and strongest multiples involve reflections at the surface or at the base of the surface low velocity layer (LVL) where the reflection coefficient is very large because of the large impedance contrast. Because of the double reflection taking place at depth, mutiples are not normally observed as distinct events unless the reflec-

tions are exceptionally high.

For the North Range environment, the most probable multiples were generated by assuming the Onaping formation as the base of the LVL, as shown in Figures 6.1a through 6.1c. The nature of the dip itself allows only very few of the reflected rays to reach the surface (assuming conventional layout) and they have to traverse a much longer path. Having suffered double bounces through a much longer path, multiples from a steeply dipping interface cannot maintain a detectable amplitude, as confirmed by Figure 6.1c. Other multiples generated with the source located between 12 km and 14 km have amplitudes which are three orders of magnitude lower than the weakest reflection. Consequently, they leave no trace at all in the synthetic section. Thus, in Sudbury in particular and in mineral exploration in general, reverberation and multiples are not expected to impose as serious a problem as in petroleum exploration in younger sedimentary basins.

## 6.2 Migration in mineral exploration

The fact that the most common form of occurrence of well known orebodies is in moderately to steeply dipping structures makes migration an indispensable processing operation in mineral exploration, particularly in the Sudbry region. More often, the target area is characterized by substantial lateral velocity variation resulting from steeply dipping formations, faults, and anticlinal and synclinal structures. In Sudbury, dips of 30° - 45° (North Range) and 50° - 70° are common features. Also, all the major rock units in Sudbury are frequently

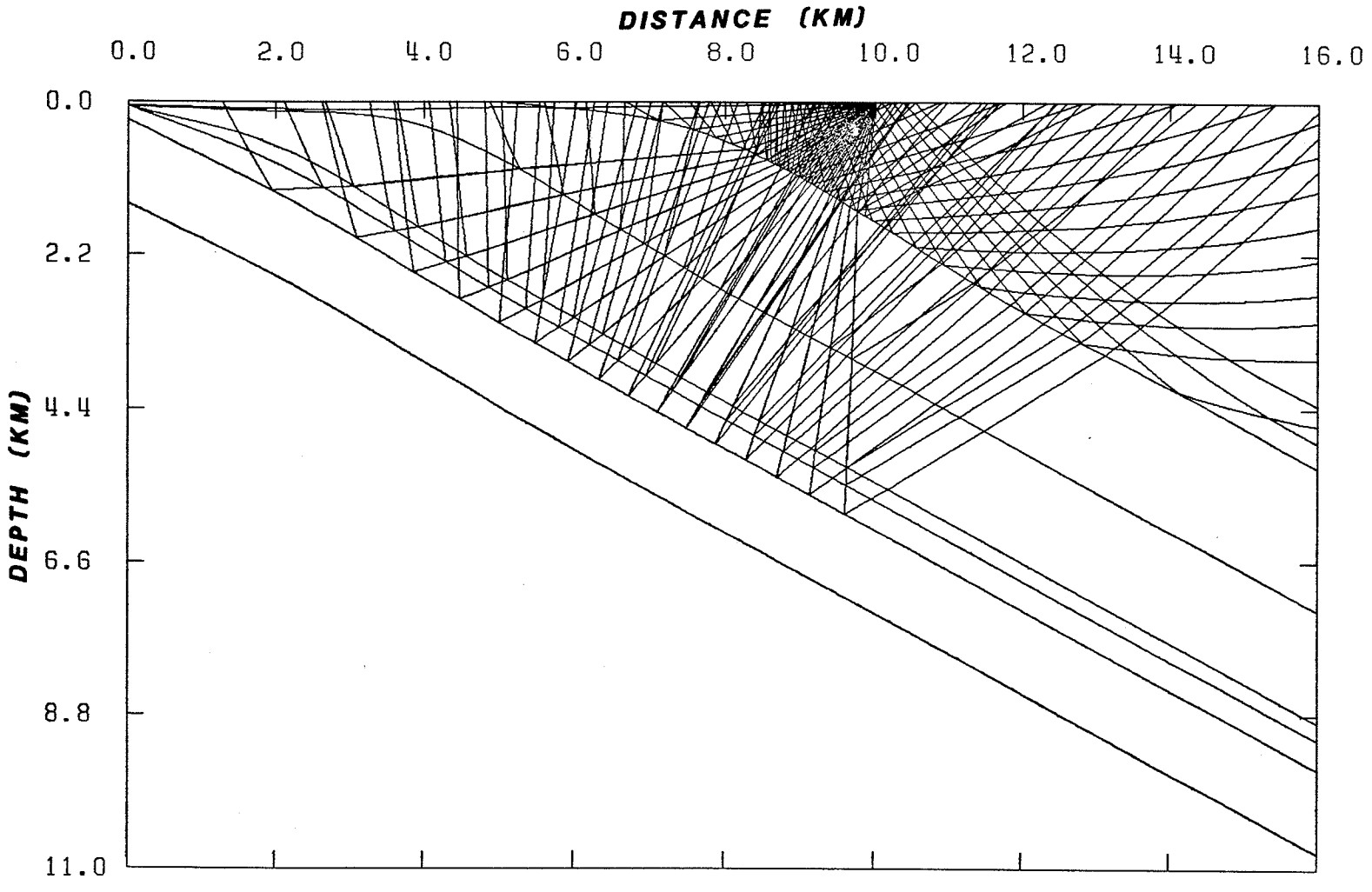


Figure 6.1. (a) Ray tracing of the deep North Range environment model with multiples from the top of the Onaping formation included.

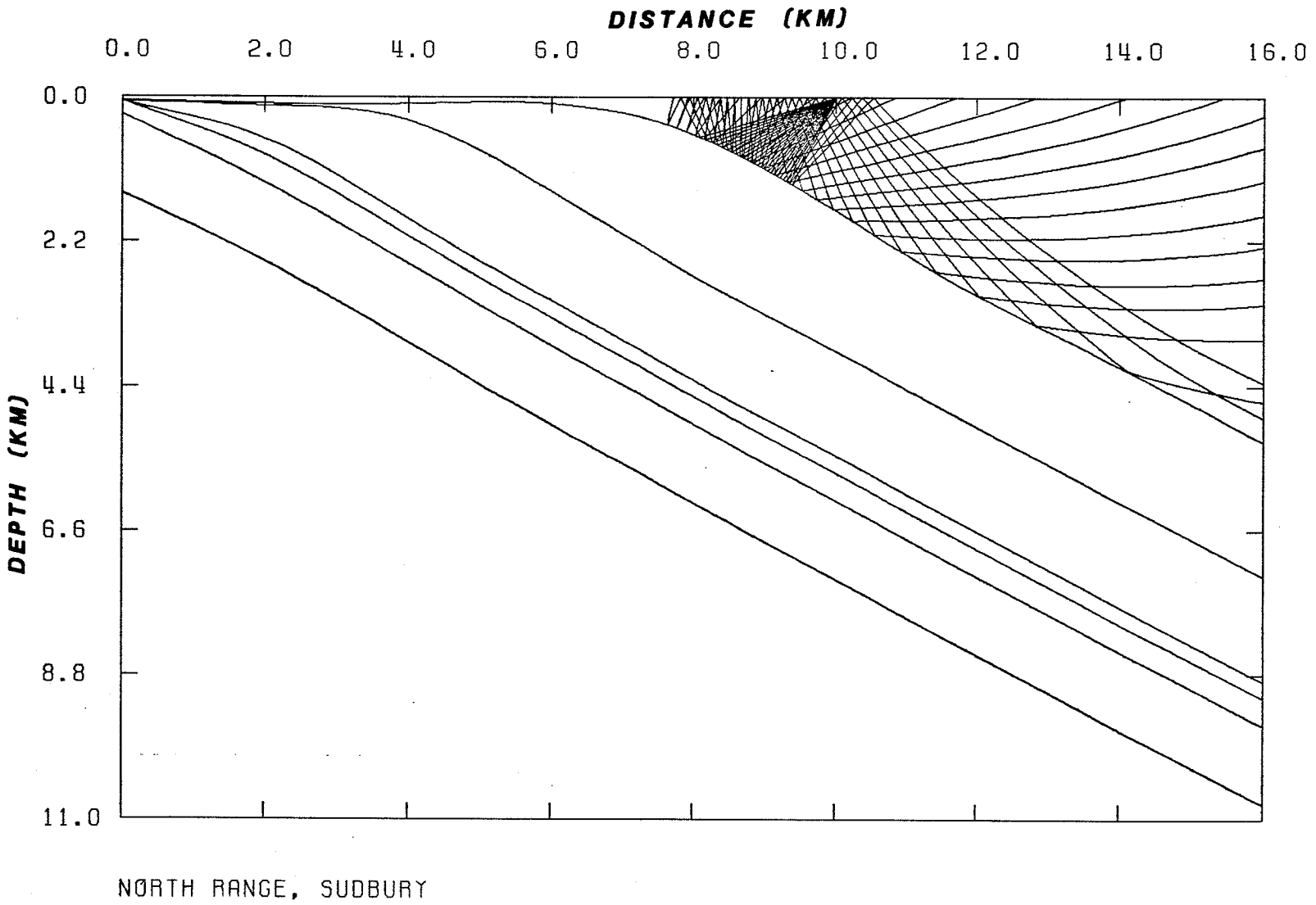


Figure 6.1. (b) The same model as in part (a) showing only multiples.

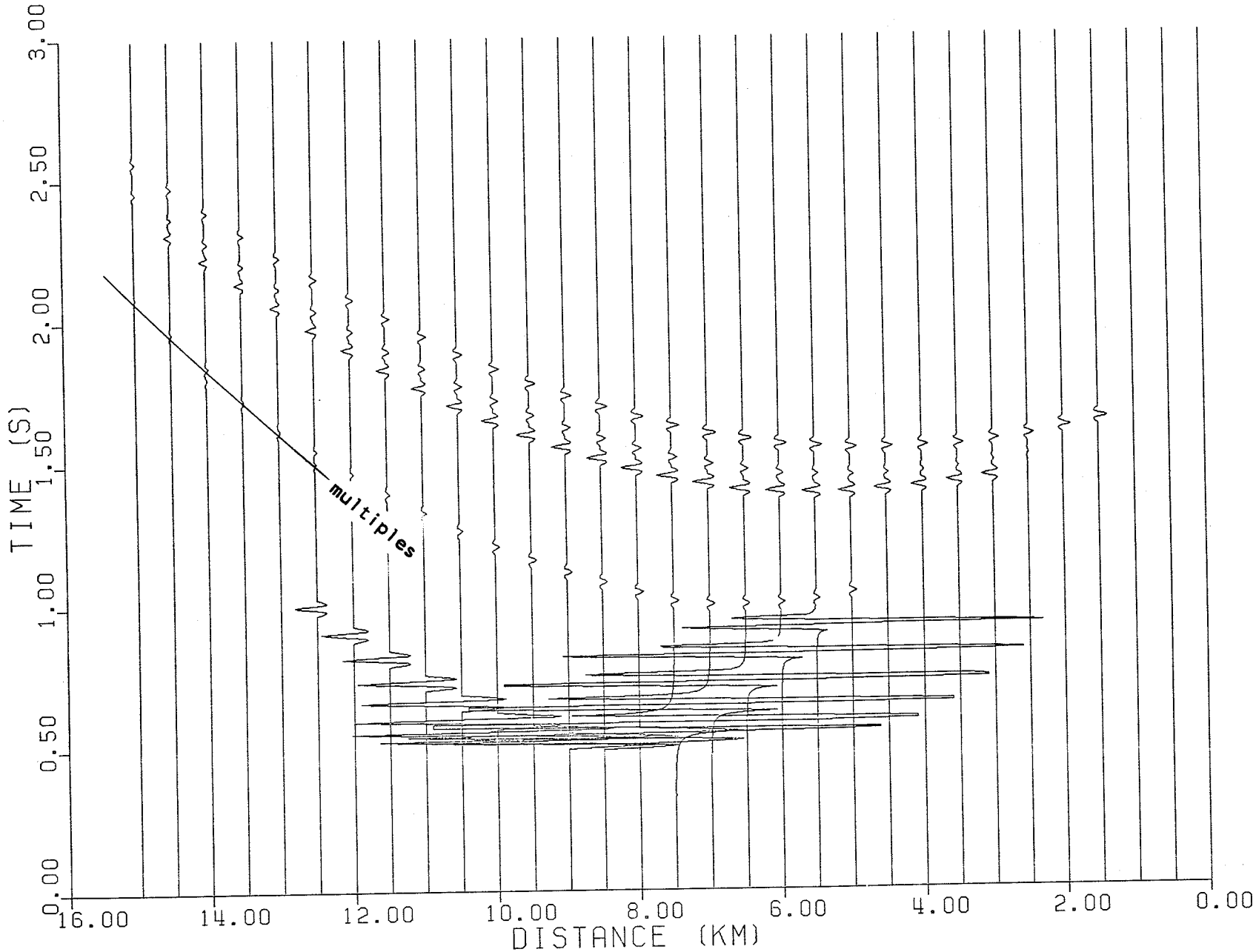


Figure 6.1. (c) Synthetic seismogram of the model shown in part (a).

cut by steeply dipping olivine diabase dykes with a thickness ranging from a few cm to 100 m (N.L.Anderson, personnal communication). Depending on the orientation of the survey line with respect to the atitude of the dykes, some of them, especially the thinner ones, will act as point diffractors. The presence of such features may eventually contaminate the seismic section with diffraction hyperbolas of varying intensity. Furthermore, the embayment structures and the associated thinning and thickening of formations will all result in significant lateral inhomogeneity in the structure. The seismic records can be hopelessly smeared by the diffraction pattern and side swaps generated by faults, anticlines, synclines, and other steeply dipping structures. In this case, the reflectors as viewed in the time section will have pronounced lateral displacement and appear to have smaller dips than the true value.

The role of migration will be to collapse the diffraction patterns generated by faults and point diffractors, to reduce the breadth of anticlines to their correct value, and to increase the breadth of synclines. Therefore, a more realistic picture of the subsurface geology will be ascertained.

At present, migration is more likely regarded as a two-stage process (Anstey, 1977) :

a) Time migration, in which the reflection segment is moved to its revised position horizontally, but in which the vertical axis is still reflection time.

b) Depth migration, in which the vertical scale is changed to depth.

The rationale behind the two stage process is that the first process which accomplishes all the objectives concerned with the collapse of diffractions and the general clarification of the structure, is not overly sensitive to the correct choice of migration velocity. However, a small error in the depth conversion velocity can lead to serious errors in the structural interpretation.

Currently, there are three major migration techiniques: diffraction (Kirchhof integral migration when high-order approximations are used), finite difference, and frequency domain migration.

The Diffraction method is the oldest of the widely used migration techniques and relies on diffraction for migrating reflections from dipping reflectors and for collapsing diffractions. The major advantage of this method is good performance with steep dip. The disadvantage is poor performance under low (S/N) (signal-to-noise) ratio (Chun and Jacewitz, 1981).

The finite difference method is based on the finite difference approximation of the wave equation for downward continuation (Claerbout, 1971; Claerbout and Doherty, 1972; Claerbout, 1976). In this method, the migration procedure is modeled by the wave equation, which will then be approximated by a simple type of equation appropriate for migration. Finally, finite difference algorithms will be employed to approximate the last equation. The method has a good performance under low (S/N) conditions, but has a relatively long computing time and difficulty in handling steep dip data (Chun and Jacewitz, 1981).

The third method, frequency domain migration, depends on two dimen-

sional (2-D) Fourier transform. It has a greater computational advantage through the use of the fast Fourier transform and it has become very popular recently (Stolt, 1978; Gazdang, 1978). Other advantages include good performance under low (S/N) conditions and excellent performance for steep dip. A disadvantage of this method is the difficulty encountered when dealing with widely varying velocity functions (Chun and Jacewitz, 1981) and narrow pass band of the seismic hardware in use.

To see how much a seismic section observed in Sudbury will depart from the real geological section, the North Range environment model was densely mapped as shown in Figure 6.2a simulating an actual seismic survey. A maximum offset distance of 250 m was used in the set-up which amounts to a 500 m split spread. The response so obtained was stacked as shown in Figure 6.2b to give a synthetic record section of the model. A comparison of the two figures reveals a substantial reduction in dip and a corresponding upward shift of the interfaces. The dip has decreased from the specified value of 30° to 18° . A shift of this magnitude can completely distort the interpreted geological result.

Because of their inherent good performance for steep dips, two of the above mentioned migration techniques; diffraction and frequency domain, would be suitable for migrating actual seismic data collected for mineral exploration purposes in a Sudbury-like area. However, frequency domain migration will be preferable for the exceptional advantage in computation. In regions of gentle dips, such as the flanks of the Sudbury area, it may be possible to use the classical manual method

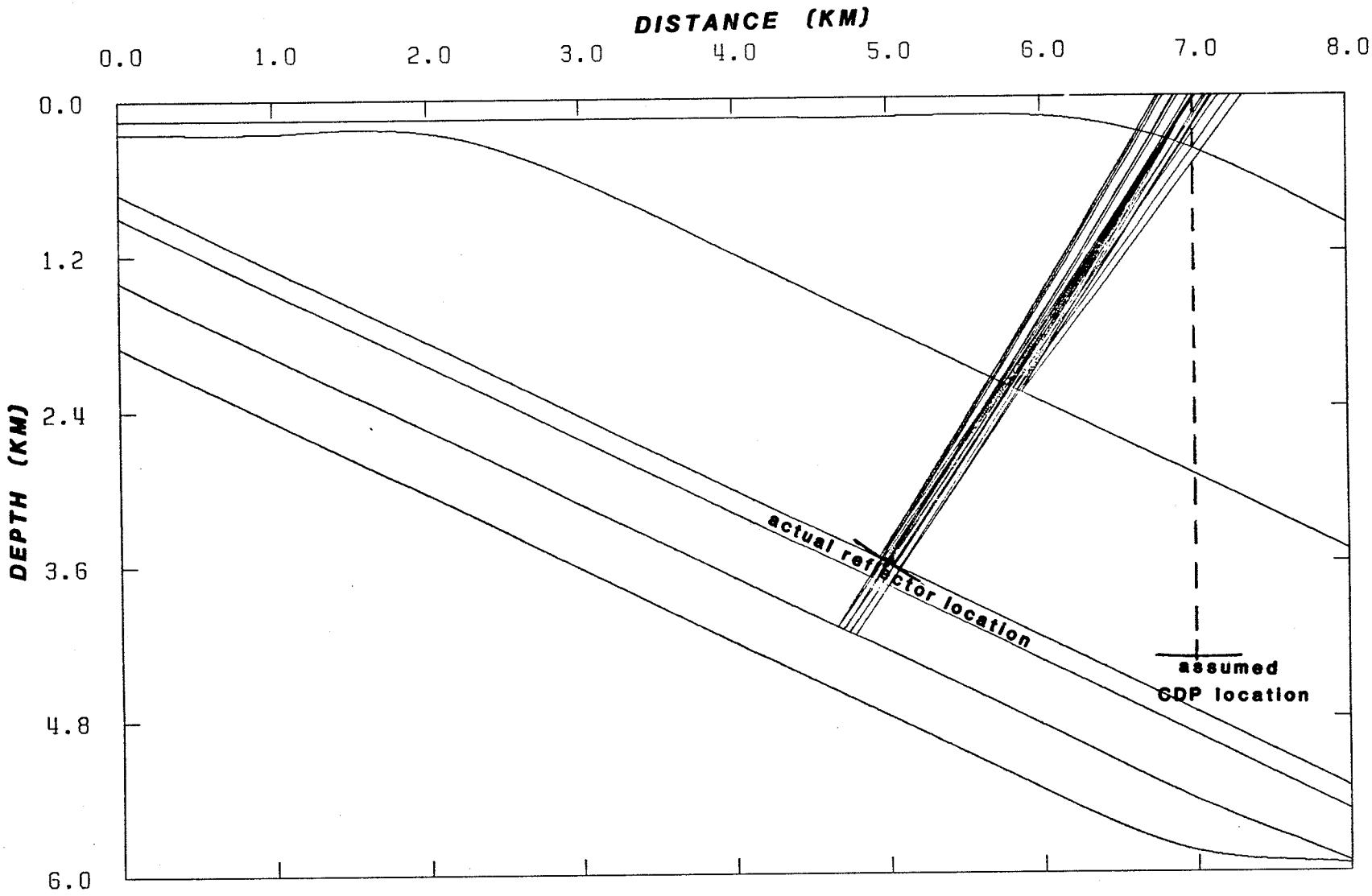


Figure 6.2. (a) Diagram showing ray paths for a split spread of 500 m. The subsurface mapping was effected by moving the source from 7.75 km to 2 km distance in steps of 250 m.

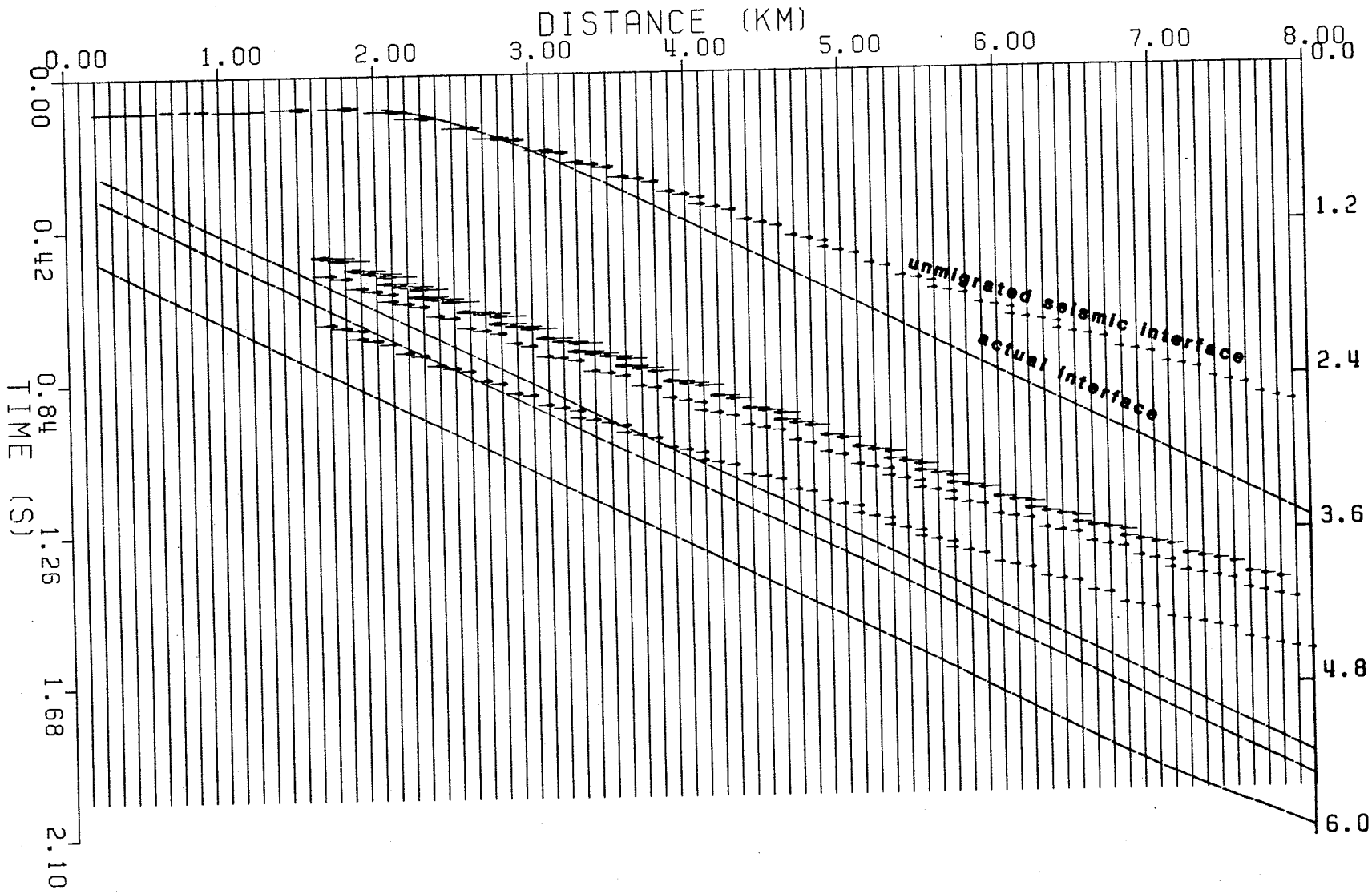


Figure 6.2. (b) Unmigrated synthetic record section of the model shown in part (a). The figure also shows the actual geological boundaries (broken lines) superimposed on the synthetic record section.

of migration.

In order to image geologic structures and stratigraphic targets that do not fit the standard two-dimensional (2-D) assumption, the data acquisition should be sufficiently dense and should have a uniform coverage of the area (Gibson et al., 1983). This kind of data can only be handled by three dimensional (3-D) migration technique, which provides the natural approach to imaging seismic wavefields recorded in the field. Fine structures such as mineralized embayments will generally have complicated seismic signatures due to out of line interference, diffractions from small obstacles and terminating reflectors. Two terminating reflectors are obvious from Figure 5.16a. Consequently, 3-D migration will be an essential and hopeful component of the processing of seismic data collected over such areas. Even though 3-D migration approach is an effective method for proper subsurface imaging of seismic data, it has its own drawback. In addition to the requirement that the data be collected over an area rather than over a single line on the earth's surface, 3-D migration involves considerably more data and more extensive processing. The storage and manipulation of such a large data volume demands very large computer capacity. More recently, efficient 3-D migration approaches, that can considerably reduce the burden of computation and data manipulation, have been introduced (Gibson et al., 1983; Jakubowicz and Levin, 1983). This and similar improvements may eliminate in the future some of the existing problems and pave the way for a routine application of 3-D method in seismic mineral exploration techniques.

## 6.3 Some aspects of seismic resolution

Seismic resolution is the ability to distinguish between the properties of two reflecting interfaces by a seismic method. The resolving power generally depends on the predominant frequency of the source energy wavelet and on the (S/N) ratio (Widess, 1973). Additional factors that come into play in seismic resolution are the form and duration of the incident wavelet, the degree to which this wavelet is known prior to analysis, and the data processing methods used.

Throughout this thesis, the impulse response of the ground motion was computed and then convolved with a velocity-type source wavelet (displayed in Figure 6.3a). This operation modifies the impulse response so that it will have a similar form as the actual output of a geophone. Recent studies show that there are three aspects that control the resolving power of a seismic signal, namely, the breadth of the central lobe, the side lobe ratio and the amplitude of the side-tail oscillations (Koefoed, 1981). In addition to resolution, there are other desirable properties of signals, such as accuracy of depth estimation and accuracy of formation thickness. A comparison of minimum phase and zero phase signals, based on the above mentioned points, reveals that zero phase signals have better resolution and more accurate estimates of reflection times and spacings (Schoenberger, 1974). Hence, the zero phase velocity-type signal of Figure 6.3a, which describes the earth particle velocity at infinity, was found more appropriate to use in this study.

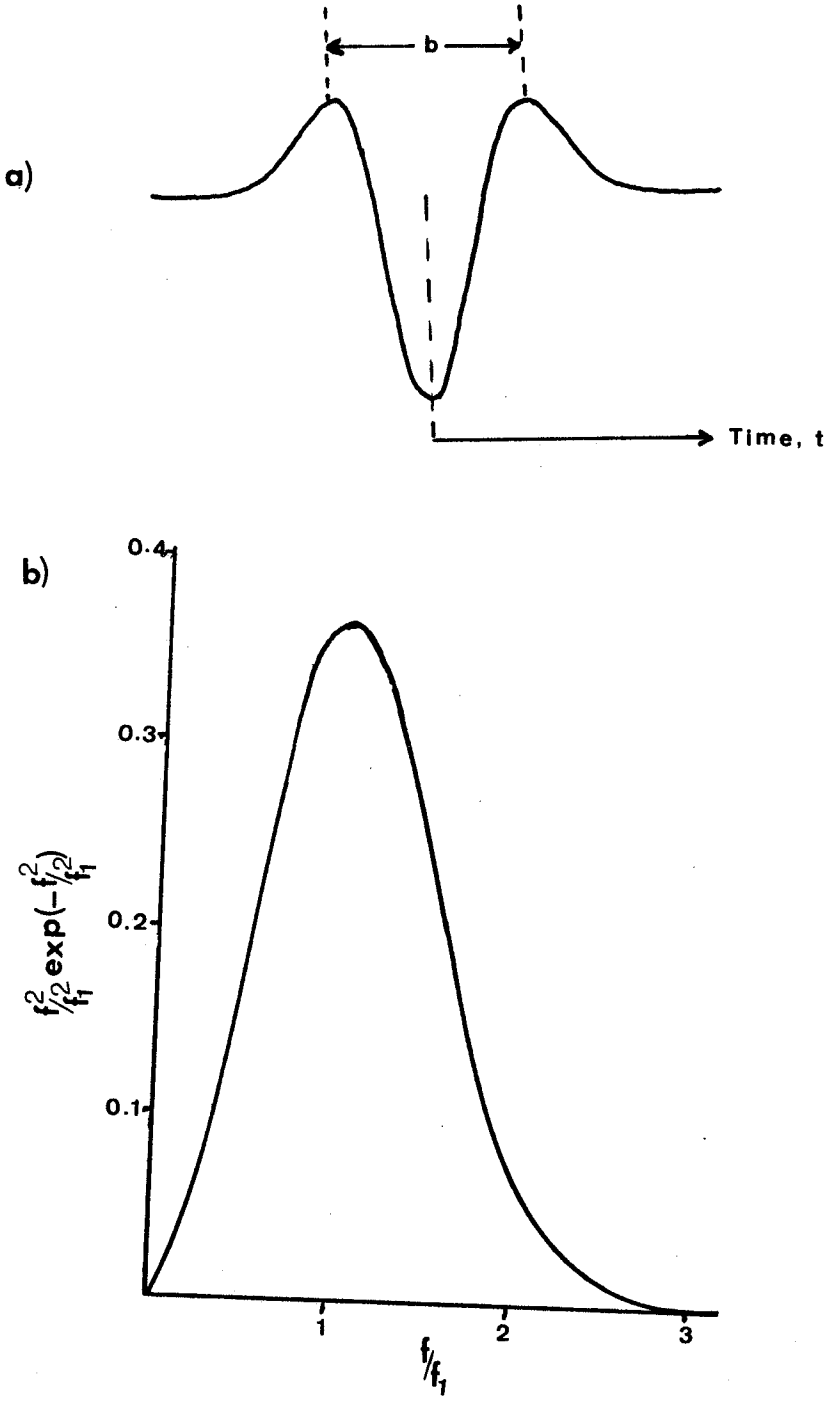


Figure 6.3. (a) Velocity-type seismic wavelet.
(b) Spectrum of the velocity type wavelet shown in part (a) (see text for explanations).

Following Ricker (1977), a velocity type seismic wavelet may be represented by an infinite integral of the form :

$$V(u|_\infty) = -\int_0^\infty \xi^2 \exp(-\xi^2) \cos\left\{\frac{2\sqrt{6}}{b} t\, d\xi \right. \quad \ldots (6.1)$$

where $\xi$ is simply a variable of integration, b is the breadth of the wavelet in seconds between its two maxima, and t is the time measured from the wavelet center. If a frequency $f_1$ is defined as

$$f_1 = \frac{\sqrt{6}}{\pi} \frac{1}{b} \quad \ldots (6.2)$$

and a variable, f, by :

$$f = f_1 \xi \quad \ldots (6.3)$$

then the integral form, equation (6.1), can be expressed as :

$$V(u|_\infty) = -\int_0^\infty \frac{f^2}{f_1^2} \exp(-f^2/f_1^2) \cos 2\pi f t \frac{df}{f_1} \quad \ldots (6.4)$$

According to equation (6.4), the wavelet is the sum of an infinite array of single-frequency sinusoidal components covering the entire range of frequencies from zero to infinite frequency. It also states that all these single frequency components are in phase at the wavelet center which accounts for the deep valley at the center of the wavelet.

The spectrum of the velocity wavelet is given in Figure 6.3b, which also indicates that the frequency of the maximum amplitude component is $f_1$. In normal exploration seismology, the predominant frequency is in the range of 15 Hz to 50 Hz. By substituting these values in equation (6.2), it is possible to determine the expected breadth (b) of the wavelet as detected by the geophones. The computed value is 0.052 second for a 15 Hz wavelet and 0.016 second for a 50 Hz wavelet.

If two interface are closely spaced, the seismic wavelets reflected from each of these interfaces will tend to overlap and form a wavelet complex, instead of a single arrival. It has been shown (Ricker, 1977) that the components of a wavelet complex can be resolved only when the wavelet centers are separated in time by an amount greater than 0.428 of the wavelet breadth. Thus, if the wavelet complex arises from the overlaping of the reflections from two interfaces, and V is the wavelet velocity in the bed lying between these two interfaces, we have :

$$t = \frac{2h}{V} \qquad \ldots (6.5)$$

where t is the time interval between the two reflections and h is the distance between the interfaces. At the resolution point, we have :

$$\frac{t}{b} = 0.428 \qquad \ldots (6.6)$$

and

$$h = 0.214bV \qquad \ldots (6.7)$$

This last expression is of vital importance in exploration seismology and it will be used to determine the minimum thickness of the bed that can be resolved by the method. In the case of Sudbury, the average layer velocity can be taken as 6.2 km/s, which gives a minimum thickness of 21 m for the high frequency (50 Hz) and 69 m for the low frequency (15 Hz).

This mathematical formulation will be valid when the wave is normal to the interfaces and it is free from any kind of distortion. In real geological conditions, where most ore-bodies occur, the above requirements are hardly met. In the synthetic seismograms of the previous chapter, wavelet breadths corresponding to 50 Hz (for the shallow models) and 15 Hz (for the deep models) were employed. For example, in Figure 5.8c, the model with 45 m thick sulphide body, a 50 Hz wavelet was used and yet the resolution was not satisfactory. If the noise introduced by the measuring instrument is also taken into account, the minimum resolvable thickness of a bed appears to be substantially higher than the values computed by the above formula.

The computation of the minimum thickness of a bed that can be resolved, given above, assumes that conventional reflection seismic techniques will be used for the actual survey. Recently, however, new high resolution seismic techniques with signal frequency content of as high as 100 or 120 Hz are becoming popular in the oil and gas industry. The new method has a broader bandwidth obtained by extending the high frequency end of the spectrum, which makes it significantly superior to the conventional seismic methods. This is primarily achieved by: 1) scaling down the explosive charge size and using single high frequency geophones instead of groups, 2) reducing the sampling interval in space and time (Ziolkowski and Lerwill, 1979; Applegate et al., 1982; Mair and Green, 1981). By this method, it will be possible to detect beds as thin as 10 m, a very desirable feature for use in Sudbury. Hence, a suitable adaptation of this technique for crystalline environments will be of paramount importance.

# Chapter 7

## SUMMARY AND CONCLUSION

The prime objective of this study has been to investigate the feasibility of applying seismic techniques to solve current exploration problems associated with deep ore-bodies. The overall procedure was essentially an understanding of the forward problem, i.e., the behavior of seismic waves traveling in rocks typically found in Precambrian mining districts. The initial stage of the study was directed towards the determination of the seismic velocity distribution in a typical mining environment, specifically the world renowned nickel-copper mining district of Sudbury, Ontario.

Using the most popular and reliable laboratory seismic velocity measuring technique, the pulse method, P-wave and S-wave velocities of core samples were determined for simulated overburden pressures of 2 MPa to 44 MPa. The range of the applied pressure in the experiment corresponds to a depth of a few meters to 2 km, and it is intended to coincide with the depth of occurrence of most known ore-bodies.

From the laboratory measured seismic velocities, it is concluded that:

1) The sudden increase in velocity in the low pressure region, up to 20 MPa, is the result of the closing of very fine cracks in the rock samples. Beyond 20 MPa, the role of applied pressure on the observed velocities continues to be less significant, i.e., it gives way to some other factors.
2) Unlike most young sedimentary rocks, the velocity of crystalline

rocks strongly depends on the chemical composition and density of the rock type, even in the low pressure region. Mafic rocks in general have higher seismic velocities than felsic rocks, felsic norite being an exception, which has a velocity that fits well in the prominent felsic group of rocks.

3) There is some indication of the effect of alteration in the measured average velocities (Figures 5.4a and 5.4b) where the two gneissic rocks (mafic gneiss and granite gneiss) tend to possess a lower velocity than their igneous counterparts. The average velocity of granite gneiss is less than the average velocity of granite breccia or micropegmatite, and the average velocity of mafic gneiss is less than the average velocity of mafic norite or oxide-rich quartz gabbro.

4) Up to a pressure of 44.2 MPa, the measured P-wave velocities are not very well governed by the linear law of the form $V = a + b\rho$ A least squares fit of a straight line to all the measured velocities at 44.2 MPa confirms that only 33.7% of the variation of velocity may be accounted for by correlation with density, which disagrees with the result obtained by Birch (1961) at 1000 MPa of pressure.

5) From laboratory measured seismic velocities, it is possible to determine the seismic wave velocity distribution of a given area with a reasonable degree of accuracy. A maximum standard deviation of only 0.203 km/s (3.3% of the mean) may be introduced in the measured velocity of a particular rock type. Velocity measurements of this nature can provide valuable data in an effort made to understand the seismic forward problem in crystalline

rock environment.

6) S-wave velocities generally show a similar pattern as the P-wave velocities except that they are less sensitive to the applied pressure, particularly in the low pressure region. Exploration techniques based on S-wave motion are not likely to be appropriate for mineral exploration, consequently, no further analysis was done on the measured S-wave velocities.

Having acquired the necessary data for the seismic velocity distribution of the area of interest, the next step was to select the appropriate theoretical approach through which the seismic response of the subsurface geology can be predicted. The most important points considered in selecting the theoretical tool were: 1) The method should comply with the requirements of the geology in the mining areas, i.e., should be able to handle both lateral and vertical inhomogeneities. 2) The method should be reasonably efficient and flexible to use.

Only the asymptotic ray theory could satisfy the above criteria; consequently all the analysis and numerical simulation undertaken in this study was based on this theory.

A preliminary analysis of the P-wave velocity and density of core samples from Sudbury mining area revealed that:

a) Massive sulphide has an exceptionally high acoustic impedance.

b) Two mafic rocks, oxide-rich quartz gabbro and mafic norite have a moderately high acoustic impedance.

c) The felsic footwall rock, granite gneiss, has the lowest acoustic impedance

A similar analysis based on the possible seismic interfaces which correspond to the respective geological boundaries shows that:

a) The reflection coefficient of all the seismic interfaces formed with massive sulphide is substantially high and it is comparable to moderately high reflection coefficients found in young sedimentary areas.

b) Three other interfaces, micropegmatite/oxide-rich quartz gabbro, oxide-rich quartz gabbro/felsic norite, and mafic norite/granite gneiss, have reflection coefficients that will be of significant importance from exploration point of view.

c) All other interfaces are characterized by generally low reflection coefficients suggesting that these interfaces may be too weak to be detected by presently available techniques.

To understand the effect of various geological structures on seismic waves, several seismic models were constructed. The input data for these models were 1) the P-wave velocity distribution as observed by laboratory measurements, and 2) geological sections typically found in the Sudbury Basin. The overall model study involved ray tracing in an assumed geological section, and generating theoretical seismograms as the seismic response of the model. Extensive use of synthetic seismograms was made as a result of which both the kinematic and dynamic characteristics of the seismic response was analyzed.

For the geological condition of the Sudbury Basin, three groups of seismic models were constructed. The first group of models represent the shallow and deep geological sections of the North Range environment. From the seismic response of these models, it is concluded that:

a) the top of the oxide-rich quartz gabbro has a uniquely strong reflection, much stronger than the reflection from the top of the micropegmatite (which is 1.8 km shallower than the former). This reflector may serve as a marker horizon in future reflection seismic surveys.

b) The reflection obtained by including a massive sulphide layer is the strongest of all, but not much exploration significance can be attached to this kind of response because of the impracticality of having a sulphide layer with that dimension.

c) A more useful and realistic response was obtained when a mafic norite layer was inserted between the felsic norite and the granite gneiss footwall. The reflection from the bottom of this layer is nearly as strong as the reflection from the top of the oxide-rich quartz gabbro. Because of the intimate association of sulphide mineralization with mafic norite sub-layer, the seismic mapping of this layer (mafic norite) will have special exploration significance.

d) The reflection from the rest of the interfaces is generally weak and not very much different from one another.

The second group of models are intended to give the seismic characteristics of the whole Sudbury Basin. For these models, geologically accepted dimensions (depth and width) of the Basin were used. The amplitude characteristics of these models was found not to be significantly different from the one observed in the first group of models. The travel time of these models, however, reveals the phase identification problem that might be encountered in a seismic survey of this scale in the Basin. A thorough investigation of such models is expect-

ed to have valuable contribution to a better understanding of the origin of the Sudbury Structure.

The third and last group of models are all small scale models which correspond to the mineralized zones in Sudbury. Considerable effort has been made to include the most essential features of the mineralized structures in both the North Range and the South Range. From the computed seismic response, it is concluded that :

a) There is a better chance of detecting the lenticular South Range ore-bodies by virtue of the strong reflecion generated from both faces (top and bottom) of the sulphide body.

b) For North Range type of ore-bodies, the seismic response appears relatively complicated, but more diagnostic features can be recognized from a careful examination of both the arrival time and the dynamic characteristics.

A review of the current seismic data processing techniques shows that:

a) Multiples and reverberation should not cause any serious impediment in a Sudbury-like environment.

b) Frequency domain migration is judged to be more suitable for improving the horizontal resolution of the seismic data collected for mineral exploration.

It should be realized, however, that all the above conclusions are based on the numerical simulations made in constructing the various seismic-geological models. Their validity greatly depends on how much the assumed parameters approximate the actual geological conditions. One of the most common and critical assumptions made in seismic mod-

elling is that of a sharp contact between layers, but in real geological conditions there will always be a transition zone of varying thickness at the boundary of two formations. It has been shown, however, that the existence of a transiton zone will not reduce the amplitude of the reflected wave as long as the thickness of the zone is less than 10% of the wavelength (approximately 20 m in Sudbury). In Sudbury, the most important contacts from seismic reflection point of view, such as the contact of the Irruptive with the footwall, are known to be reasonably sharp (Dence, 1978; N.L. Anderson, personnal communication). Even the contact considered as very gradational (the contact between felsic norite and mafic norite) has a thickness of 2 - 8 m (Dence, 1978), which is sufficiently thin not to cause any reduction of amplitudes. On these grounds, a considerable degree of optimism can be attached to all the conclusions made in this study.

## References

Aki, K., and Richards, P., 1980, Quantitative seismology, theory and methods, Volumes I and II : Freeman and Company, San Francisco.

Anstey, N.A., 1977, Seismic interpretaion, The physical aspects: International Human Resources Development Corporation, Part 7, Migration pp. 474-513.

Applegate, J.K., Emila, D.A., Neitzel, E.B., and Donaldson, P.R., 1982, High resolution seismic study in the Gas Hills uranium district, Wyoming: Geophysics, Vol.47, pp. 1355-1374.

Ari Ben-Menham, and Sarva Jit Singh, 1981, Seismic waves and sources: Springer-Verlag, New York, pp. 420-621.

Berry, M.J., 1973, The structure of the crust and upper mantle in Canada: Tectonophysics, Vol.20, pp. 183-201.

Berry, M.J., and Fuchs, K., 1973, Crustal structure of the Superior and Grenville Provinces of the Northeastern Canadian Shield: Bulletin of the Seismological Society of America, Vol.63, pp. 1393-1432.

Birch, F., 1960, The velocity of compressional waves to 10 kilobars, Part 1: Journal of Geophysical Research, Vol.65, pp. 1083-1102.

Birch, F., 1961, The velocity of compressional waves to 10 kilobars, Part 2: Journal of Geophysical Research, Vol.66, pp. 2199-2223.

Braile, L.W., and Smith, R.B., 1975, Guide to the interpretation of crustal refraction profiles: Geophysical Journal of the Royal Astronomical Society, Vol.40, pp. 145-176.

Card, K.D., and Hutchinson, R.W., 1972, The Sudbury structure, its geological setting: In New developments in Sudbury Geology, J.V. Guy-Bray (editor) The Geological Association of Canada, special paper No 10, pp. 67-78.

Cerveny, V., 1979, Ray theoretical seismograms for laterally inhomogeneous structures: Journal of Geophysics, Vol.46, pp. 335-342.

Cerveny, V., and Hron, F., 1980, The ray series method and dynamic ray tracing system for three-dimensional inhomogeneous media: Bulletin of Seismological Society of America, Vol.70, pp. 47-77.

Cerveny, V., Molotov, I.A., and Psenick, I., 1977, Ray method in Seismology, Praha: Univerzita Karlova.

Creveny, V., and Ravindara, R., 1971, Theory of seismic head waves: University of Toronto Press, Toronto, 1971.

Chapman, C.H.,1978, A new method for computing synthetic seismograms:

Geophysical Journal of the Royal Astronomical Society, Vol.54, pp. 481-518.

Christensen, N.I., 1979, Compressional wave velocities in rocks at high tempretures and pressures, critical thermal gradients, and crustal low-velocity zones: Journal of Geophysical Research, Vol.84, pp. 6849-6857.

Chun, J.H., and Jacewitz, C.A., 1981, Fundamentals of frequency migration: Geophysics, Vol.46, pp. 717-733.

Claerbout, John F., 1971, Toward a unified theory of reflection mapping: Geophysics, Vol.36, pp. 467-481.

Claerbout, John F., 1976, Fundamentals of geophysical data prcessing: McGraw-hill, New York pp. 227-263.

Claerbout John f., and Doherty, S., 1972, Downward continuation of seismic reflection profiles: Geophysics, vol.37, pp. 741-768.

Cook, F.A., Brown, L.D., and Oliver, J.E., 1980, Southern Applachian and the growth of continents: Scientific American, Vol. 243, No.4, pp. 156-170.

Cowan, J.C., 1968, The geology of the Strathcona Ore Deposit: Canadian Mining and Metallurgical Bulletin, Vol.61, pp. 38-54.

DeLandro, W., and Moon, W., 1982, Seismic Structure of Superior-Churc -hill Precambrian boundary zone: Journal of Geophysical Research (Red), Vol.87, pp. 6884-6888.

Dence, M.R., 1978, Sudbury and Brent excursions, guide book, Laurentian University, Sudbury, Ontario, pp. 1-28.

Dietz, R.S., 1964, Sudbury structure as an astrobleme: Journal of geology, Vol.72, pp. 412-434.

Dietz, R.S., 1972, Sudbury astroblem, splash emplaced sub-layer and possible cosmogenic ores: In New developments in Sudbury Geology, J.V.Guy-Bray (editor), The Geological Association of Canada, special paper No.10, pp. 29-40.

Dohr, G.P., and Meissner. R., 1975, Deep crustal reflections in Europe: Geophysics, Vol.40, pp. 25-39.

Elliot, C.L., 1967, Some application of seismic refraction techniques in mining exploration: In Seismic Refraction Prospecting, A.W.Musgrave (editor), Society of Exploration Geophysicists, Tulsa, Ok., pp. 522-538.

Fairbairn, H.W., Faure, G., Pinson, W.h., and Hurley, P.m., 1968, Rb-Sr whole-rock age dating of the Sudbury loplith and basin sediments: Canadian Journal of Earth Sciences, Vol.5, pp. 707-714.

Fairbairn, H.W., Hurley, P.M., Card, K.D., and Knight, C.J., 1969, Correlation of radiometric ages of Nipissing diabase and Huronian metasediments with Proterozoic orogenic events in Ontario: Canadian Journal of Earth Sciences, Vol.6, pp. 489-497.

Frazer, N.L., and Phinney, R.A., 1980, The theory of finite frequency body wave synthetic seismograms in inhomogeneous elastic media: Geophysical Journal of Royal Astronomical Society, Vol.63, pp. 691-717.

French, B.M., 1967, Sudbury Structure, Ontario, Some petrographic evidence for origin by meteorite impact: Science, Vol.156, pp. 1094-098.

French, B.M., 1972, Shock-metamorphic features in the Sudbury Structure, A review: In New developments in Sudbury Geology, J.V.Guy-Bray (editor), The Geological Association of Canada, special paper, No.10, pp. 19-28.

Fuchs, K., and Muller, G., 1971, Computation of synthetic seismograms with the reflectivity method and comparison with observation: Geophysical Journal of the Royal Astronomical Society, Vol.23, pp. 417-433.

Gazdag, R., 1978, Wave equation migration with the phase shift method: Geophysics, Vol.43, pp. 1342-1351.

Gibbins, W.A., and McNutt, 1975, The age of the Sudbury Nickel Irruptive and Murray Granite: Canadian Journal of Earth Sciences, Vol.12, pp. 1970-1989.

Gibson, B., Larner, K., and Levin, S., 1983, Efficient 3-d migration in two steps: Geophysical Prospecting, Vol.31, pp. 1-33.

Gilbert, F., and Helmberger, D.V., 1972, Generalized ray theory for a layered sphere: Geophysical Journal of Royal Astronomical Society, Vol.27, pp. 58-80.

Green, A.G., 1981, Results of seismic reflection survey accross the fault zone between the Thompson Nickel Belt and the Churchill Tectonic Province, Northern Manitoba: Canadian Journal of Earth Sciences, Vol.18 pp. 13-25.

Green, A.G., Anderson, N.L., and Stephenson, O.G., 1979, An expanding spread seismic reflection survey across the Snake Bay-Kakagi Lake Greenstone Belt, Northwestern Ontario: Canadian Journal of Earth Sciences, Vol.16, pp. 1599-1612.

Green, A.G., Stephenson, O.G., Mann, G.D., Kanasewich, E.R., Cumming, G.L., Hajnal, Z., Mair, J.A., and West, G.F., 1980, Cooperative seismic surveys across the Superior-Churchill boundary in Southern Canada: Canadian Journal of Earth Sciences, Vol.17, pp. 617-632.

Hajnal, Z., and Stauffer, M.R., 1975, The application of seismic

reflection techniques for subsurface mapping in the Precambrian Shield near Flin Flon, Manitoba: Canadian Journal of Earth Sciences, Vol.12, pp. 2036-3047.

Hall, D.H., and Hajnal, Z., 1973, Deep seismic studies in Manitoba: Bulletin of the Seismological Society of America, Vol.63, pp. 885-917.

Hall, D.H., and Hajnal, Z., 1969, Crustal structure of Northwestern Ontario: refraction seismology: Canadian Journal of Earth Sciences, Vol.6, pp. 81-100.

Helmberger,D.V., 1968, The crust-mantle transition in the Bering Sea: Bulletin of Seismological Society of America, Vol.58, pp. 179-214.

Helmberger, D.V., 1972, Long period body-wave propagation from 4° to 13° : Bulletin of Seismological Society of America, Vol.62, pp. 325-341.

Hilterman, F.J., 1970, Three dimensional seismic modeling: Geophysics, Vol.35, pp. 1020-1037.

Hobson, G.D., 1966, A shallow seismic experiment in permafrost, Klondike area, Yukon Territory: In report of activities, Geological Survey of Canada, paper 66-2: 10-14.

Hobson, G.D., 1967, Seismic methods in mining and groundwater exploration: In Mining and groundwater geophysics, L.W.Morley (editor), Geological Survey of Canada, Economic Geology Report, No.26, pp. 148-176.

Hobson, G.D., and Grant, A.C., 1964, Tracing buried river valleys in the Kirkland Lake area of Ontario with a hammer seismograph: Canadian Mining Journal, April: pp. 79-83.

Hong, T.L., and Helmberger, D.V., 1977, Generalized ray theory for a dipping structure: Bulletin of the Seismological Society of America, Vol.67, 995-1008.

Hong, T.L., and Helmberger, D.V., 1978, Glorified optics and wave propagation in nonplanar structure: Bulletin of the Seismological Society of America, Vol.68, pp. 1313-1330.

Hood, P.J., 1961, Paleomagnetic study of the Sudbury Basin: Journal of Geophysical Research, Vol.66, pp. 1235-1241.

Hood, P., 1978, Finite difference and wave number migration: Geophysical Prospecting, Vol.26, pp. 773-789.

Hron, F., 1971, Criteria for selection of phases in synthetic seismograms: Bulletin of Seismological Society of America, Vol.61, pp. 765-779.

Hron, F., and Kanasewich, E.R., 1971, Synthetic seismograms for deep seismic sounding studies using Asymptotic ray theory: Bulletin of Seismological Society of America, Vol.61, pp. 1169-1200.

Hughes, D.S., and Cross, J.H., 1951, Elastic wave velocities in rocks at high pressures and temperatures: Geophysics, Vol. 16, pp. 577-593.

Hughes, D.S., and Kelly, J.L., 1952, Variation of elastic wave velocity with saturation in sandstone: Geophysics, Vol.17, pp. 739-752.

Jakubowicz, H., and Levin, S., 1983, Asimple exact method of 3-D migration - theory: Geophysical Prospecting, Vol.31, pp. 34-56.

Kaarsberg, E.A., 1975, Elastic-wave velocity measurements in rocks and other materials by phase-delay methods: Geophysics, vol.40, pp. 955-960.

King, M.S., 1966, Wave velocities in rocks as a function of changes in overburden pressure and pore fluid saturants: Geophysics, Vol.31, pp. 50-73.

Koefoed, O., 1981, Aspects of vertical seismic resolution: Geophysical Prospecting, Vol.29, pp. 21-30.

Korgh, T.E., McNutt, R.H., and Davis, G.l., 1982, Two high precision U-Pb zircon ages for the Sudbury Nickel Irruptive: Canadian Journal of Earth Sciences, Vol.19, pp. 723-728.

Kosminskaya, I.P., and Riznichenko, Y.V., 1964, Seismic studies of the earth's crust in Eurasia: In Solid earth and interface phenomena, H.Odishaw (editor), Research in Geophysics, Vol. 2, Cambridge: M.I.T. press

Lang, A,H., Goodwin, A.M., Mullingan, R., Whitmare, R.R.E., Gross, G.A., Boyle, R.W., Johnston, A.G., Chamberlain, J.A., and Rose, E.R., 1970, Geology and economic minerals of Canada: Geological Survey of Canda, pp. 151-226.

Langston, C.A., 1977, The effect of planar dipping structure on source and receiver responses for constant ray parameters: Bulletin of Seismological Society of America, Vol.67, 1029-1050.

Larochelle, A., 1969, Preliminary results of a study of paleomagnetism of the Sudbury Irruptive: Geological Survey of Canada, paper 69-19.

Mair, J.A., and Green, D.E., 1981, High resolution seismic reflection profiles reveal fracture zones within a 'homogeneous' granite batholith: Nature, Vol.294 3 December, pp. 439-442.

Matsushima, S., 1981, Compressional and shear wave velocities of

igneous rocks and volcanic glasses to 900° C and 20 Kbar : Tectonophysics, Vol.75, pp. 257-271.

May, B.T., and Hron, F., 1978, Synthetic seismic sections of typical petroleum traps: Geophysics, Vol.43, pp. 1119-1147.

Meissner, R., 1967, Exploring deep interfaces by seismic wide angle measurements: Geophysical Prospecting, Vol.15, pp. 598-617.

Meissner, R., 1973, The Moho as a transition zone: Geophysical Surveys Vol.1, pp. 995-216.

Meissner, R., and Fakhimi, M., 1977, Seismic anisotropy as measured under high-pressure, high-temperature conditions: Geophysical Journal of Royal Astronomical Society, Vol.49, pp.133-143.

Mereu, R.F., and Hunter, J.A., 1969, Crustal and upper-mantle structure under the Canadian Shield from project Early Rise data: Bulletin of the Seismological Society of America, Vol:59, pp. 147-155.

Morgan, N.A., 1969, Physical properties of marine sediments as related to seismic velocities: Geophysics, Vol.34, pp. 529-545.

Noponen, I., Heikkinen, P., and Mehrotra, S., 1979, Applicability of seismic reflection sounding in regions of Precambrian Geology: Geoexploration, Vol.17, pp. 1-9.

Nur, Amos, and Simmons, Gene, 1969, The effect of saturation on veloccity in low porosity rocks: Earth and Planetary Science Letters Vol.7, pp. 183-193.

O'Doherty, R.F., and Anstey, N.A., 1971, Reflection on amplitudes: Geophysical Prospecting, Vol.19, pp. 430-458.

Oliver, J., and Kaufman, S., 1977, Complexities of the deep basement from seismic reflection profiling: In The earth's crust, Geophysical monograph ser., J.G.Heacock (editor), A.G.U. Washington, D.C., Vol.20, pp. 243-253.

Overton, A., 1972, A seismic experiment over a metallic sulphide deposit: In Report of activities, part A, Geological Survey of Canada, paper 72-1A. p. 57.

Overton, A., 1976, Seismic velocity measurements on samples and sulphide ore-bodies: In Report of activities, part A, Geological Survey of Canada, paper 76-1A, p.485.

Pattison, Edaward F., 1979, The Sudbury sublayer: Canadian Mineralogist Vol.17, pp. 257-274.

Peredery, W.V., 1972, Chemistry of fluidal glasses and melt bodies in the Onaping formation: In New developments in Sudbury Geology, J.V.Guy-Bray (editor) The Geological Association of Canada,

special paper No.10, pp. 49-59.

Pilant, W.L., 1979, Elastic Waves in the earth: Developments in solid earth geophysics 11, Elsevier Publishers, Amsterdam, pp. 195-280.

Popelar, J., 1972, Gravity interpretation of the Sudbury Area: In New developments in Sudbury Geology, J.V.Guy-Bray (editor) Geological Association of Canada, special paper No.10 pp. 103-115.

Ricker, N.H., 1977, Transient waves in visco-elastic media: Elsevier Publishers, Amsterdam, pp. 37-95.

Robertson, P.B., and Grieve, R.A.E., 1975, Impact structures in Canada Their recognition and characteristics: The Journal of the Royal Astronomical Society of Canada, Vol. 69, pp. 1-21.

Robinson, E.A., 1982, Migration of seismic data as W.K.B. approximation: Geoexploration, 20 pp. 7-30.

Schoenberger, M, 1974, Resolution compaprison of minimum-phase and zero-phase signals: Geophysics, Vol.39, pp. 826-833.

Sharma, P.V., 1976, Geophysical methods in geology: Elsevier Publishers, Amsterdam, pp. 7-85.

Simmons, G., 1964, Velocity of compressional waves in various minerals at pressures to 10 kilobars: Journal of Geophysical Research, Vol.69, pp. 1117-1121.

Smithson, S.B., Shive, P.N., and Brown, S.K., 1977, Seismic velocity, reflections and structure of the crystalline crust: In The earth's crust, Geophysical monograph ser., Vol.20. Edited by J.G. Heacock. A.G.U. Washington, D.C., pp. 254-270.

Sopher, S.R., 1963, Paleomagnetic study of the Sudbury Irruptive: Geological Survey of Canada Bulletin, Vol.90.

Souch, B.E., Podolosky, T., and Geological staff, The International Nickel Company of Canada, Limited, 1969, The sulphide ores of Sudbury, their particular relationship to a distinctive inclusion-bearing facies of the Nickel Irruptive: Economic Geology Monograph 4, pp. 252-261.

Speers, E.C., 1957, The age relation and origin of the Sudbury breccia: Journal of Geology, Vol.65, 497-514.

Spencer, James W. Jr., and Nur, Amos M., 1976, The effects of pressure, temperature, and pore water on velocities in Westerly Granite: Journal of Geophysical Research, Vol.81, pp. 899-904.

Stockwell, C.H., 1961, Structural provinces, Orogenies and time classification of rocks of the Canadian Precambrian Shield: Geological Survey of Canada, paper 64-17.

Stockwell, C.H., Mcylynn, R.F., Emslie, B.V., Sanford, A.W., Donaldson, J.A., Fahring, W.F., and Curie, K.L., 1970: Geology and economic minerals of Canada, pp. 43-150.

Stolt, R.H., 1978, Migration by Fourier transform: Geophysics Vol.43, pp. 23-48.

Toksoz, M.N., Chung, C.H., and Timur, A., 1976, Velocities of seismic waves in porous rocks: Geophysics, Vol.41, 621-645.

Tucker, P.M., and Yorston, H.J., 1973, Pitfalls in seismic interpretation: Society of Exploration Geophysicists, monograph series No.2.

Van Schumus, W.R., 1965, The geochronology of the Blind River-Bruce Mines area, Ontario, Canada: Journal of Geology, Vol.73, pp. 755-780.

Wabaso, C.E., and Mereu, R.F., 1978, The feasibility of delineating non-layered anomalous velocity zones by a combination of fan shooting and least-squares analysis: Canadian Journal of Earth Sciences, Vol.15, pp. 1642-1652.

Widess, M.B., 1973, How thin is a thin bed ? : Geophysics, Vol.38, pp. 1176-1180.

Wiggins, R.A., and Helmberger, D.V., 1974, Synthetic seismogram computation by expansion in generalized rays: Geophysical Journal of the Royal Astronomical Society, Vol.37, pp. 73-90.

Wyllie, M.R.J., Gregory, A.R., and Gardner, G.H.F., 1958, An Experimental investigation of factors affecting elastic velocities in porous media: Geophysics, Vol.23, pp. 459-493.

Young, R.A., 1979, Seismic crustal structure, Northwest of Thunder Bay, Ontario, Ph.D thesis, University of Toronto, PP. 31-40.

Ziolkowoski, A., and Lerewill, W.E., A simple approach to high resolution seismic profiling for coal: Geophysical Prospecting, Vol.27, pp. 360-393.

# APPENDIX

## PROGRAM TRACE

The seismic modelling throughout this thesis was made possible through the use of the computer program called TRACE. The main function of this program is to compute traveltimes and the corresponding amplitude and phase of all arrivals. Unlike the "shooting" and the "bending" methods of ray path calculation which involve iterative procedures in one way or the other, the method used by the program is relatively straightforward. In this method, the starting point(source) and the initial direction of the ray are specified, and the ray path calculation is done in steps of time-increment. The time-increment generally depends on the scale of the model and the complexity of the structure; more complex structures require short time-increment. This, however, results in long computing time and more computer storage. Besides, for the same number of interfaces, more rays will be required to map a complicated structure than a simple layered one. All these effects ultimately add up to make ray path calculation of a complicated structure rather expensive.

The computation procedure begins with the construction of a 2-dimensional rectangular grid, horizontal axis stands for distance(x), and vertical axis (positive downward) stands for depth(z). The grid is usually uniformly spaced with respect to the x-axis, but the vertical spacing will depend on the thickness of the layers in the structure. Thus, the geological boundaries(seismic interfaces) will be constructed by specifying the position of the boundary at each grid point. This process will be repeated for each boundary in the structure. For a

complicated structure, very closely spaced grid points will be required, i.e., more input data should be fed to the computer.

Once the structure is constructed in the above manner, the next step will be to include the P-wave velocity in the model. This is done again by supplying the P-wave velocity at each grid point. For each grid point there will be two velocity values, one for the upper medium and another one for the lower medium. A sample input data is shown in Figure(A1). The velocity between grid points is determined by interpolating the values at the grid points. The interpolation procedure is facilitated through the use of a special subroutine based on cubic splines.

The last set of input data contains the source position, initial direction of the ray, time increment, number of rays required to map a given interface, and the type of ray(reflected, refracted, multiples, etc, ). This part will be repeated as many times as the number of interfaces in the model.

The output of the program is a plot showing the geological structure with ray paths (Figure A2) and the necessary information for generating synthetic seismograms. The data includes the travel time, geophone position, amplitude, phase, and ray type. A separate program called SYNART utilizes this data to generate the synthetic seismogram of the given model as shown in Figure (A3).

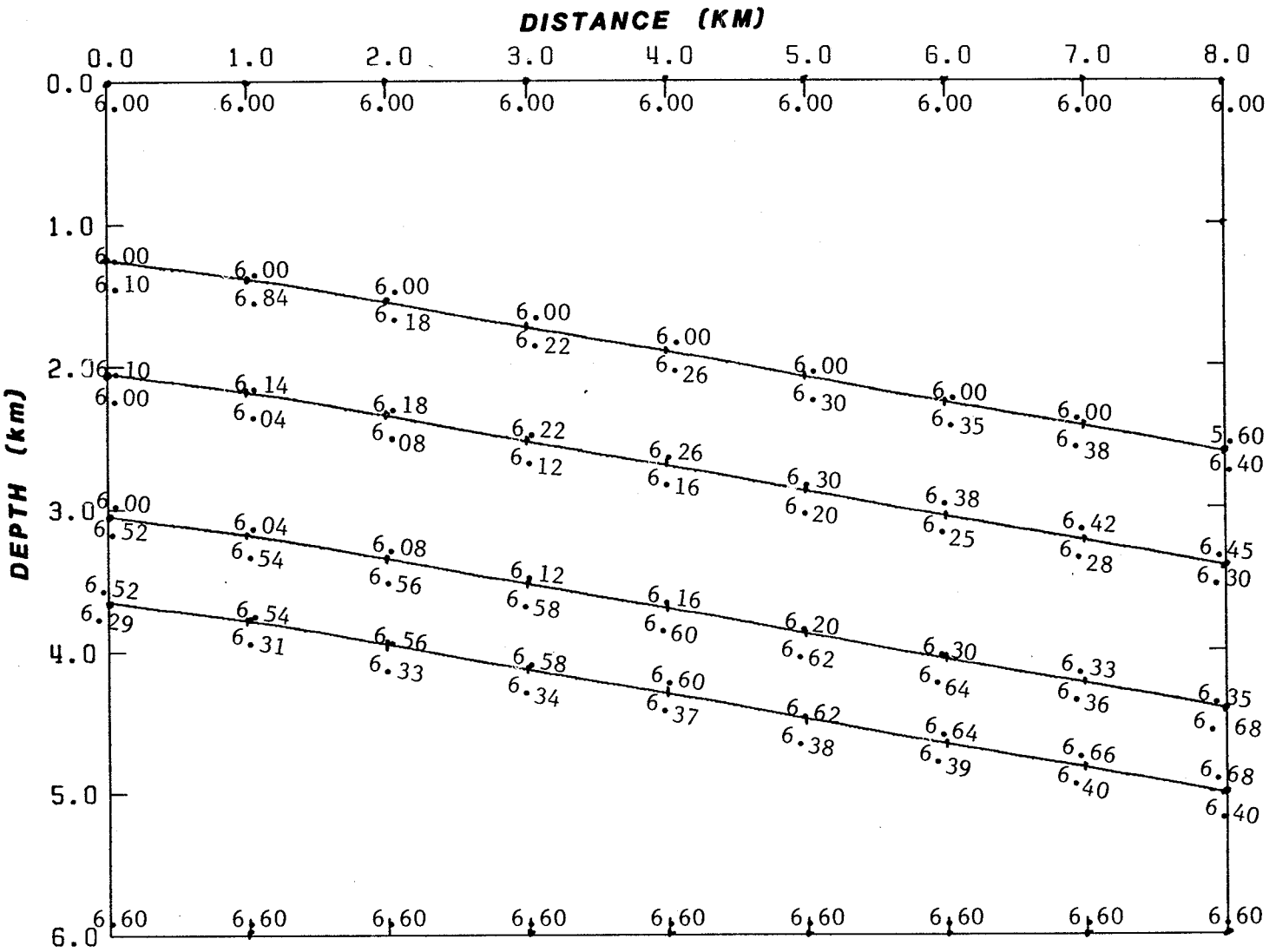


Figure A1. Sample input data for program TRACE.

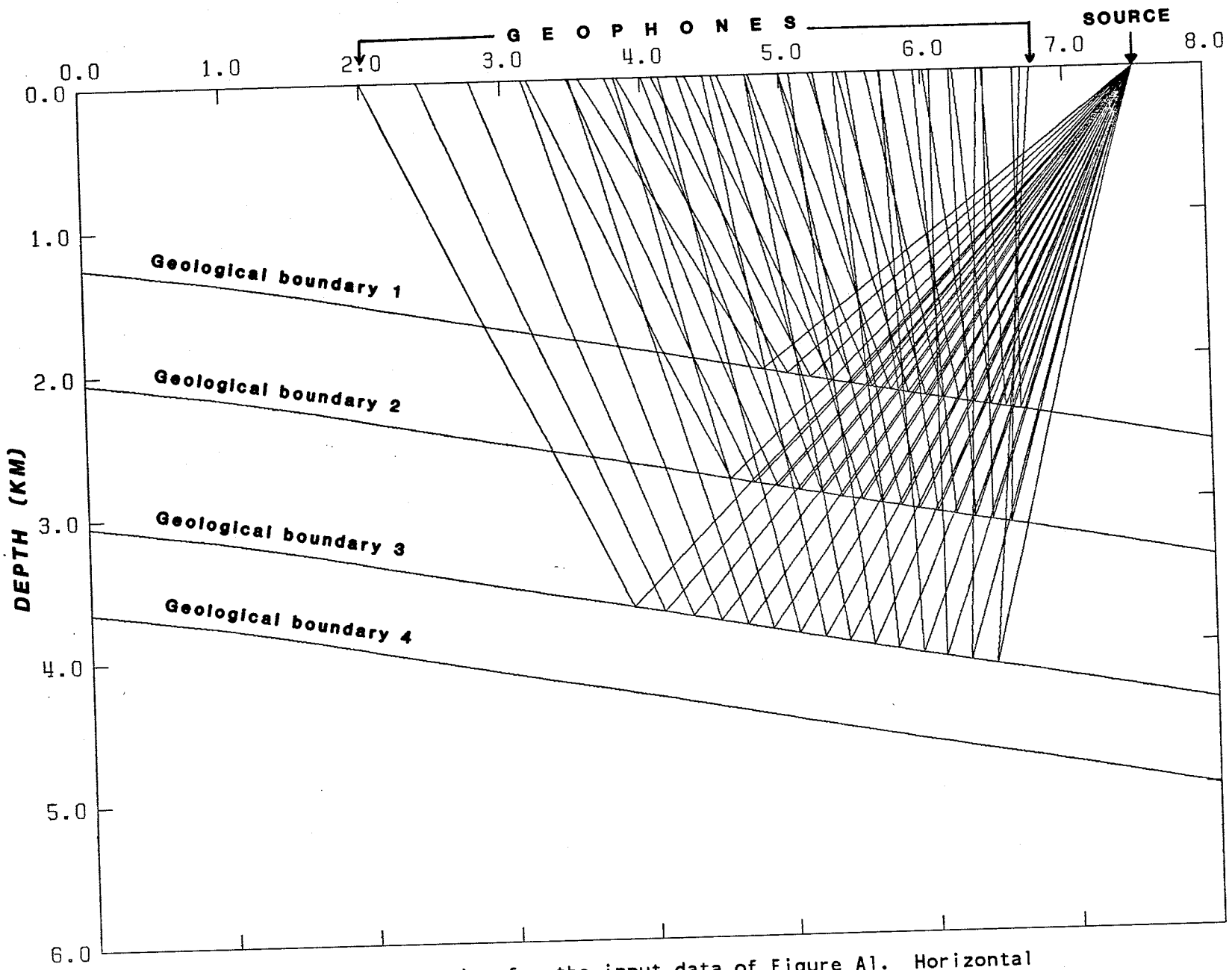


Figure A2. Ray tracing for the input data of Figure A1. Horizontal axis represents distance in km.

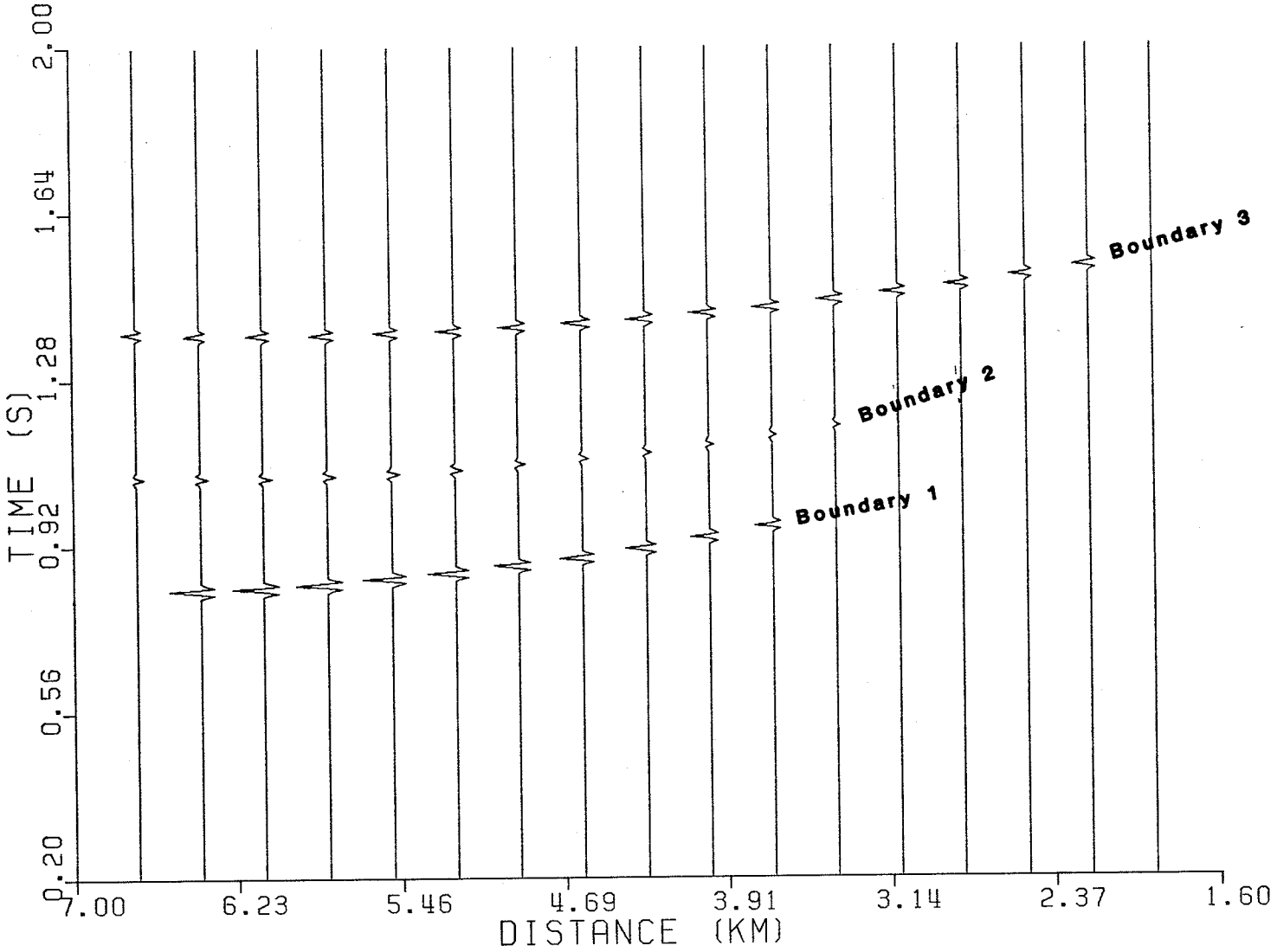


Figure A3. Synthetic seismogram of the model shown in Figure A2. Only reflections from the top three geological boundaries are shown.